DOT/FAA/CT-ACD33092/2

COPY 1

PROCEEDINGS OF THE FOURTH MLS MATH MODEL USER GROUP MEETING
NOVEMBER 6 & 7, 1991
FAA TECHNICAL CENTER

DEC 9 1991
TECHNICAL CENTER LIBRARY
ATLANTIC CITY INTL AIRPORT, NJ 08405

Linda Pasquale
Jesse D. Jones
Coordinators

November 1991

Engineering, Research, and Development Service
Concepts Analysis Division
FAA Technical Center
Atlantic City International Airport, N.J. 08405

TABLE OF CONTENTS

	Page
MEETING AGENDA	iii
ATTENDANCE LIST	v
FAA MLS PROGRAM - Steven Wolf	1
MILITARY MLS PROGRAM - Gerry Headley	42
BENDIX MLS PROGRAM - Dave Huntington	49
RUNWAY HUMP MODELING - Kent Chamberlin	63
AZIMUTH GROUND CROSSFALL EFFECTS - Al Lopez	74
ELEVATION DIFFRACTION ERROR - Kazunobu Koremura	88
THE DME/P MODEL - Jesse Jones	99
VALIDATION OF THE DME/P MODEL - Stephan Kruger	101
DME/P CRITICAL AREAS - Jaikishan Rajendran	113
DIFFRACTION AT A RECTANGULAR PLATE - Michael Kleintz	132
SPECULAR GROUND REFLECTIONS - Hollis Ryan	164

MLS MATHEMATICAL MODEL USER GROUP MEETING
AGENDA

NOVEMBER 6-7, 1991
FAA TECHNICAL CENTER
ATLANTIC CITY INTERNATIONAL AIRPORT, NJ 08405

DAY 1 - NOVEMBER 6, 1991

Morning Session - 9:00 to 12:00

Welcome	
MLS Program Overview	Steve Wolf, FAA
Military MLS Program	Gerry Headley, USAF
Bendix MLS Program	Dave Huntington, Bendix

Lunch - 12:00 to 1:00

Afternoon Session - 1:00 to 4:00

GELTI Demonstration	Kent Chamberlin, U. of N.H.
Azimuth Ground Crossfall Effects	Al Lopez, ARL Associates
Elevation Diffraction Error	Kazunobu Koremura, ENRI

DAY 2 - NOVEMBER 7, 1991

Morning Session - 9:00 to 12:00

The DME/P Model	Jesse Jones, FAA
Validation of the DME/P Model	Stefan Kruger, O.U.
DME/P Critical Areas	Jaikishan Rajendran, O.U.

Lunch - 12:00 to 1:00

Afternoon Session - 1:00 to 4:00

Electromagnetic Reflection and Diffraction	Michael Kleintz, DLR
Specular Ground Reflections	Hollis Ryan, CTA Inc.
General Discussion	

MLS MATH MODEL USER GROUP MEETING - NOVEMBER 6-7, 1991

ATTENDANCE LIST

Mr. Glen Adams
MiTech, Inc.
820 First St., NE, Suite 600
Washington, DC 20002
202-408-2150

Mr. Joe Acoraci
Allied-Signal/Bendix
1300 East Joppa Road
Baltimore, MD 21204
410-583-4345

Mr. Alf W. Bakken
Civil Aviation Administration Technical Center
P.O. Box 16, N-1330
Oslo Lufhavn, Norway
47-2-59-3303

Mr. Michael Biggs
Allied-Signal/Bendix
1300 East Joppa Road
Baltimore, MD 21204
410-583-4621

Mr. Michael Braasch
Avionics Engineering Center
Stocker Center, Ohio University
Athens, OH 45701-2979
614-593-1522

Mr. Chris Burr
Civil Aviation Authority
45-59 Kingsway, CAA House, Room K420
London, England WC2B 6TE
44-71-832-6016

Mr. Ed Butterly
CTA Incorporated
English Creek Center
McKee City, NJ 08232
609-484-5006

Dr. Kent Chamberlin
University of New Hampshire
Kingsbury Hall
Durham, NH 03824-3591
603-863-3766

Mr. Elmer Clausen
Bell Aerospace Textron
P.O. Box 1
Buffalo, NY 14240-0001
716-298-6597

Mr. Jan-Hein van Dronkelaar
National Aerospace Laboratory
P.O. Box 90502, Anthony Fokkerweg 2
1059 CM Amsterdam, The Netherlands
31-20-511-3583

Mr. Roger Holm
Civil Aviation Administration
P.O. Box 8124 Dep.
N-0032
Oslo 1, Norway
47-2-94-2225

Mr. Mahbue Hoque
Bellcore, NJ
201-829-2970

Mr. Jim Howell
Raytheon Corporation, A-26
Boston Post Road
Wayland, MA 01778
508-440-6453

Mr. Dave Huntington
Allied-Signal/Bendix
1300 East Joppa Road
Baltimore, MD 21204
410-583-4281

Mr. Bob Ibach
Wilcox Electric, Inc.
2001 N.E. 46th St.
Kansas City, MO 64116
816-453-2600

Ms. Marjorie Luke Johnson
ARINC Research Corporation
2551 Riva Road
Annapolis, MD 21401
410-266-2268

Mr. Jesse Jones
FAA Technical Center, ACD-330
Atlantic City International Airport
NJ 08405
609-484-4573

Mr. Scott Kennett
E-Systems
2268 South 3270 West
Salt Lake City, UT 84119
801-974-7586

Mr. Michael Kleintz
DLR, Institut fur Hochfrequenztechnik
D-8031 Oberpfaffenhofen
Post Wessling/Obb., Germany
49-81-53-28-379

Mr. Kozunobu Koremura
Landing Aides Section, E.N.R.I.
6-38-1, Shinkawa, Mitaka
Tokyo 181, Japan
81-422-41-3175

Mr. Stephan Kruger
Avionics Engineering Center
Stocker Center, Ohio University
Athens, OH 45701-2979
614-593-1529

Mr. Al Lopez
ARL Associates
Four Sarina Drive
Commack, NY 11725
516-499-2987

Mr. Mike Mehth
FAA Technical Center, ACN-260
Atlantic City International Airport
NJ 08405
609-484-4932

Mr. Henry Nguyen
Allied-Signal/Bendix
1300 East Joppa Road
Baltimore, MD 21204
410-583-5923

Ms. Linda Pasquale
FAA Technical Center, ACD-330
Atlantic City International Airport
NJ 08405
609-484-6806

Mr. Jaikishan Rajendran
Avionics Engineering Center
Stocker Center, Ohio University
Athens, OH 45701-2979
614-593-1529

Dr. Bernd Rode
DLR, Institut fur Hochfrequenztechnik
D-8031 Oberpfaffenhofen
Post Wessling/Obb., Germany
49-8153-28-357

Mr. Charles Rosario
FAA National Headquarters, ASE-300
800 Independence Avenue, SW
Washington, DC 20591
202-646-2061

Dr. Hollis Ryan
CTA Incorporated
English Creek Center
McKee City, NJ 08232
609-645-5029

Mr. Joseph M. Sammon
FAA Technical Center, RJO/ACN-260
Atlantic City International Airport
NJ 08405
609-484-4024

Mr. Gary Viviani
Textron Defense Systems
201 Lowell Street, MS 3286
Wilmington, MA 01887
508-657-1319

Mr. John Warren
FAA Technical Center, ACN-260
Atlantic City International Airport
NJ 08405
609-484-6436

Mr. Steven Wolf
FAA National Headquarters, AND-30
800 Independence Avenue, SW
Washington, DC 20591
202-267-5833

STEVEN WOLF
FAA MLS PROGRAM OFFICE

MLS PROGRAM OVERVIEW

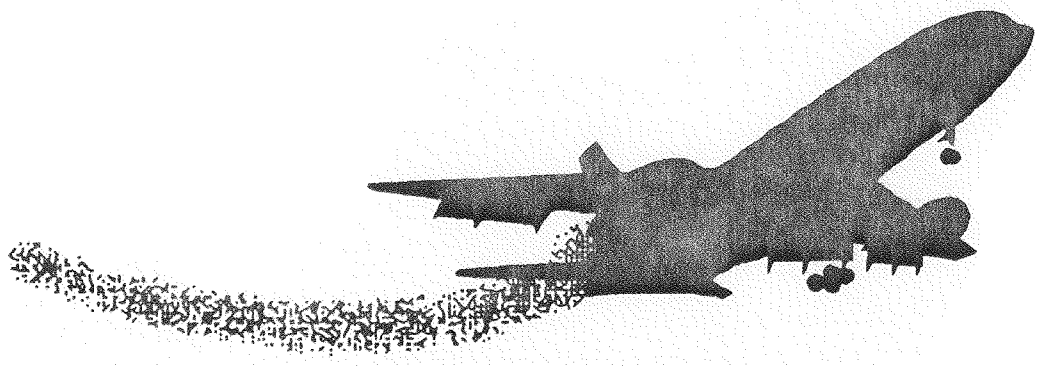

FAA MLS Program

Current and Projected Precision Approach Requirements

	Year		
	1989	*2000*	*2010*
Existing CAT I Landing Systems	757	—	—
Existing CAT II/III Landing Systems	74	—	—
New Candidates for a CAT I Landing System	303	456	506
New Candidates for a CAT II/III Landing System	151	363	423
Total CAT I Systems (Existing & Candidates)	**1382**	**1524**	**1563**
Total CAT II/III Systems (Existing & Candidates)	**225**	**467**	**527**
Total Number of Precision Landing Systems (Existing & Candidates)	**1464**	**1787**	**1877**

Why MLS?

- Frequencies
- ATC Benefits
- G/A Precision Approaches
- CAT II/III Approaches
- Rotorcraft

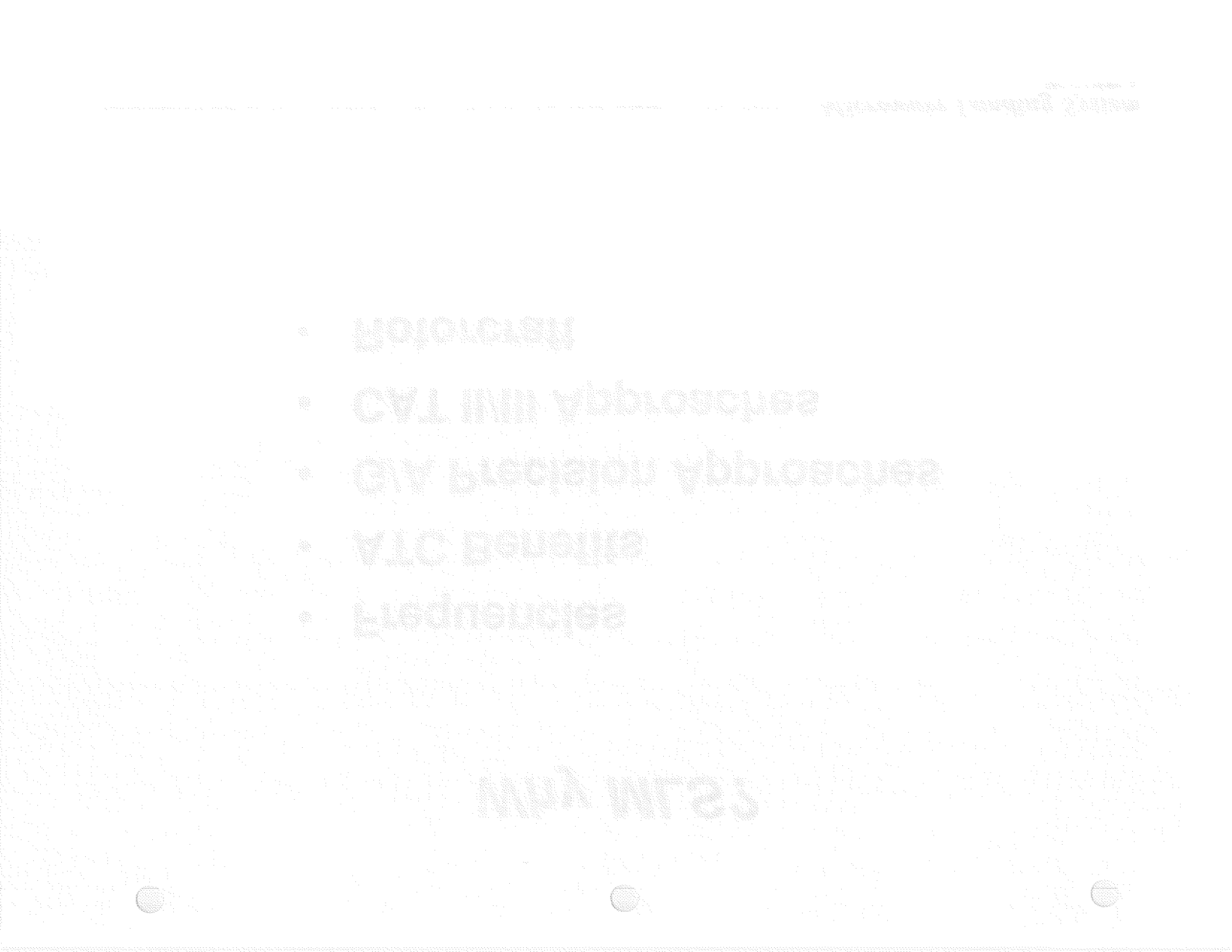

MLS Demonstration Program

- Nine Economic And Operational Evaluations
- All Projects Nearing Completion
- Industry Participation
- Results Available

ILS/MLS Frequency Study

Objective: ***Determine The Imminence And Severity Of ILS/MLS Frequency Congestion And FM Interference***

- **ILS Analysis**
- **MLS Analysis**

ILS/MLS Frequency Study (Cont'd)

MIT's Computer Simulation Tool Designed To:

- Perform Analyses Of In-Band And Out-Of-Band Interferences
- Assess Interference Within The Service Volumes
- Predict Channel Capacities In Selected Major Metropolitan Areas

ILS/MLS Frequency Study (Cont'd)

Results

- 173-203 Channel Assignments Required; 100 Cannot Be Assigned
- 252 Channel Assignments Required; 80 Cannot Be Assigned
- Total Shortfall of 180; 85 Due To FM Interference
- MLS Can Be Assigned Well Into 21st Century Without Exceeding Capacity

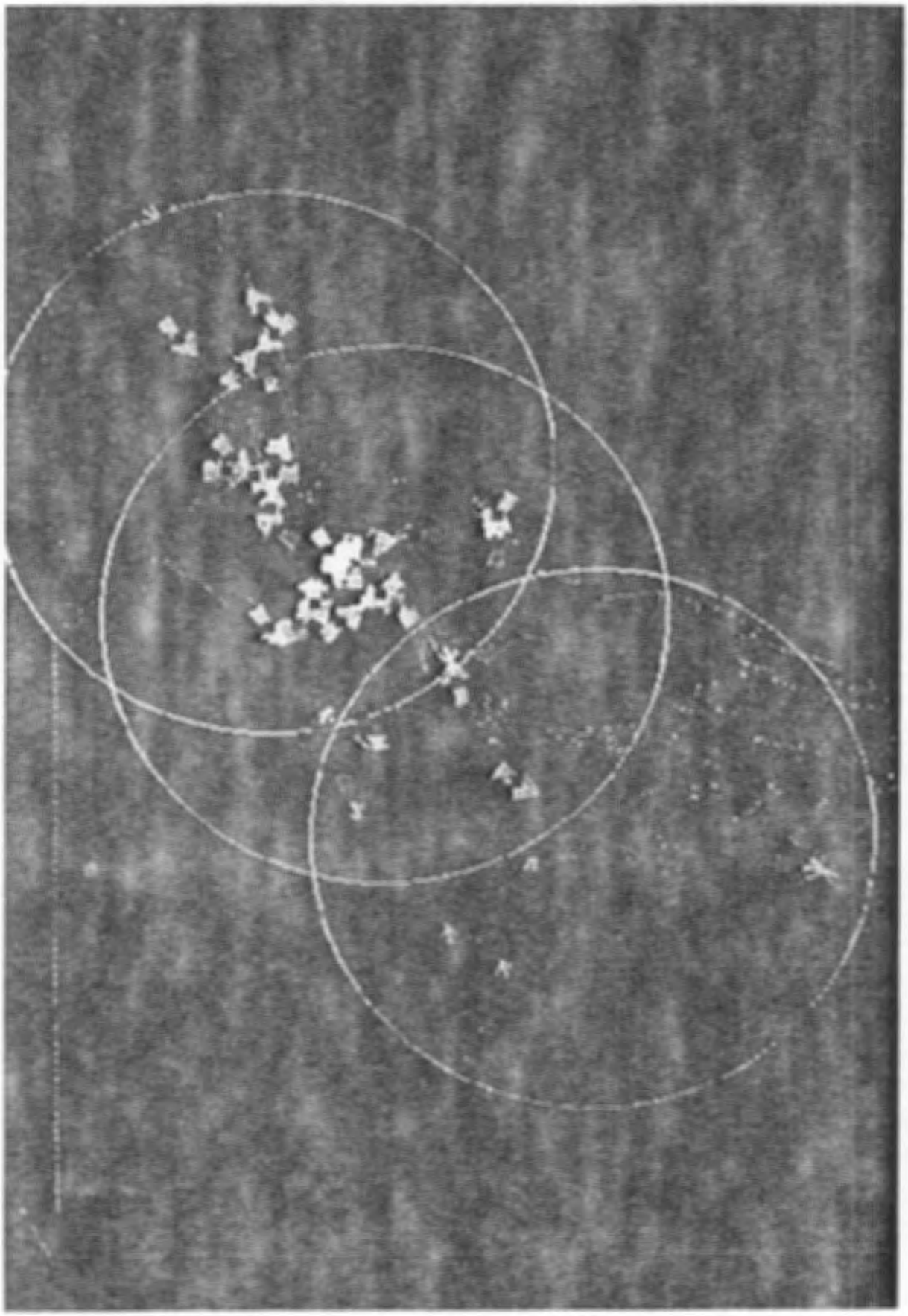

Evaluation Of Widebody Curved/ Segmented Approaches

Objective: Solve Human And Technical Issues For Curved Approaches

- **NLR Study (Netherlands)**
  - **747 Simulator - Hand Flown Flight Director**
  - **39 747 Line Crews**
  - **580 Approaches, 84 Departures**
  - **Final Segment Length - 0.7 To 3.0 NM**

Evaluation Of Widebody Curved/ Segmented Approaches (Cont'd)

- NLR Conclusion - Approaches/Departures Feasible
  - Insidious Failures
- McDonnell Douglas MD-11 Simulator
  - Control Laws, Aerodynamics, Cockpit Displays, Certification

Pilot Acceptance Of Minimum Straight Final Length In NLR Simulation

Pilot Acceptance (%)	Minimum Straight Final Length (Nautical Miles)
100	3.0
80	2.0
40	1.5

Evaluation Of Advanced Procedures

Objective: Determine Economic And Operational Benefits Of MLS In Multi-Airport Environments

- Results of New York And San Francisco Demonstration
  - User Benefits From Reduced Delay & Shortened Path
  - New York $30M, San Francisco $20M Annually
  - Independent Airport Operations
  - Pilot Acceptance Of MLS
  - Controllers Managed Mix Of ILS And MLS

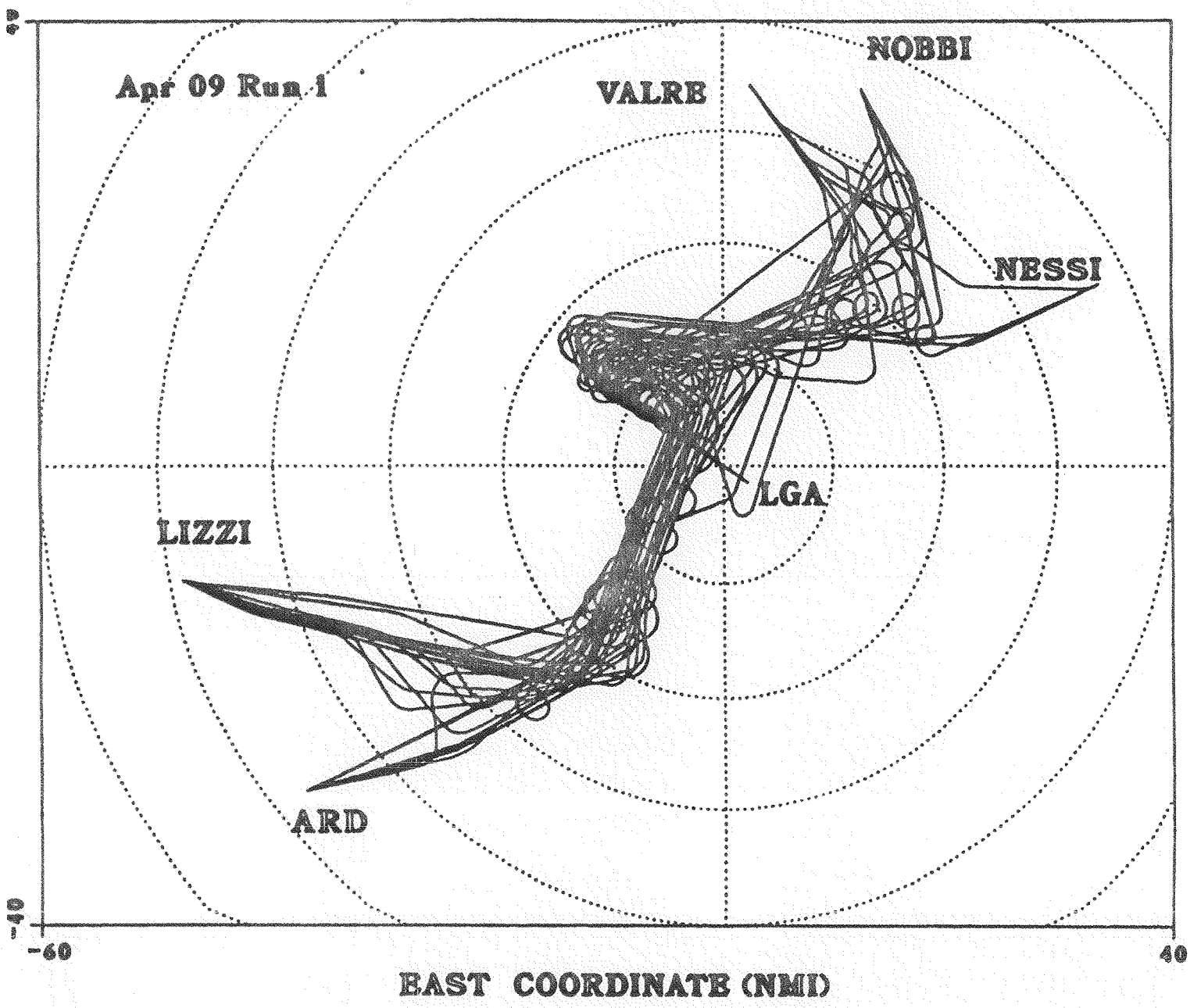
Apr 09 Run 1
NOBBI
VALRE
NESSI
LGA
LIZZI
ARD
-60
40
EAST COORDINATE (NMI)

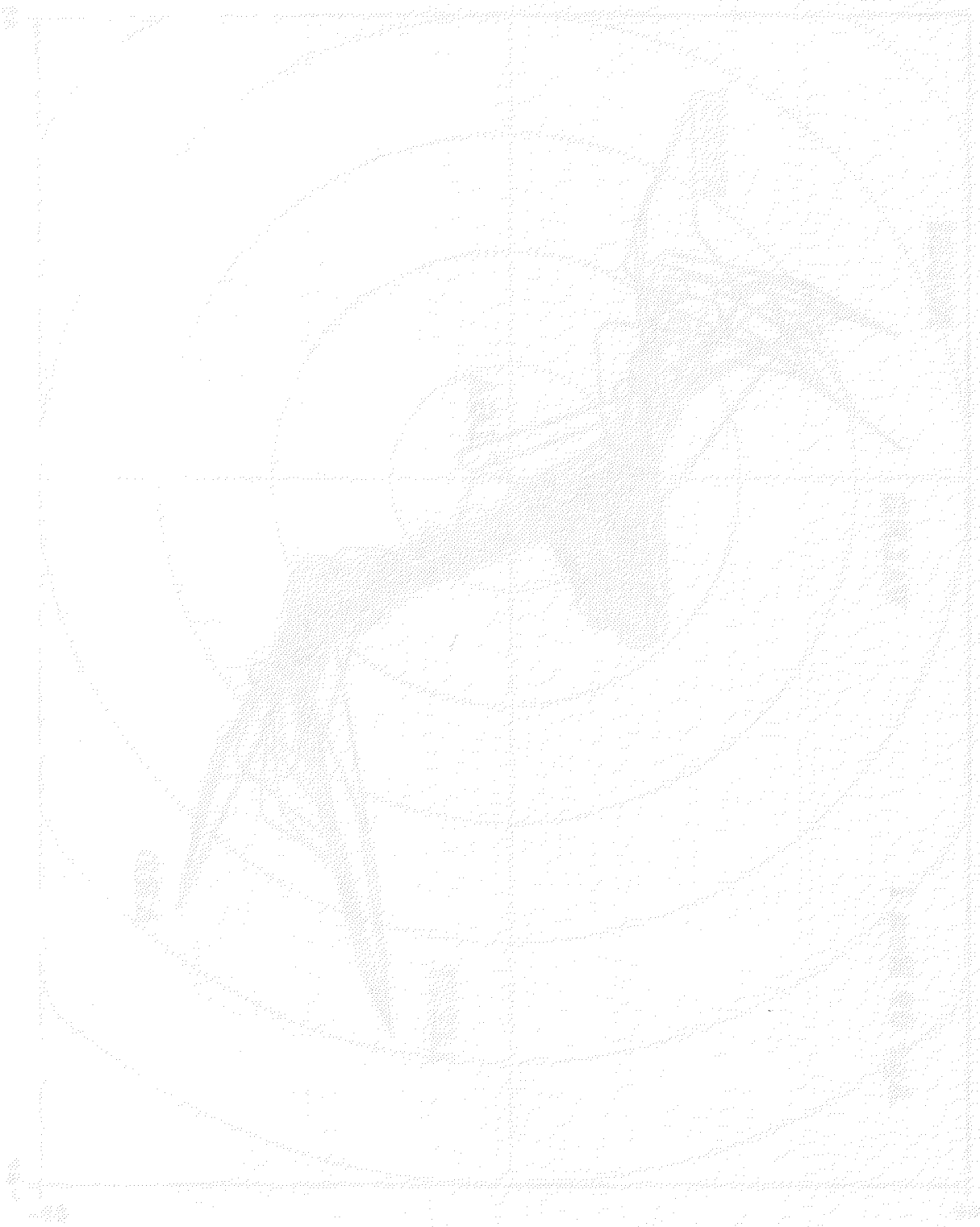

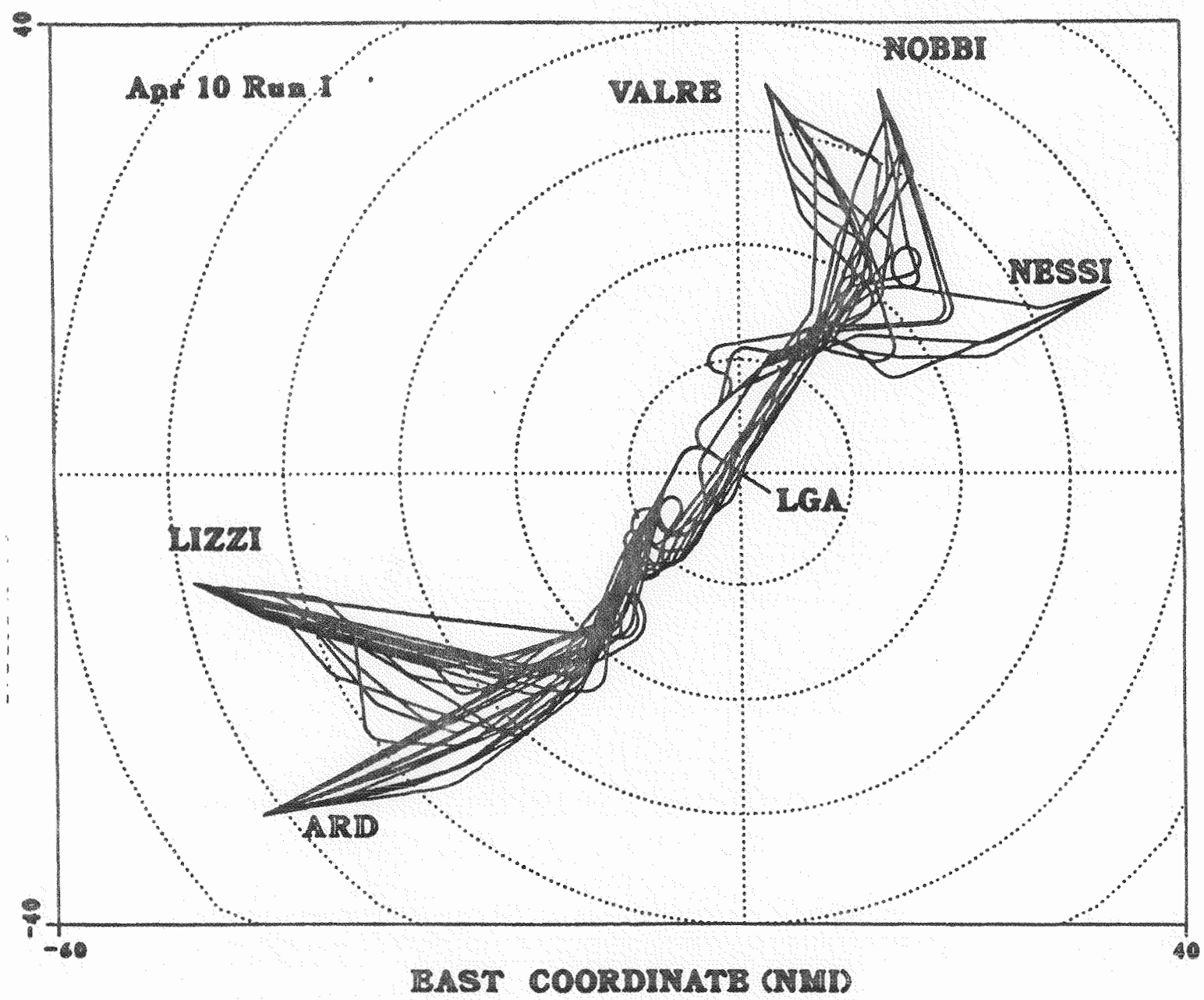
Apr 10 Run 1
NOBBI
VALRE
NESSI
LGA
LIZZI
ARD
40
-40
-60
40
EAST COORDINATE (NMI)

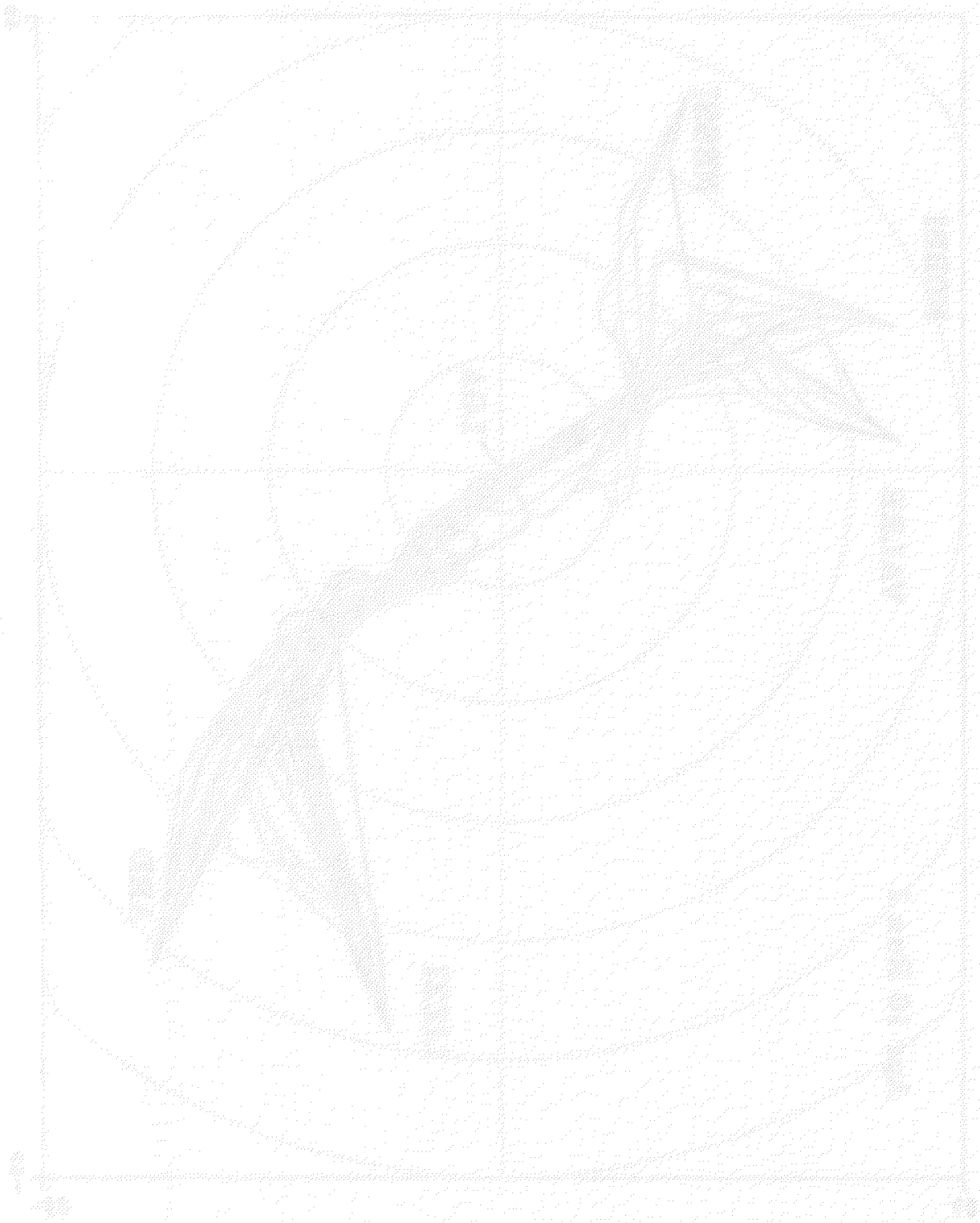

Assessment Of MLS Avionics Costs

Objective: Develop costing models for airlines and industry

- **Detailed Industry Survey**
- **Retrofit vs. New**
- **Acquisition, Installation, Maintenance**
- **Certification**

MLS Avionics Costs - Procurement And Installation

	Carrier Aircraft		General Aircraft		Commuter	Rotorcraft
	Boeing	McDonnell Douglas	Executive	Recreational		
Existing Aircraft	$ 124,900	$ 125,900	$ 112,600	$ 6,150	$ 124,900	$ 122,600
New Aircraft	$ 84,000	$ 63,300	$ 82,500	$ 6,150	$ 84,000	$ 57,800

Existing aircraft are retrofit to CAT I. New aircraft to CAT III. Costs are per aircraft include avionics procurement and installation, including wiring and antennas.

- 48 Types To Certify - $9.7M To $26M

Assessment Of MLS Alternatives

Objective: Review possible alternative precision approach systems

- ILS
- FMS/ILS
- GPS
- Synthetic Vision

ILS

- Findings
  - ILS Disturbed By Overflights
  - MLS Unaffected
  - MLS Smoother Than CAT I ILS
  - MLS Accuracy

FMS/ILS

- Flight Demo - Limited Capability
  - Minimum 3.9 Mile Final
- Issues
  - Minimum Final Straight Segment
  - Define And Follow Track
  - Protected Airspace
  - FMS Vertical Navigation To ILS Glide Slope Capture

Top-Level Evaluation Of GPS For Precision Approach

Evaluation Criteria

Accuracy

Degree Of Agreement Between Measured And True Position

Integrity

Ability Of System To Provide Timely Warning When Position Error Exceeds A Specified Limit

Protection Limit – Position Error Which Shall Not Be Exceeded Without Warning

Time-To-Alarm – Maximum Time Allowed Between Exceeding The Protection Limit And Receipt Of Warning By Users

Availability

Probability Of Obtaining A Specified Level Of Service At An Arbitrary Time And Location In The Service Area

"Specified Level Of Service" Typically Includes Both Accuracy And Integrity

Availability For Precision Approach

CONFIGURATION	PROBABILITY OF UNAVAILABILITY		
	Category I	Category II	Category III
Unehanced	1.3×10^{-1}	1	1
Augmented GPS constellation			
24 + 6 satellites	2.3×10^{-2}	1	1
24 + 12 satellites	3.3×10^{-3}	1	1
24 + 18 satellites	7.7×10^{-4}	1	1
24 + 24 satellites	2.3×10^{-4}	1	1
Two geostationary satellites	6.2×10^{-2}	1	1
Pseudolites			
One per runway	1.6×10^{-2}	1	1
Two per runway	7.3×10^{-4}	1	1
GPS/GLONASS	5.7×10^{-4}	1	1

- No Configuration Has Unavailability Within Factor-Of-10 Of Less-Stringent Requirement (2.0×10^{-5})

GPS Results

- Unenhanced GPS Will Not Satisfy CAT I, II, III Precision Approaches
  - Availability
  - Accuracy
  - Integrity
- Enhanced GPS Can Meet Near CAT I Precision Approaches
  - Differential Ground Stations
  - Datalink
  - Integrity Monitor
  - GPS Receiver - Carrier Phase Measurements
  - INS Integration With GPS
  - GPS And GLONASS Constellations - Combined Receiver
- GPS Will Not Satisfy CAT II, III Requirements

EVS Investigation Overview

Sensors

- Forward-Looking InfraRed (FLIR)
- MilliMeter Wave (MMW) Radar

Objective

- Assess Feasibility Of Current And Project Future State Of The Art (SOTA)

Methodology

- Review Current Technology And Trends (Personal Knowledge, Meetings With Government And Industry)
- Generate Simulated EVS Images For Several Altitude And Weather Conditions

Development Of DME/P Interrogators

Objective: Provide units for evaluation program

- Six Units - SEL
- Two Prototypes-Option 20
- Contract Awarded - Delivery Dec '91

MLS Avionics Certification

Objective: Assure certification of airborne equipment

- Upgrade FAA Aircraft - King Air 200 To CAT II With Curved Approach Capability
- MD - 11 Preliminary MLS Certification Data
  - Certification In Fall '91 - Customer Interest
- B - 747 Certified For CAT III
- Midway Airlines DC-9
- MLS/GPS Receiver

MLS User Financial Analysis

A Well Defined Scope Was Essential In Structuring The Analysis Methodology. This Analysis Was Limited To The Following:

- 54 "Select" Airports With Basic Extrapolation To The NAS
- Two User Groups: Air Carrier And Commuter/Air Taxi/Executive
- FAA Forecasts, Data, And Models Provided Primary Data Input. Airport And Related Outside Study Information Were Used Where Appropriate
- The Current ILS Plus Planned Growth Was Baseline For Comparison

MLS User Financial Analysis (Cont'd)

Primary Cost Assumptions Include:

- Congress Will Appropriate The Necessary Funds
- The ICAO Standard For ILS Receiver Upgrade Will Be Met By 1998
- Fleet Size For Analytical Purposes Is 9000 Aircraft
- Fleet Growth Is Expected To Be Approximately 2 Percent Per Year
- Average Aircraft Life Is 25 Years And 4 Percent Is Retired Each Year
- Stage 2/3 Noise Issue Is Independent Of This Analysis

MLS User Financial Analysis (Cont'd)

User Costs . . .

The Real Cost To The Users For MLS Avionics Is Calculated By Taking The Difference Between The Expected Costs Required To Continue With ILS And The Anticipated Cost To Equip With MLS

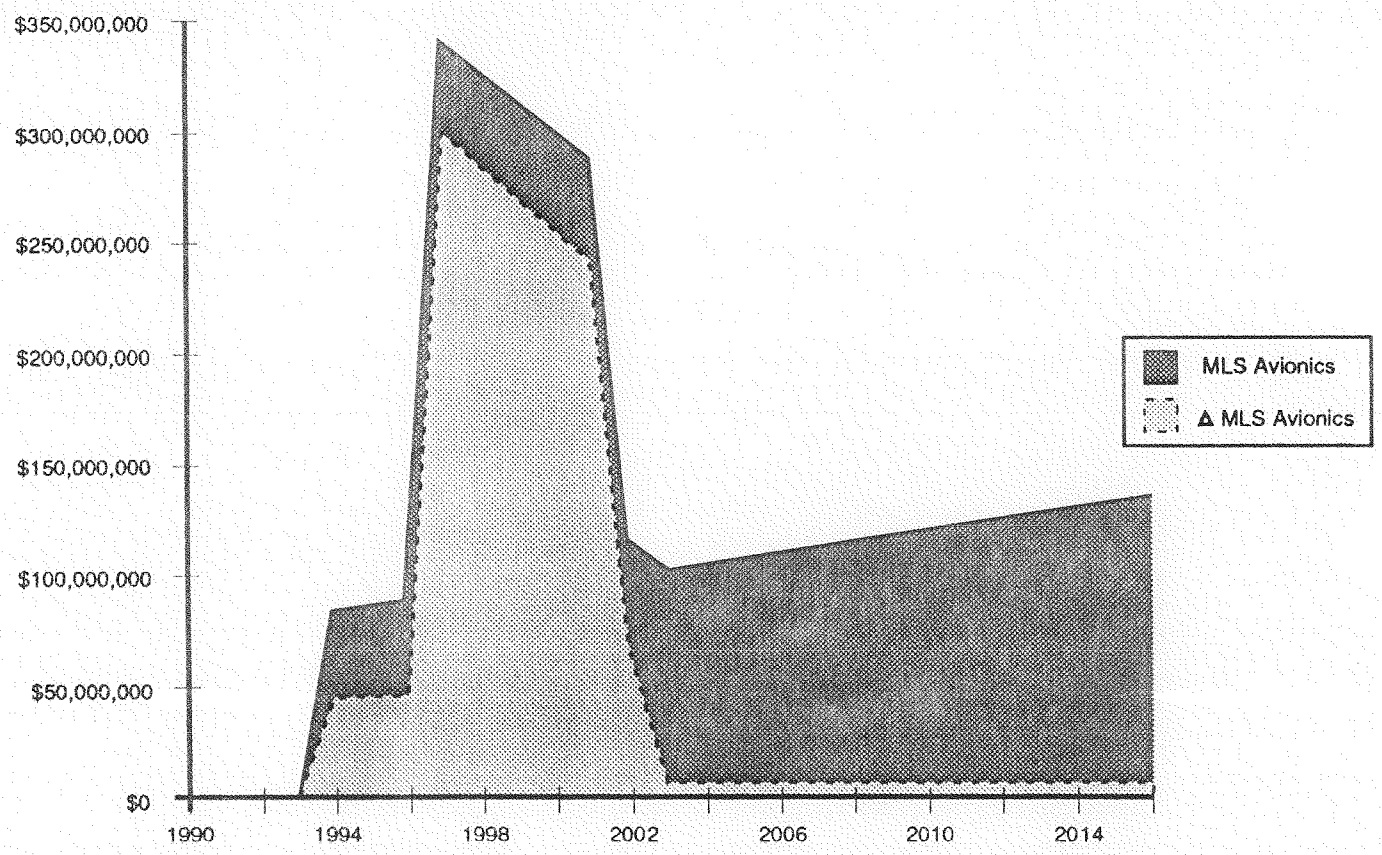

MLS User Financial Analysis (Cont'd)

User Benefits . . .

Total MLS User Benefits Average Approximately 300 Million Per Year Once The Transition Is Completed

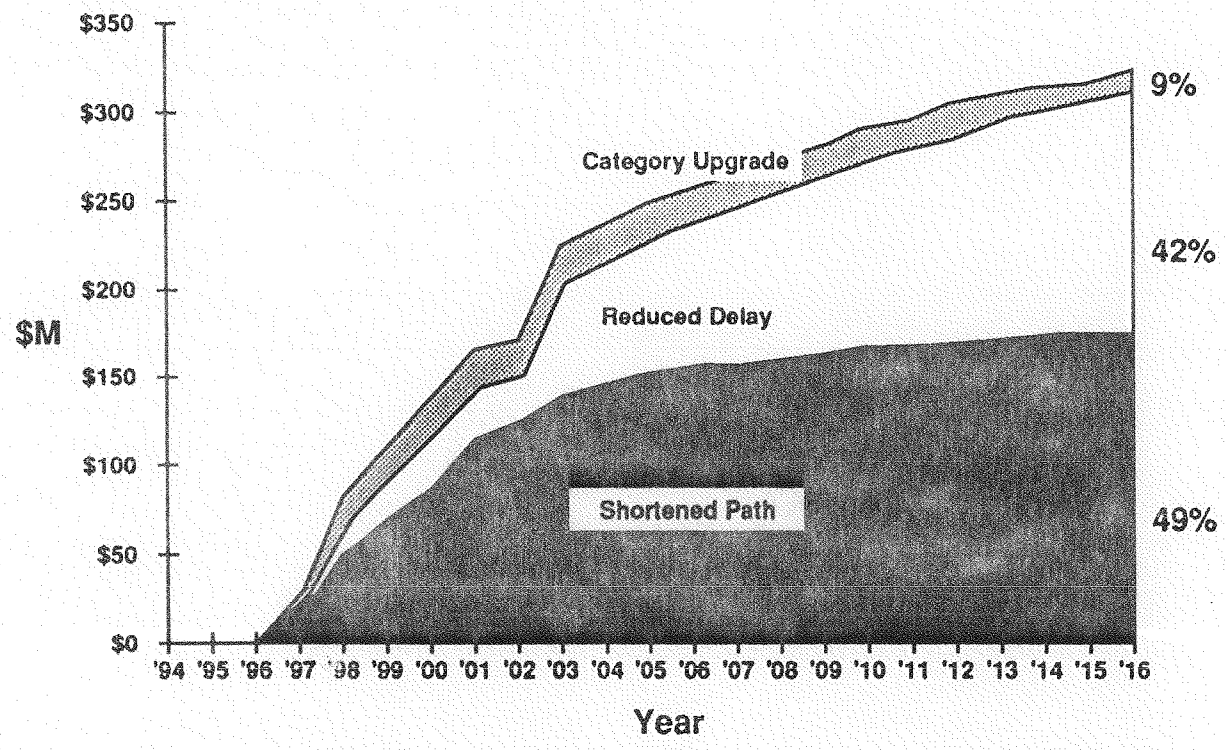

MLS User Financial Analysis (Cont'd)

The Financial Analysis Of MLS At 54 Airports Was Roughly Extrapolated To The Entire NAS. These Results Show:

For The Sample Of 54 Airports:

Cost: 1.7B Benefits 4.6B

For The National Airspace System:

Cost: 1.7B Benefits 5.8B

Note: Projected Over 20 Years

MLS User Financial Analysis (Cont'd)

...While The Second Demonstrates The Impact Of DME/P Interrogator Costs On The Overall Financial Results

Case 1: DME/P Interrogator Cost Is Reduced To $18,000 Per Unit (~ 50%). Assumes That ILS Base Case Will Equip With DME/P Beginning 1994 As Well

Cost: 1.2B Benefits 4.6B

Case 2: DME/P Is Not Needed For The Future Precision Approach Using MLS

Cost: 877M Benefits 4.6B

Note: Projected Over 20 Years

Other Projects/Activities

International Activities

- Canada
  - Approval To Purchase 147 Systems
  - 42 Systems - Micronav
- MLS Tests
  - United Kingdom - B-757, Cardiff/Heathrow And B-767 Certification
  - France - Charles De Gaulle
  - Spain - Ground Systems Tests

36

International Activities

- Canada
  - Approval To Purchase 147 Systems
  - 42 Systems - Miscoray
- MLS Tests
- United Kingdom - B-737, Cardiff/Heathrow and B-757 Certification
- France - Orly Charles De Gaulle
- Spain - Ground System Tests

International Activities (Cont'd)

- MLS Tests
  - Norway - Ground System Tests
  - Netherlands - Schiphol Airport
  - Australia - Ground System Tests
  - China - 2 Systems
- Taiwan - 2 MLS
- USSR

DOD Activities

- DOD Precision Landing Standard For Year 2000
- Contract With CMC To Design And Produce 1078 Receivers
- Development Contract Dec '89 - Production Contract in '93 For 8700 Dual MLS/ILS Receivers
- Bell Contract For Up To 132 Tactical Ground Systems
- 405 Fixed - Base Systems Through The FAA

DOD Activities

MLS Acquisition Schedule

- Two Systems Contract Award - Apr '90
- 2 - 26 Systems - Contract Award - Jun '91
- Category II/III Prototypes
  - 2 Contractors - Separate Designs
  - 6 - 12 Systems Per Contractor Production Contract - Same Contractors Award Early '95 - First Delivery Late '96

MLS Program Schedule

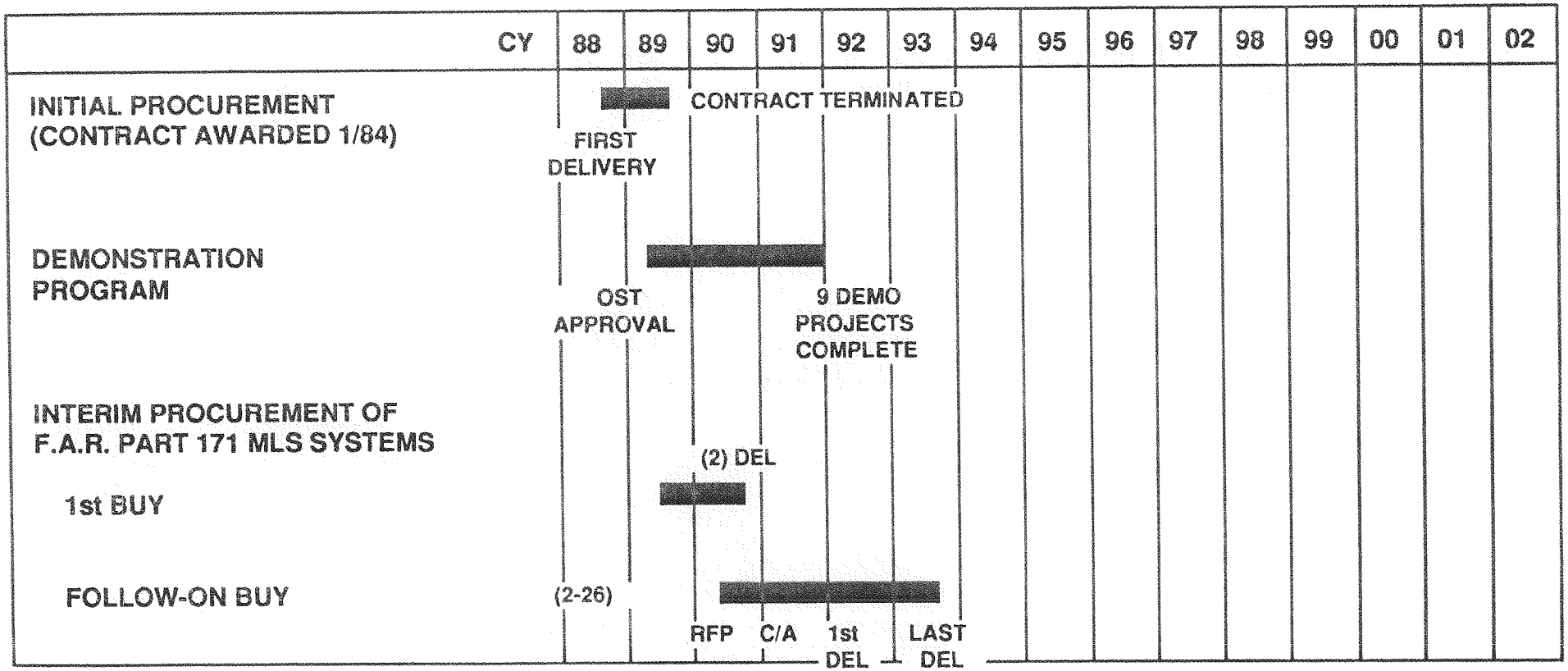

Microsoft Corporation

MLS Program Schedule (Cont'd)

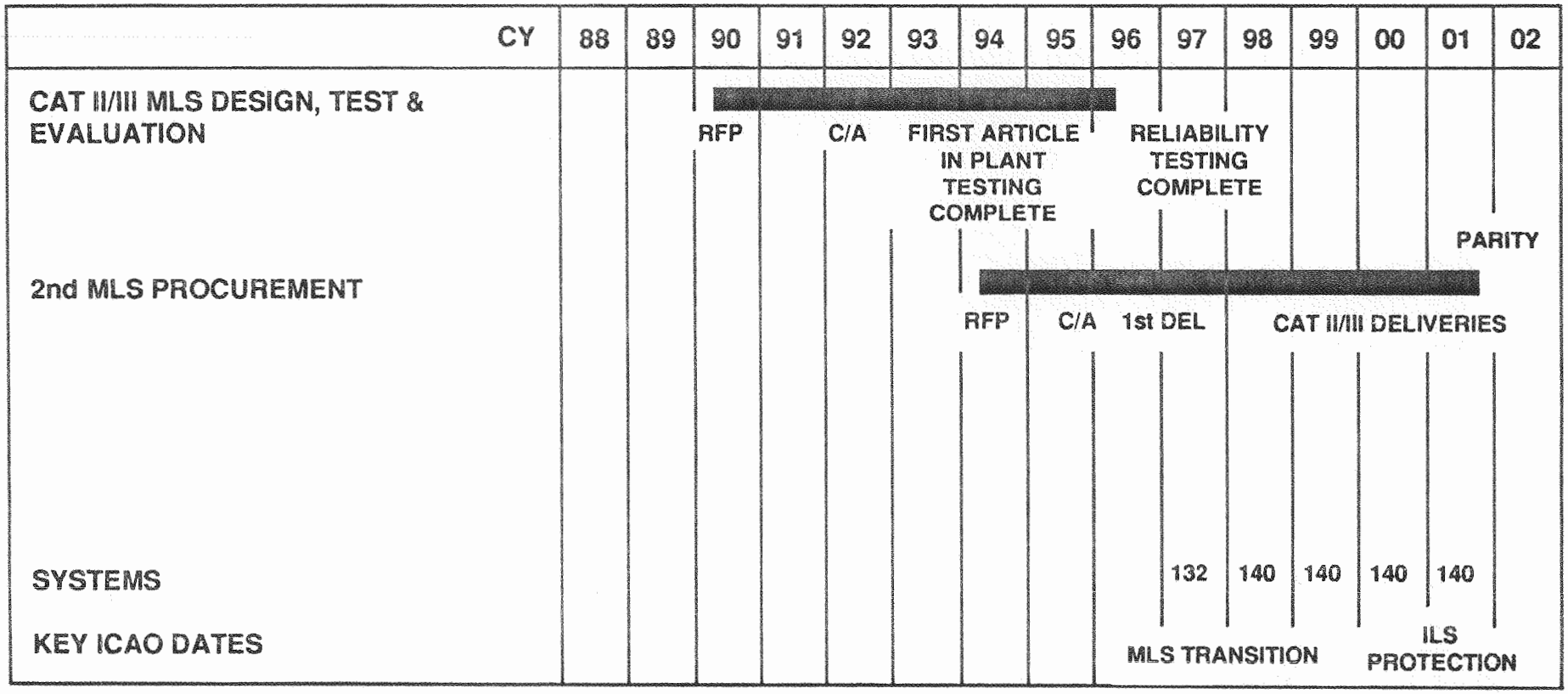

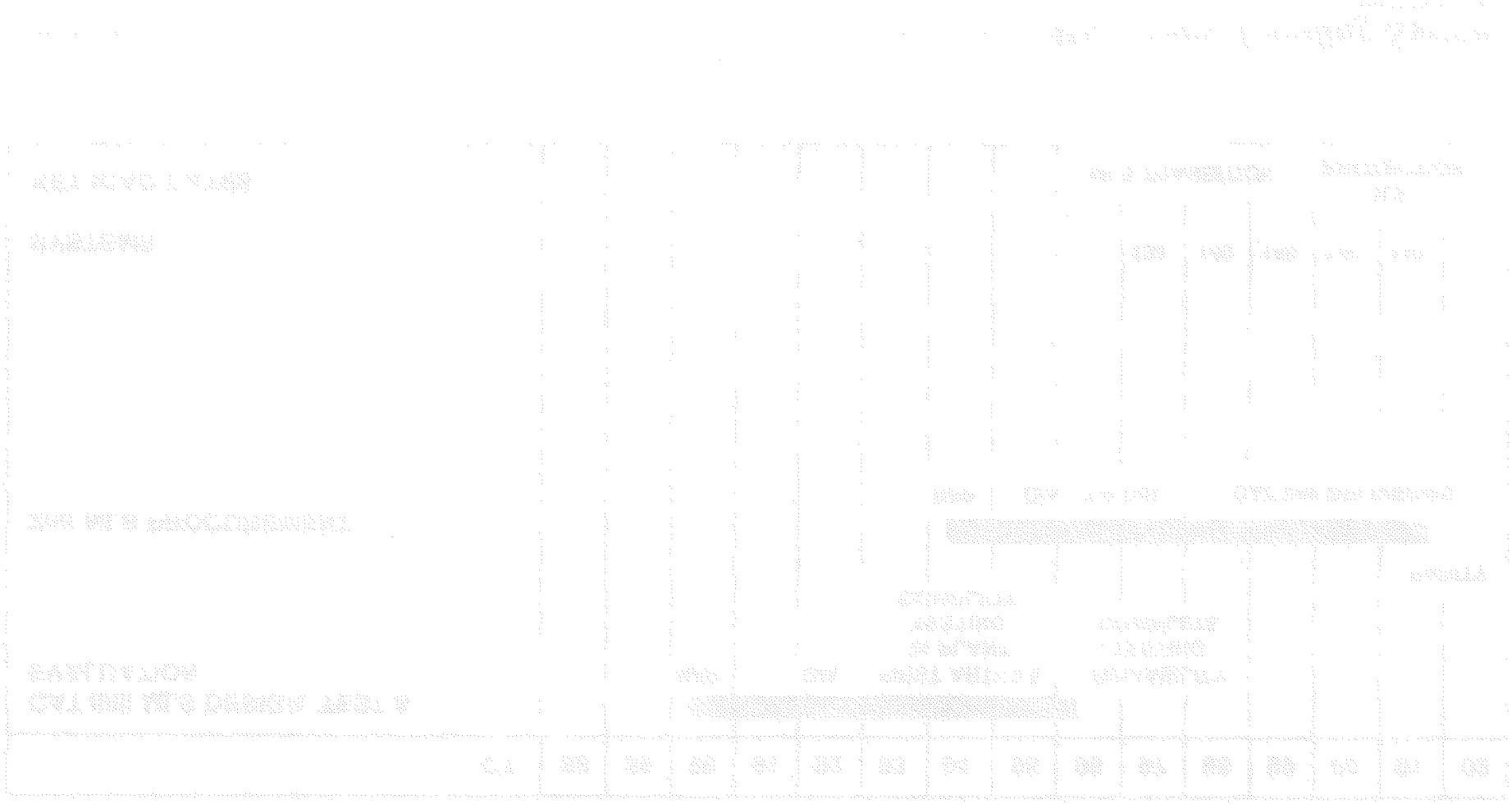

GERRY HEADLEY
USAF

MILITARY MLS PROGRAM

TECHNICAL CENTER/DOD

JOINT MLS PROJECTS

DOD MLS PROJECTS

* CMLSA RECEIVER

* MULTI-MODE RECEIVER

* MOBILE MLS

* MMLSA

CMLSA RECEIVER

* DT&E AT TECHNICAL CENTER

* OT&E AT TECHNICAL CENTER AND OTHER SITES

* ADDITIONAL FLIGHTS REQUIRED

- YOUNGSTOWN LIAGAY MACHINE

- OAKS VS ARLINGTON CRAIG TWO OAKS KILLS

- WEST VS ARLINGTON CARLEN

GREGY BELLEAND

MULTI-MODE RECEIVER

* ILS, MLS, CARRIER LANDING

* NAVY AT TECHNICAL CENTER

  - CH-53
  - F18

MOBILE MLS

* MILITARY TACTICAL MLS

* 750 LBS.

* TESTING AT BELL IN APRIL

* TECHNICAL CENTER TESTS START IN MAY

MMLSA

* ILS/MLS RECEIVER

* THREE MANUFACTURERS

* ALL TESTING AT TECHNICAL CENTER

DAVE HUNTINGTON
ALLIED-SIGNAL/BENDIX CORPORATION

BENDIX MLS PROGRAM

MLS MATHEMATICAL MODEL USERS GROUP MEETING

FAA TECHNICAL CENTER, ATLANTIC CITY

NOVEMBER 6,7 1991

BENDIX COMMUNICATIONS DIVISION

1) MLS CAT I OVERVIEW

2) MATH MODELING FOR MLS CAT I SITE ENGINEERING

3) MLS CAT I SITE LOCATIONS

4) PRELIMINARY SIMULATIONS OF RUNWAY HUMP SHADOWING

5) SYSTEMS ANALYSIS TO INCLUDE EFFECTS OF RUNWAY HUMPS, SHADOWING, UNWANTED REFLECTIONS

6) MLS AIRCRAFT ANTENNA PERFORMANCE USING GTD ANALYSIS

GA/1-2695

FAR 171 MLS ACCELERATED SCHEDULE

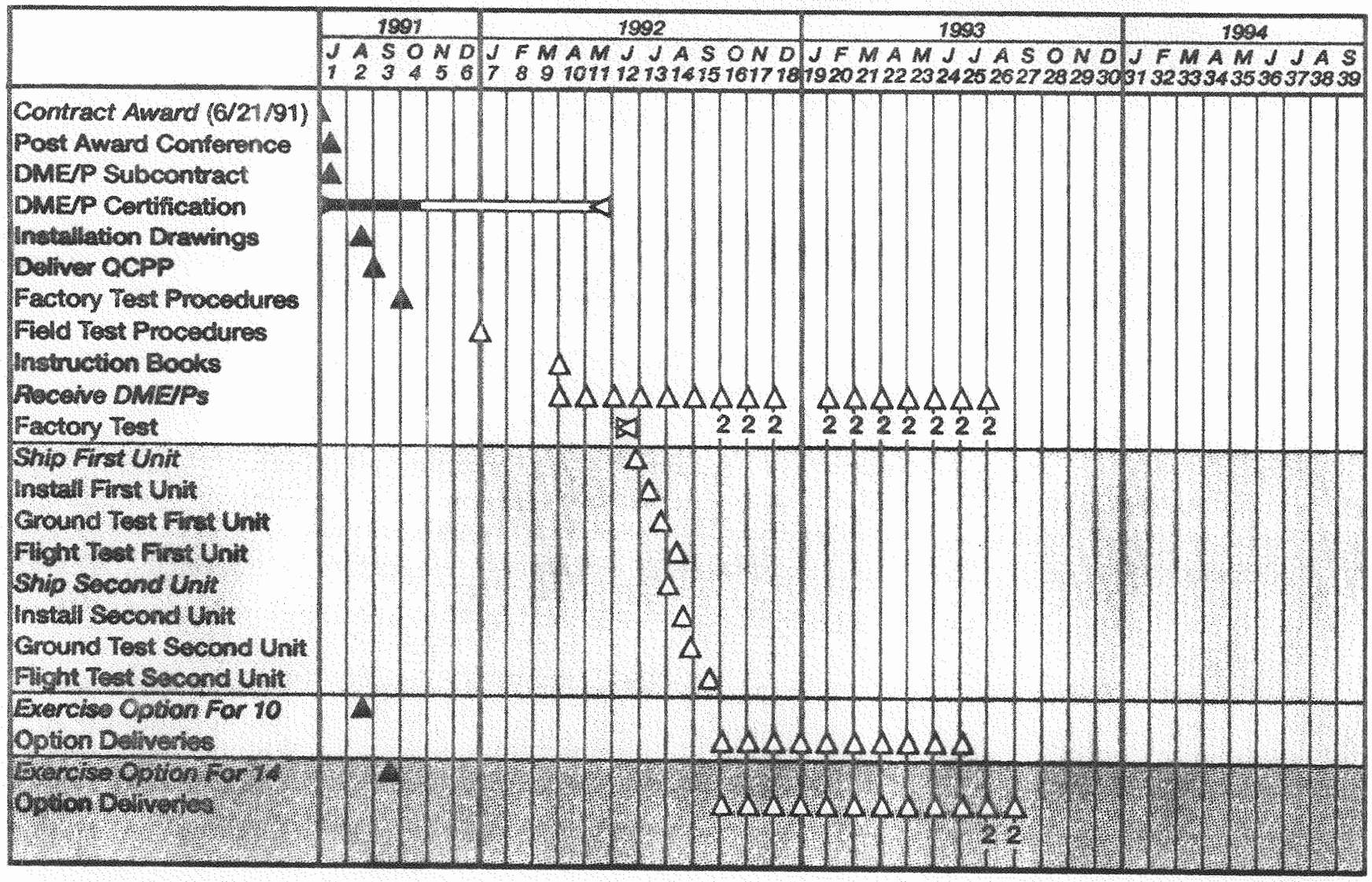

Allied-Signal Aerospace Company

Bendix Communications Division

Allied Signal

GA/1-3120

MLS CATEGORY I GROUND SYSTEMS

CUSTOMER: FAA *CONTRACT NUMBER: DTFA01-91-C00021*

- MANUFACTURE, DELIVER, INSTALL 26 GROUND SYSTEMS
  - 2° AZIMUTH STATION (±40° COVERAGE)
  - 1.5° ELEVATION STATION
  - PRECISION DISTANCE MEASURING EQUIPMENT (DME/P)
  - REMOTE CONTROL AND STATUS UNIT (RCSU)

- MAINTENANCE SUPPORT EQUIPMENT/SERVICES
  - SPARES KIT AT EACH SITE
  - STANDARD TEST EQUIPMENT AT EACH SITE
  - PORTABLE MLS RECEIVER AT EACH SITE
  - OPERATOR AND MAINTENANCE TRAINING
  - CONTRACTOR REPAIR SERVICE (CRS)
  - ENGINEERING SUPPORT SERVICES

- DELIVERABLE DATA ITEMS
  - INSTALLATION/SITE PREPARATION PLANS
  - FACTORY ACCEPTANCE TEST PROCEDURES
  - FIELD ACCEPTANCE TEST PROCEDURES
  - QUALITY CONTROL PROGRAM PLAN

GOVERNMENT RESPONSIBILITIES

- LIST OF SITES FOR INSTALLATION
- FACILITIES, INCLUDING CONCRETE FOUNDATIONS, CABLING, RCSU SPACE
- LAND ACQUISITION FOR ESTABLISHMENT OF THE FACILITY
- TRANSMISSION FREQUENCIES AND IDENTIFICATION CODES
- LOCATION OF RCSU EQUIPMENT INSTALLATION
- AIRPORT DRAWING PACKAGE, INCLUDING EXISTING SITE DRAWINGS, EQUIPMENT ROOM LAYOUTS
- GOVERNMENT COMMISSIONING FLIGHT INSPECTION

- ENVIRONMENTAL CONSIDERATIONS FROM: WINDSOR
  LANDMARKS' SOTHEBY'S ROOM PROFILE
- WINDOW DAMAGE WORKS' MOTIONS EXISTING SALE
- LOCATION OF MORE ENVIRONMENTAL INSTITUTION
- LANDMARKS' AUTOMOBILES AND DEMOLITION CODES
- FIND VOCATION FOR ENVIRONMENTAL OF THE WORTH
  CURTAIN' WORK SHOP
- FACTORS' MOTIONS CONCRETE KOMMANDANTE
- FIRE OF BUSS FOR INSTITUTION

GOVERNMENT RESPONSIBILITIES

SUBCONTRACTS

STANDARD ELEKTRIK LORENZ (SEL)

- MANUFACTURE DME/P
- PROVIDE ENGINEERING SUPPORT
- INITIALLY, PROVIDE CRS FOR DME/P
- SUPPORT FAR 171 APPROVAL PROCESS

BENDIX FIELD ENGINEERING CORP

- OPERATOR TRAINING
- MAINTENANCE TRAINING
- INSTALLATION SUPPORT

MATH MODELING FOR MLS CAT I SITE ENGINEERING

* **PRESENT CONTRACT WITH FAA FOR 26 CAT I SYSTEMS**
    - 26 Deliverable Systems (FAA FAR-171 Approved)
    - Each deliverable system includes:
        - 2.0 deg AZ antenna
        - 1.5 deg EL antenna
        - DME/P
        - Generic Installation Drawing Package
            - Footprints
            - Installation
            - Field monitor location limits
            - Signal and power cable interfaces
    - Delivery starts June 1992
        - Delivery rate 1 per month for 26 months

* **PRESENT CONTRACT WITH JIL THRU FAA FOR SITE ENGINEERING**
    - On-Site engineering at all 26 locations per FAA requirements
    - Task will influence flight procedures per user requirements
    - Generic installation drawing package adapted for specific location
    - Math Modeling may be required at some locations
        - Humped runways
        - Collocation with existing facilities
            - Localizers
            - Glide slopes
            - Approach lights
            - ADF
            - ADF
            - AWOS
            - Weather stations
            - Existing and future buildings
        - Aircraft blockage and shadowing

MLS CAT I SITE LOCATIONS

SITE	LOCATION	* POSSIBLE MATH MODELING
1	Seattle WA (SEA)	TB, SB, BR, AR
2	Pullman-Moscow WA (PUW)	
3	Portland OR (POX)	
4	Dutch Harbor AK (DUT)	
5	San Francisco CA (SFO)	ST, TB
6	Philadelphia PA (PHL)	
7	Eagle CO (EGE)	
8	Laconia NH (LAC)	
9	Flagstaff AZ (FLG)	
10	Lebanon NH (LEB)	
11	Steamboat Springs CO (SBS)	
12	Mieggs Field IL (CGR)	BR
13	Dallas-FT.Worth TX (DFW)	BR
14	Midway Airport IL (MDW)	
15	Wash National Wash DC (DCA)	
16	Laguardia Airport NY (LGA)	
17	Fayetteville AR (FYV)	
18	Buffalo NY (BUF)	
19	Omaha NE (OMA)	
20	Roanoke VA (ROA)	HR
21	NY Wall Street Heliport (NWS)	BR
22	FT. Smith AR (FSM)	
23	San Jose CA (SJC)	
24	Oakland CA (OAK)	
25	Taiwan	
26	Taiwan	

Other Airpots being considered:

	Bethal AK	HR
	Dillingham AK	HR
	St. Mary's AK	ST
	Unalakheat AK	

* Legend

HR humped runway
ST sloped terrain
TB terrain blockage
SB shadowing by buildings
BR building reflections
AR aircraft reflections

PRELIMINARY SIMULATIONS OF RUNWAY HUMP SHADOWING

AIRPORT RUNWAY TERRAIN WITH HUMP

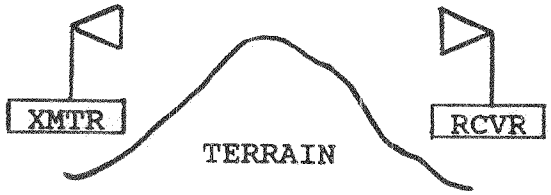

MODELS FOR HUMP IN TERRAIN

1) KNIFE EDGE

- o Straight forward computation
- o Crude model
- o Results questionable

2) CYLINDER

- o GTD computation *
- o Computational difficulties in shadow region and at small grazing angles

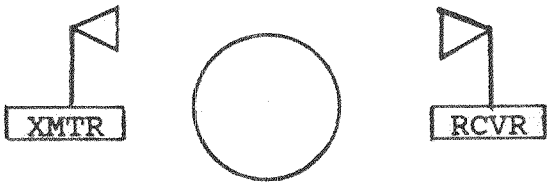

3) PLATES

- o GTD computation *
- o Computational difficulties in shadow region and at small grazing angles

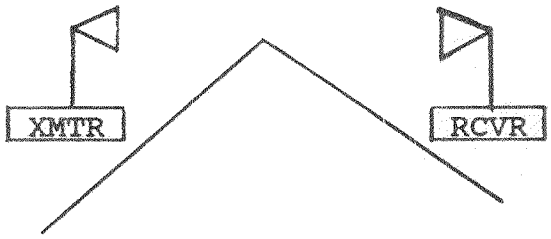

4) CYLINDER AND PLATES

- o GTD computation *
- o Computational difficulties in shadow region and at small grazing angles

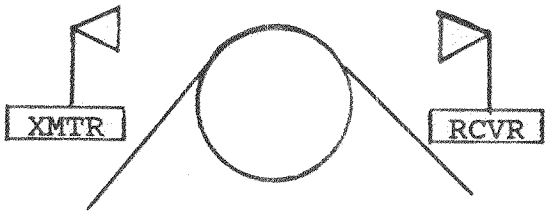

* Ohio State University GTD Basic Scattering Code

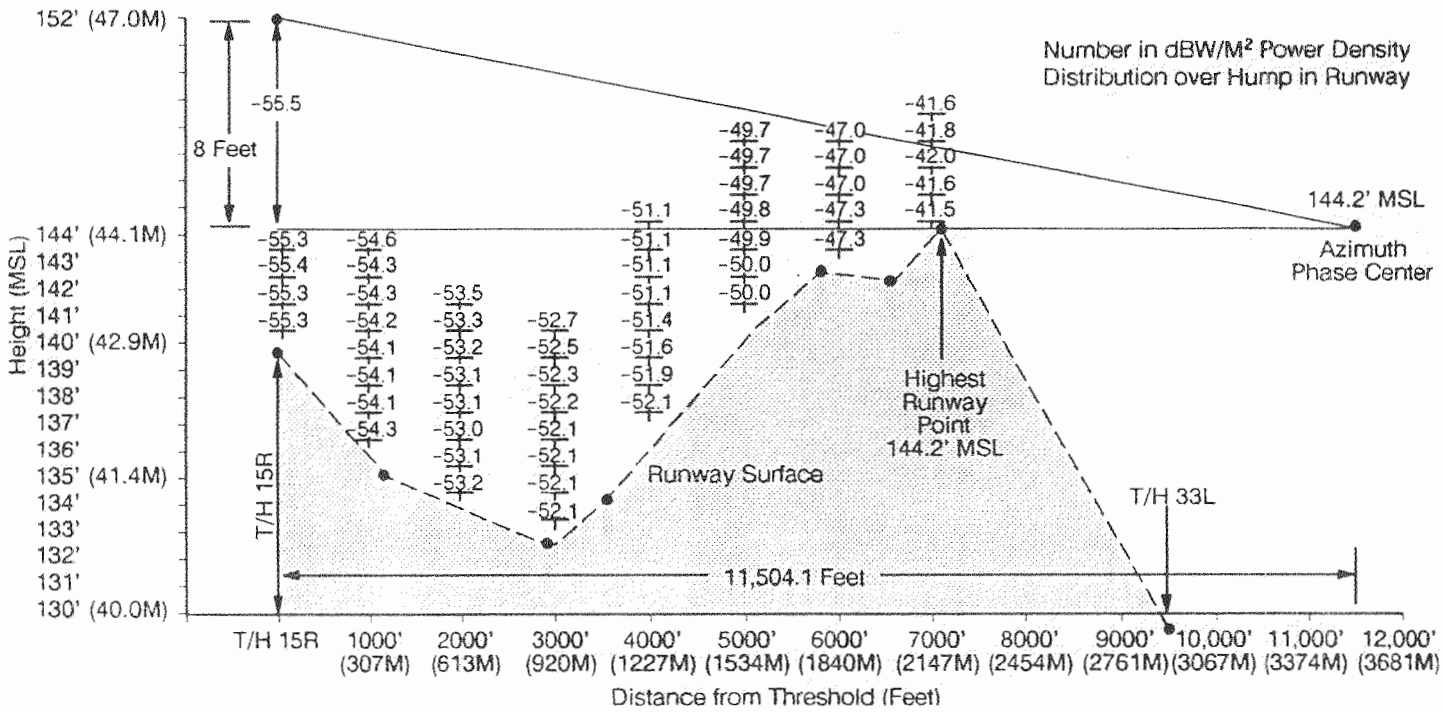

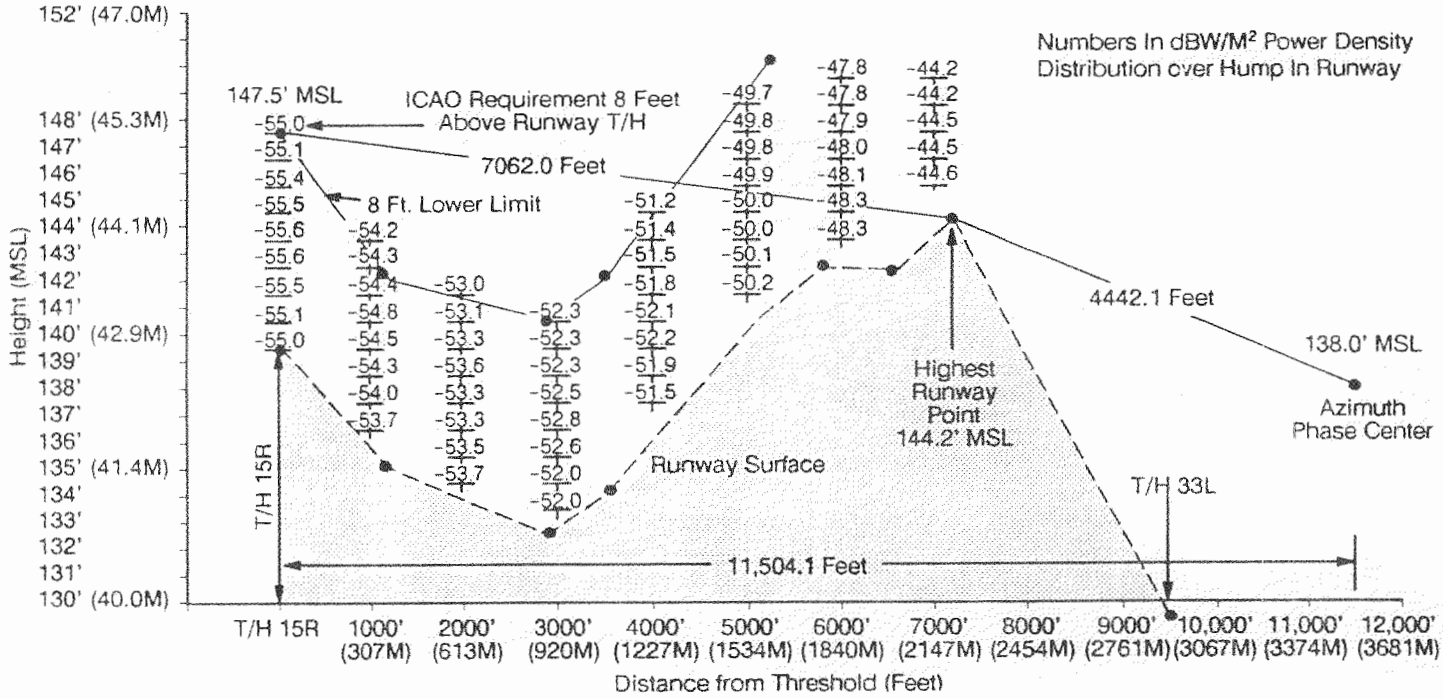

MLS AZIMUTH ANTENNA
POWER DENSITY ANALYSIS ON RUNWAY WITH HUMP

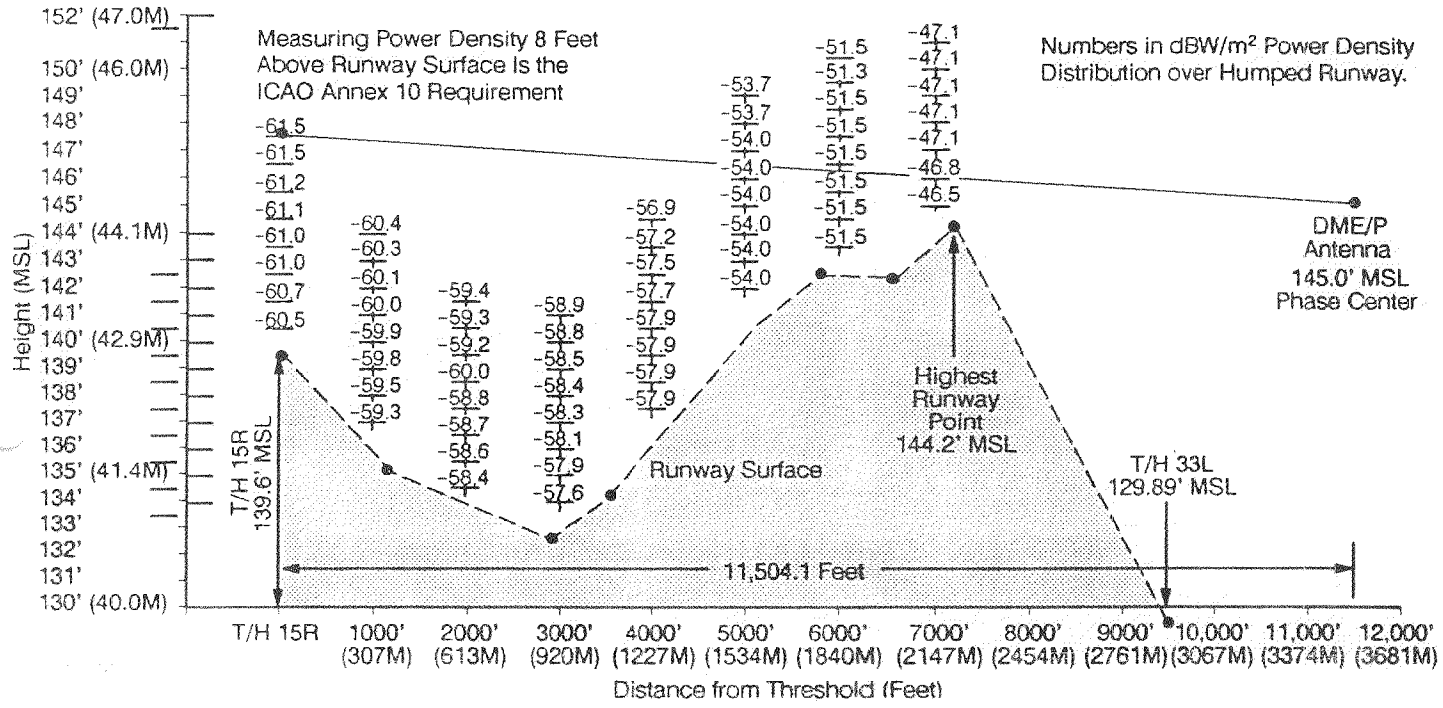

MLS DME/P ANTENNA
POWER DENSITY ANALYSIS ON RUNWAY WITH HUMP

MLS AIRCRAFT ANTENNA PERFORMANCE USING GTD ANALYSIS

- GTD analysis is used to determine optimum aircraft antenna locations to assure required MLS performance

- Computed GTD aircraft antenna pattern used to determine if the resulting RF signal at the MLS receiver is within the system power budget

- GTD technique verified at FAATC (Hanger 301) in 1978
  - Measured and GTD computed antenna patterns were compared for a North American Rockwell T-39

- Supplemental Type Certification (STC) approved using GTD
  - Location of MLS aircraft antennas using GTD is approved without flight testing

- GTD code utilized is the Ohio State University Airborne Antenna Radiation Pattern Code

- Aircraft Modeled
  - Boeing 737
  - Boeing 727
  - Boeing 707
  - EC-135
  - C-141
  - North American Rockwell T-39
  - Cessna Citation II
  - Cessna Citation III
  - Cessna 421
  - Cessna 441
  - Beech 200
  - Gulfstream GIII
  - Rockwell Saberliner
  - Piper Cheyenne
  - DeHavilland Dash 7
  - Embraer EMB-120
  - Aerospatiale ATR-42
  - Dassault Falcon 900
  - Mitsubishi Diamond II

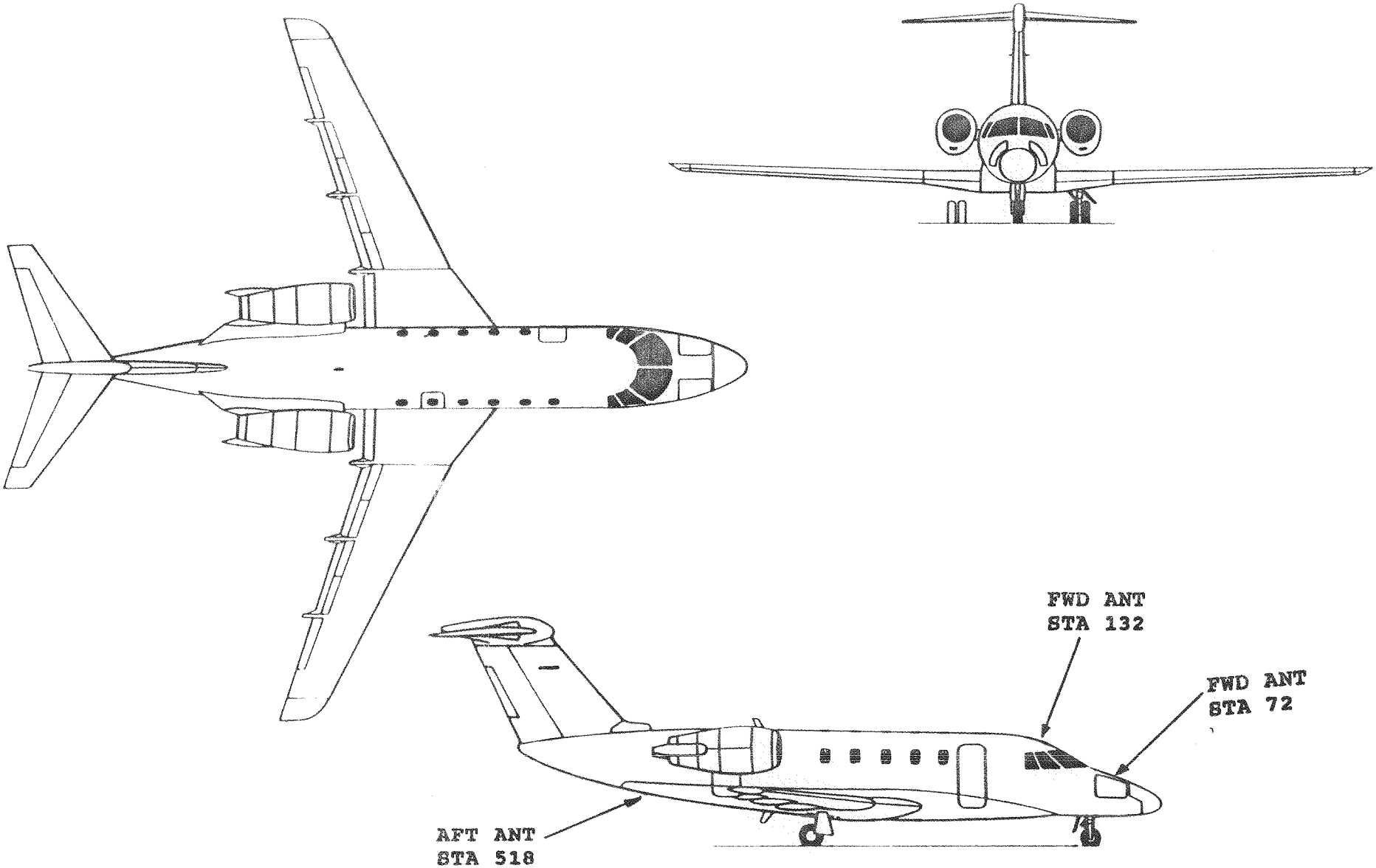

CESSNA CITATION III
MLS ANTENNA INSTALATION

TAIL

AFT ANT
STA 518

FWD ANT
STA 132

FWD ANT
STA 72

NOSE

PITCH

YAW

ROLL

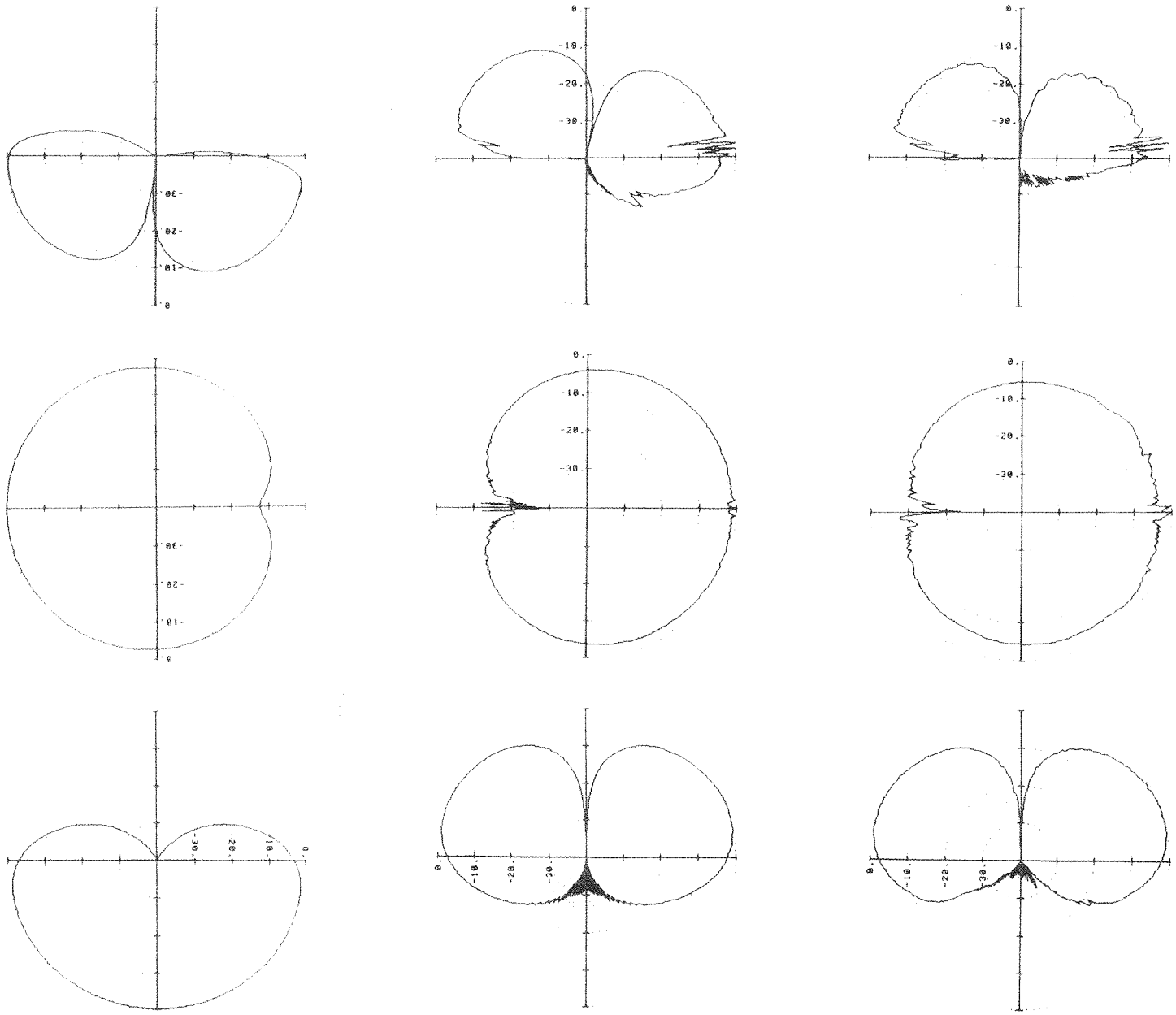

CESSNA CITATION III
GTD COMPUTED MLS ANTENNA PATTERNS

KENT CHAMBERLIN
UNIVERSITY OF NEW HAMPSHIRE

RUNWAY HUMP MODELING

Runway Hump Modeling at the University of New Hampshire

Dr. Kent Chamberlin

Today's Topics

- Overview of the GELTI Propagation Model
- The ATLM
- Model Validation Efforts to Date

[illegible]

- ITD - simulated Loss Due to Terrain Obstruction

- Considers Multiple Propagation Mechanisms
  - Up to 16 Rays and Ray Combinations

- Accounts for finite conductivity and local surface roughness

- Includes Adjacent Edge Diffraction Effects

Ray Types Considered in ITD

1. [illegible]
2. [illegible]
3. [illegible]
4. [illegible]
5. [illegible]
6. [illegible]
7. [illegible]
8. [illegible]
9. [illegible]
10. [illegible]
11. [illegible]
12. [illegible]
13. [illegible]
14. [illegible]
15. [illegible]
16. [illegible]

Verification of Propagation Models (Adjacent-Edge Diffraction)

Impetus: Divergence in measured and modeled data near ground plane for Denver path involving adjacent-edge diffraction

Approach: Implement a theoretically-correct numerical solution based upon Huygen's Principle

Adjacent-Edge Diffraction

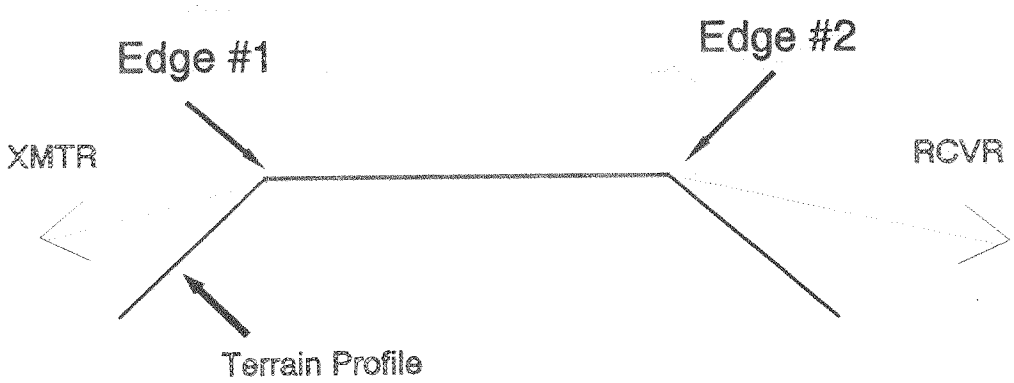

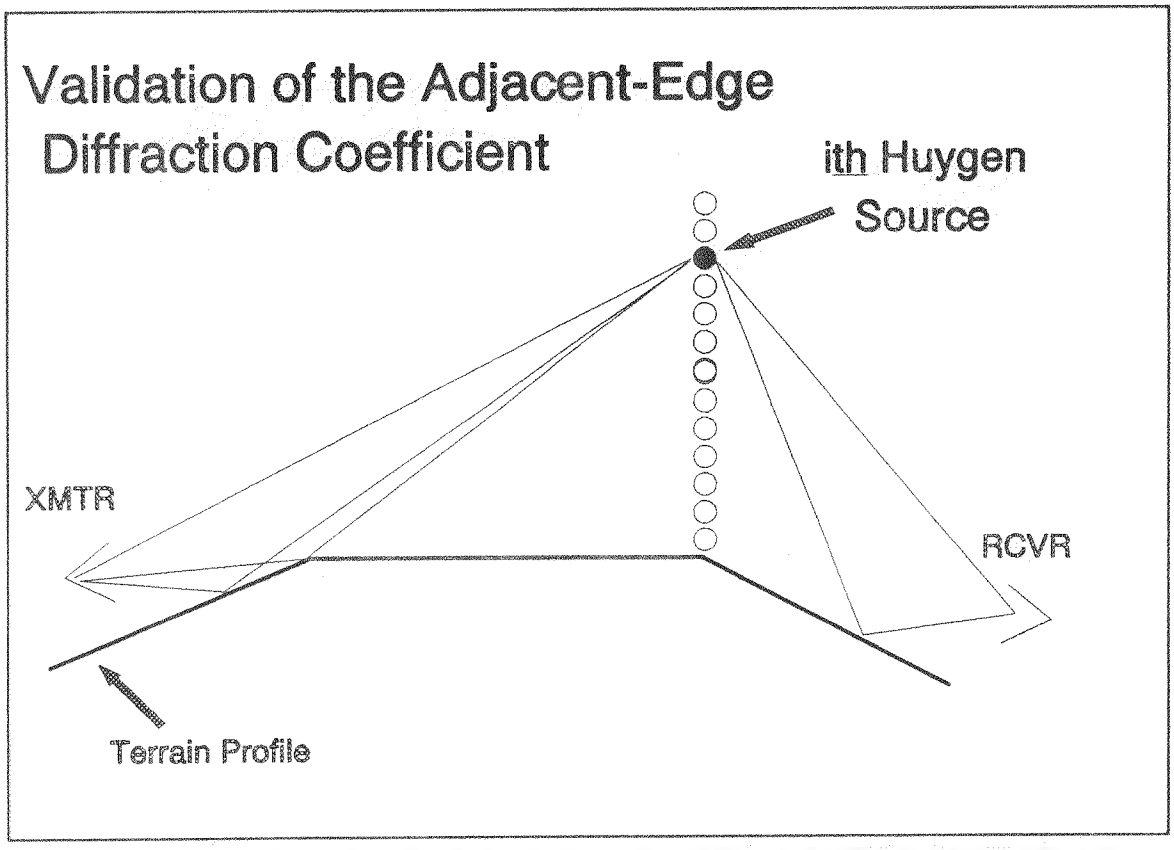
Validation of the Adjacent-Edge
Diffraction Coefficient
ith Huygen
Source
XMTR
RCVR
Terrain Profile

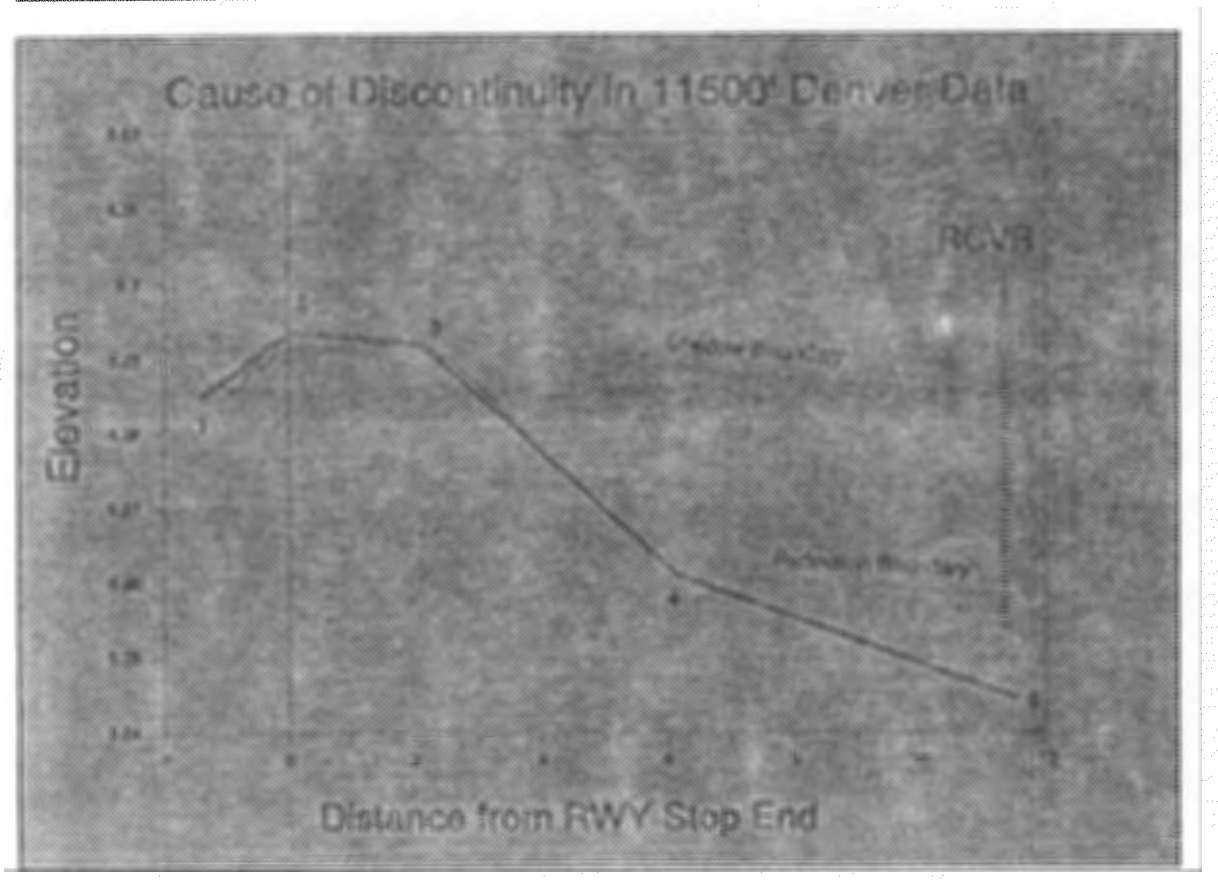
Cause of Discontinuity In 11500' Denver Data
RCVR
Elevation
Distance from RWY Stop End

Chris Penney "Validation of the Diffraction Coefficient for Finitely Conducting, Locally Rough Surfaces"

David Miller "A Hybrid Electromagnetic Propagation Model for Calculating Adjacent-Edge Diffraction"

The Automated Terrain Linearization Model

- Converts raw terrain data into GELTI input file
  Consistent GELTI results from user to user

- Provides graphical display of data
  Aids in error checking of input data and model operation

- Requires little expertise on the part of the user
  GELTI output is now user independent

Terrain Data Requirements

- Terrain elevation as a function of distance along the runway centerline
- Must have sufficient number of points to represent predominant terrain features
- Accuracy should be within ±6 inches in elevation

Yuma, Arizona

- Measurements taken at 2 receiver locations

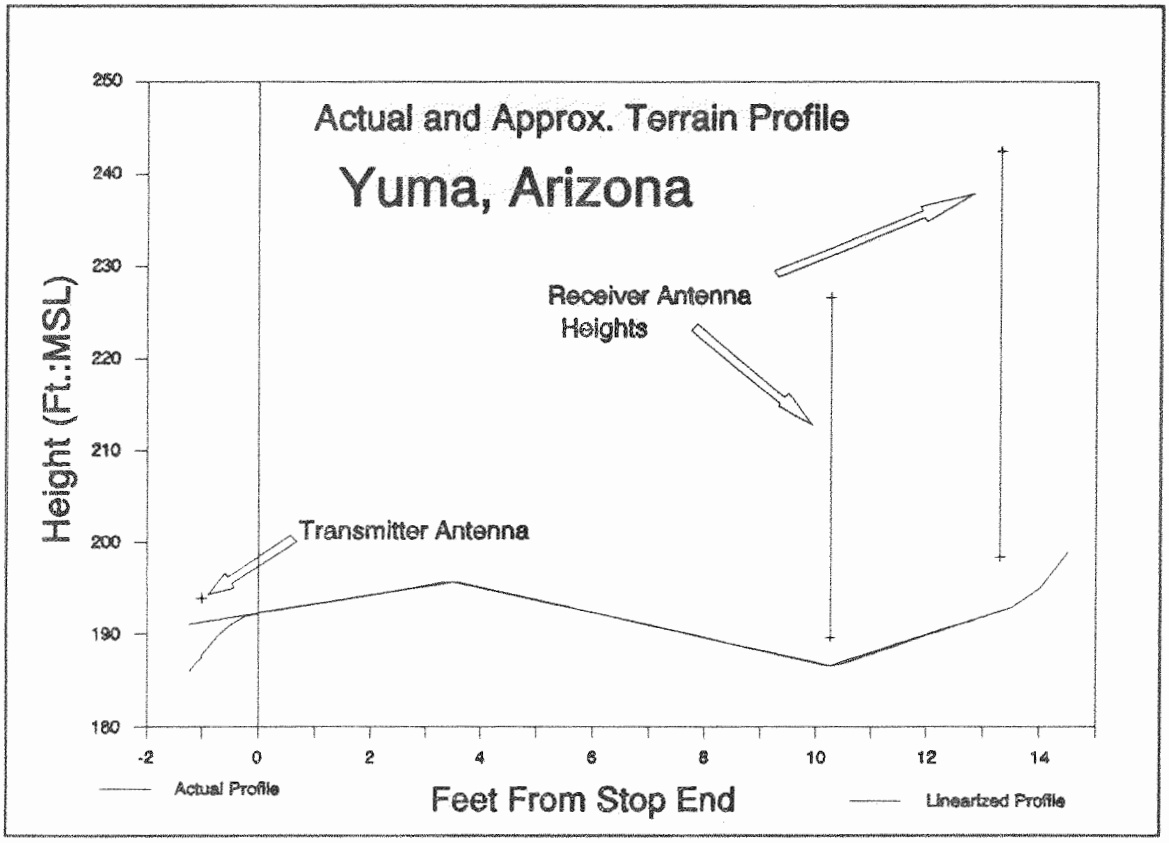
Actual and Approx. Terrain Profile
Yuma, Arizona
Receiver Antenna Heights
Transmitter Antenna
Height (Ft.:MSL)
250
240
230
220
210
200
190
180
-2
0
2
4
6
8
10
12
14
Actual Profile
Feet From Stop End
Linearized Profile

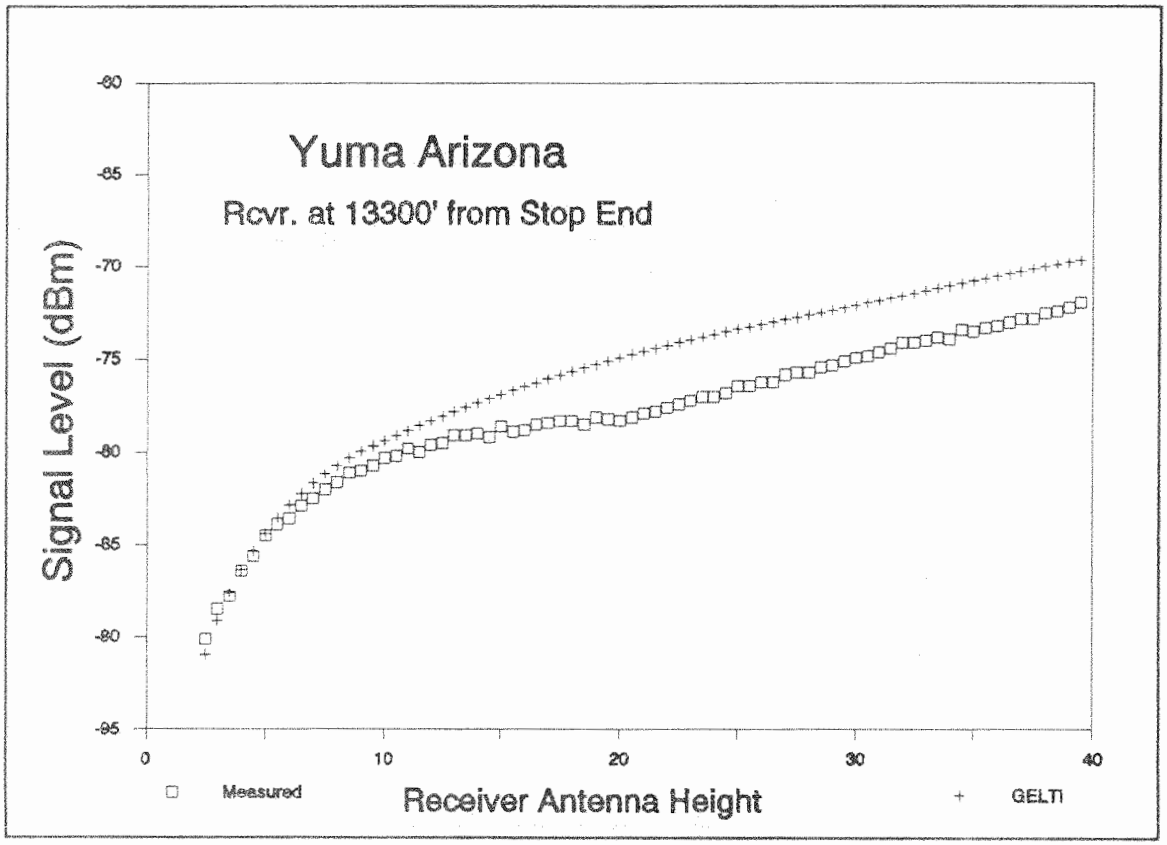
Yuma Arizona
Rcvr. at 13300' from Stop End
Signal Level (dBm)
-60
-65
-70
-75
-80
-85
-90
-95
0
10
20
30
40
Measured
Receiver Antenna Height
GELTI

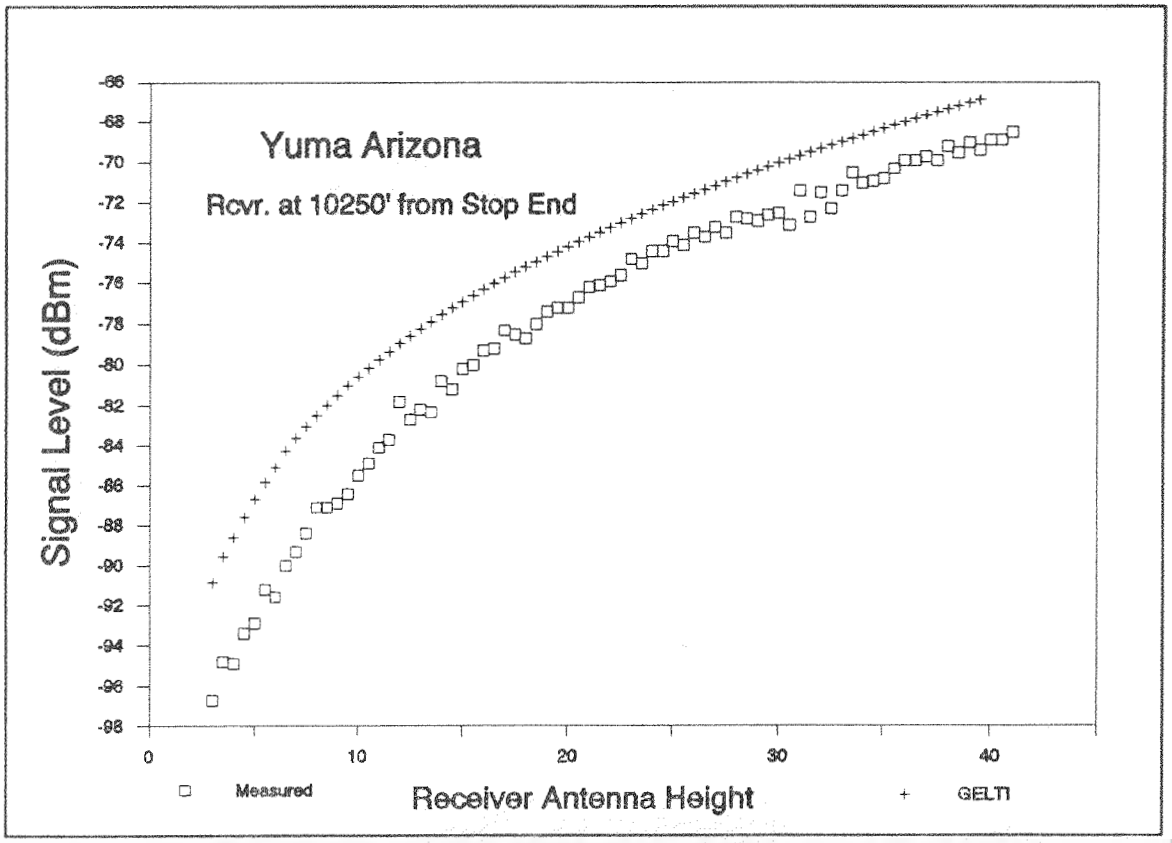

Roanoke, Virginia

Measurements taken at 2 receiver locations

Multipath observed at RWY Threshold

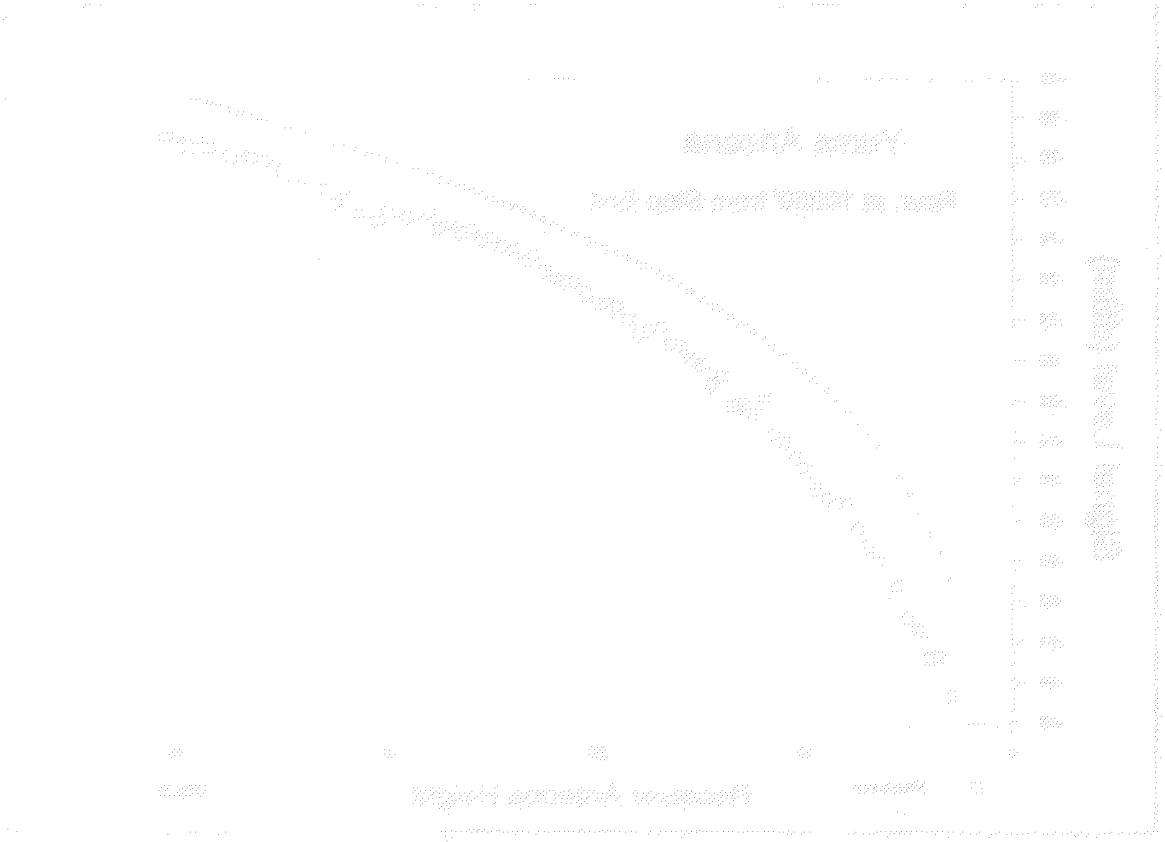

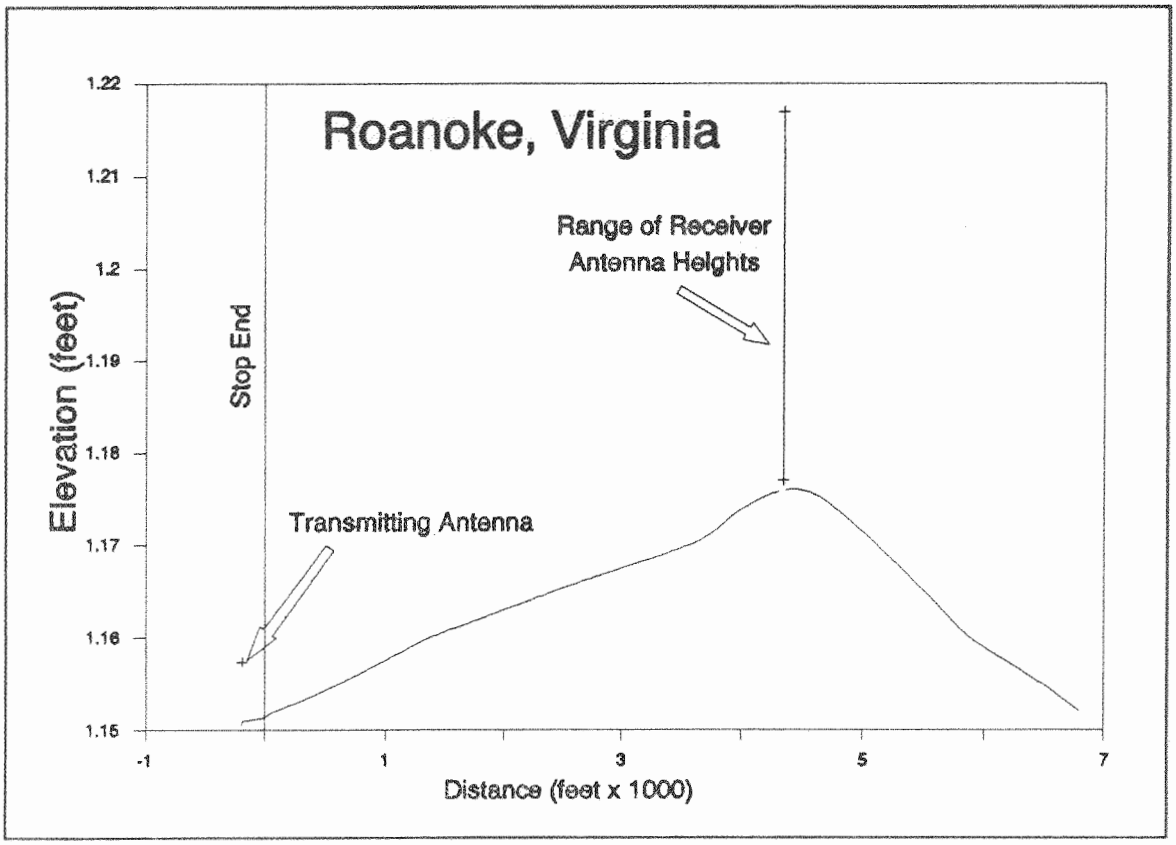
Roanoke, Virginia
Range of Receiver Antenna Heights
Stop End
Transmitting Antenna
Elevation (feet)
1.22
1.21
1.2
1.19
1.18
1.17
1.16
1.15
-1
1
3
5
7
Distance (feet x 1000)

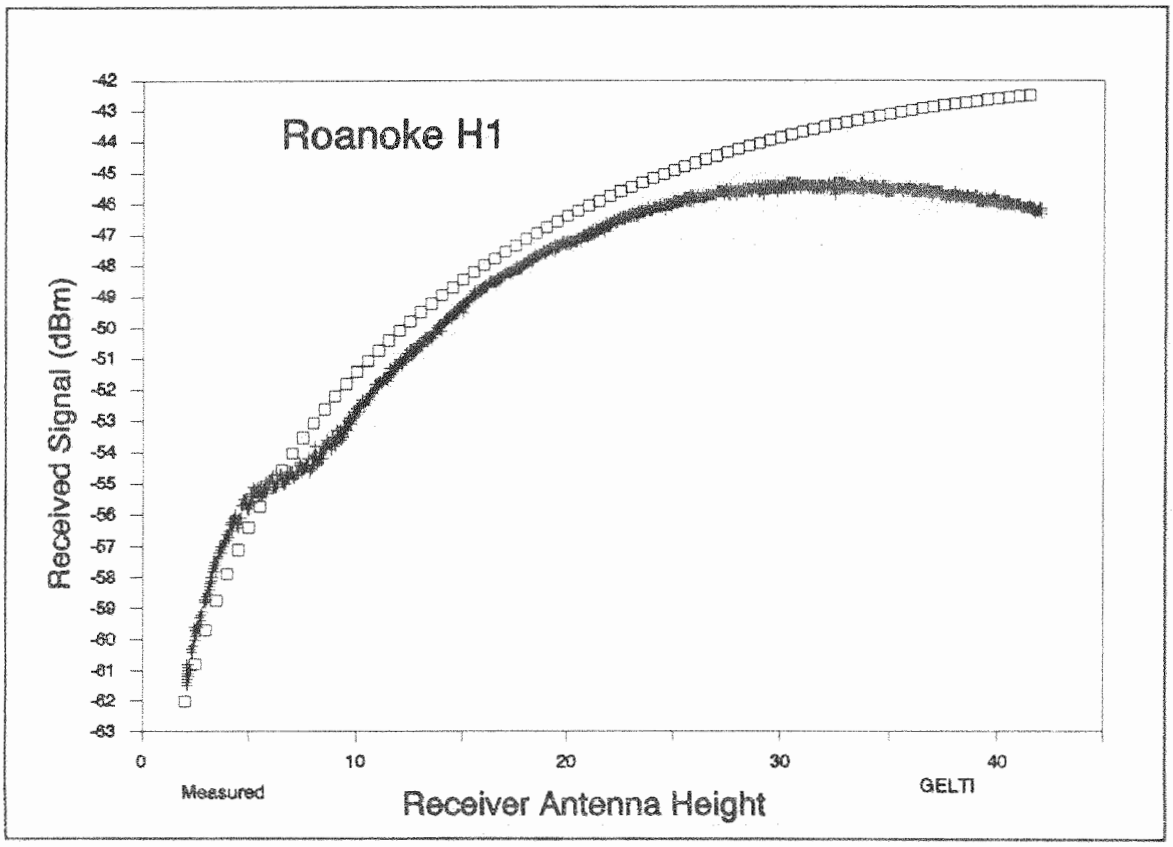
Roanoke H1
Received Signal (dBm)
-42
-43
-44
-45
-46
-47
-48
-49
-50
-51
-52
-53
-54
-55
-56
-57
-58
-59
-60
-61
-62
-63
0
10
20
30
40
Measured
GELTI
Receiver Antenna Height

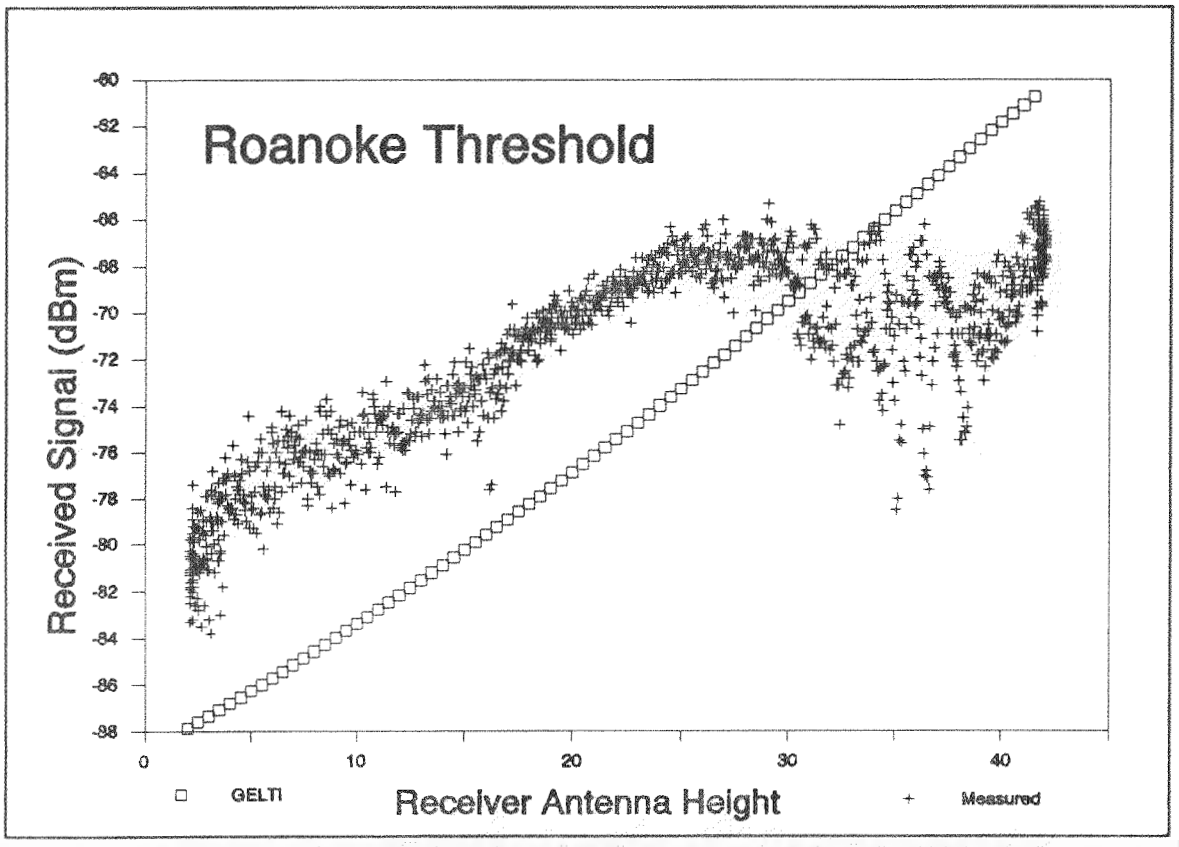

Conclusions - Recommendations

- The capability to model accurately the effects of bumpy runways has been validated
- Approach to modeling terrain effects can be extended to other navigation systems
- Additional validation data should be collected

AL LOPEZ
ARL ASSOCIATES

AZIMUTH GROUND CROSSFALL EFFECTS

MLS AZIMUTH ANTENNA
GROUND CROSSFALL CONSIDERATIONS

ALFRED R. LOPEZ

ARL ASSOCIATES
FOUR SARINA DRIVE
COMMACK, NY 11725

- o INTRODUCTION
- o GROUND CROSSFALL PROBLEM DEFINITION
- o IN-BEAM MULTIPATH CHARACTERISTICS
- o MULTIPATH SEPARATION ANGLE RELATIONSHIP TO:
  - CROSSFALL ANGLE
  - ELEVATION ANGLE
- o CROSSFALL ERROR FORMULA
- o RESULTS
- o SUMMARY

INTRODUCTION

IT HAS BEEN RECOGNIZED THAT THE GROUND REFLECTION FOR THE AZ ANTENNA CAN CAUSE SIGNIFICANT ERROR. THE VERTICAL APERTURE SIZE FOR THE AZ ANTENNA MUST BE SUFFICIENTLY LARGE TO SATISFY THE 8 dB/° SLOPE REQUIREMENT AT 0° ELEVATION AND THE SIDELOBE REQUIREMENTS IN THE NEGATIVE ELEVATION DIRECTIONS. I AM NOT AWARE OF ANY QUANTITATIVE RELATIONSHIP BETWEEN THE 8 dB/° (20 WAVELENGHT VERTICAL APERTURE SIZE) SLOPE REQUIREMENT AND A PERFORMANCE PARAMETER. DURING THE EVOLUTION OF MLS, AZ PATH FOLLOWING NOISE (PFN) ERRORS ON FINAL APPROACH WERE OBSERVED AND ATTRIBUTED TO GROUND REFLECTIONS. A LARGE VERTICAL APERTURE SIZE TO PROVIDE A SHARP BOTTOM SIDE CUTOFF OF THE BEAM WAS HELPFUL IN SUPPRESSING THESE EFFECTS.

THIS PAPER PRESENTS SOME SIMPLE CONCEPTS THAT QUANTIFY THE RELATIONSHIP BETWEEN PFN ON FINAL APPROACH AND THE VERTICAL APERTURE SIZE FOR THE AZ ANTENNA. GROUND CROSSFALL (LATERAL TILT OF THE GROUND REFLECTION ZONE) GENERATES A TILTED GROUND IMAGE THAT CREATES SIGNIFICANT IN-BEAM MULTIPATH.

AZIMUTH ANTENNA GROUND CROSSFALL

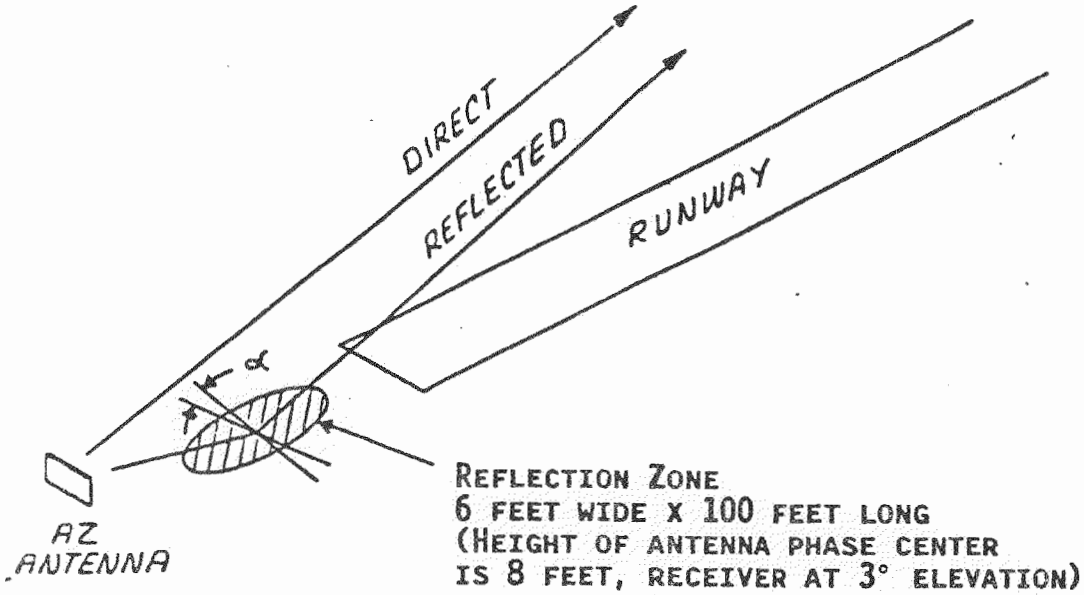

GROUND CROSSFALL PROBLEM

BECAUSE THE AZ EQUIPMENT HAS TO PROVIDE SERVICE DOWN TO ESSENTIALLY 0° ELEVATION, A VERY STRONG GROUND REFLECTION IS INHERENT. IN THE LIMIT OF 0° ELEVATION THE REFLECTION COEFFICIENT APPROACHES -1. THE PRIMARY REFLECTING SURFACE (REFLECTION ZONE) IS AN ELLIPSE WITH A MINOR AXIS, a

$$a=\sqrt{\lambda \times R_0}$$

AND THE MAJOR AXIS $b = a/\sin\theta$.

IF THE MINOR AXIS IS HORIZONTAL THEN THE REFLECTED SIGNAL HAS THE SAME CODING AS THE DIRECT SIGNAL AND, CONSEQUENTLY, IT DOES NOT CAUSE AN ERROR. IF THE MINOR AXIS IS ROTATED AN ANGLE α (CROSSFALL ANGLE) THEN THE REFLECTED SIGNAL DOES NOT HAVE THE SAME CODING AS THE DIRECT SIGNAL AND CAN CAUSE AN ERROR. TYPICALLY, THE REFLECTION ZONE IS LOCATED ABOUT 200 FEET IN FRONT OF THE AZ ANTENNA WHEN THE AIRCRAFT IS AT THE OUTER MARKER AND MIGRATES ONTO THE RUNWAY SURFACE AS THE AIRCRAFT APPROACHES TOUCHDOWN.

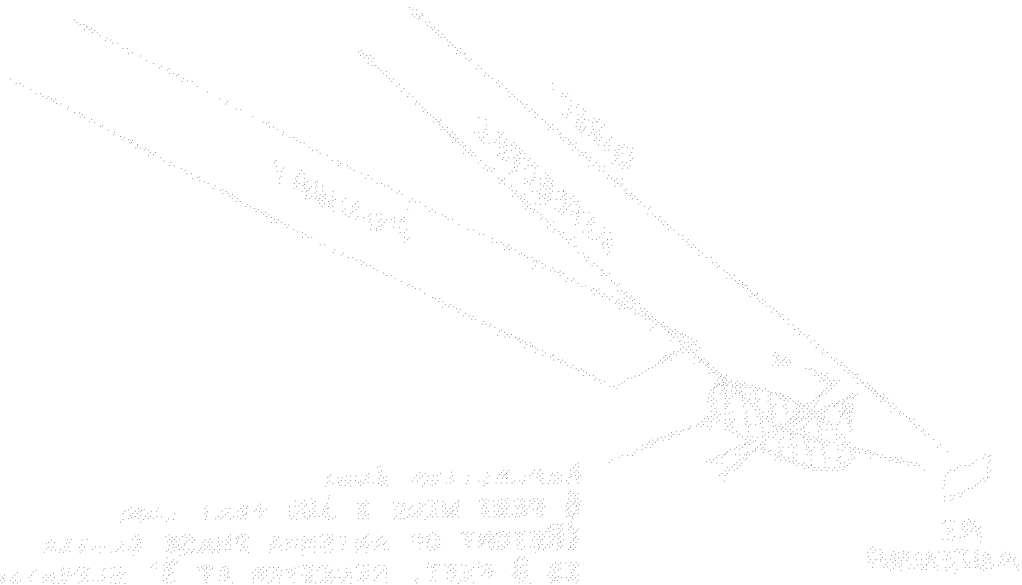

GROUND IMAGE ANGLE = 2 TIMES CROSSFALL ANGLE

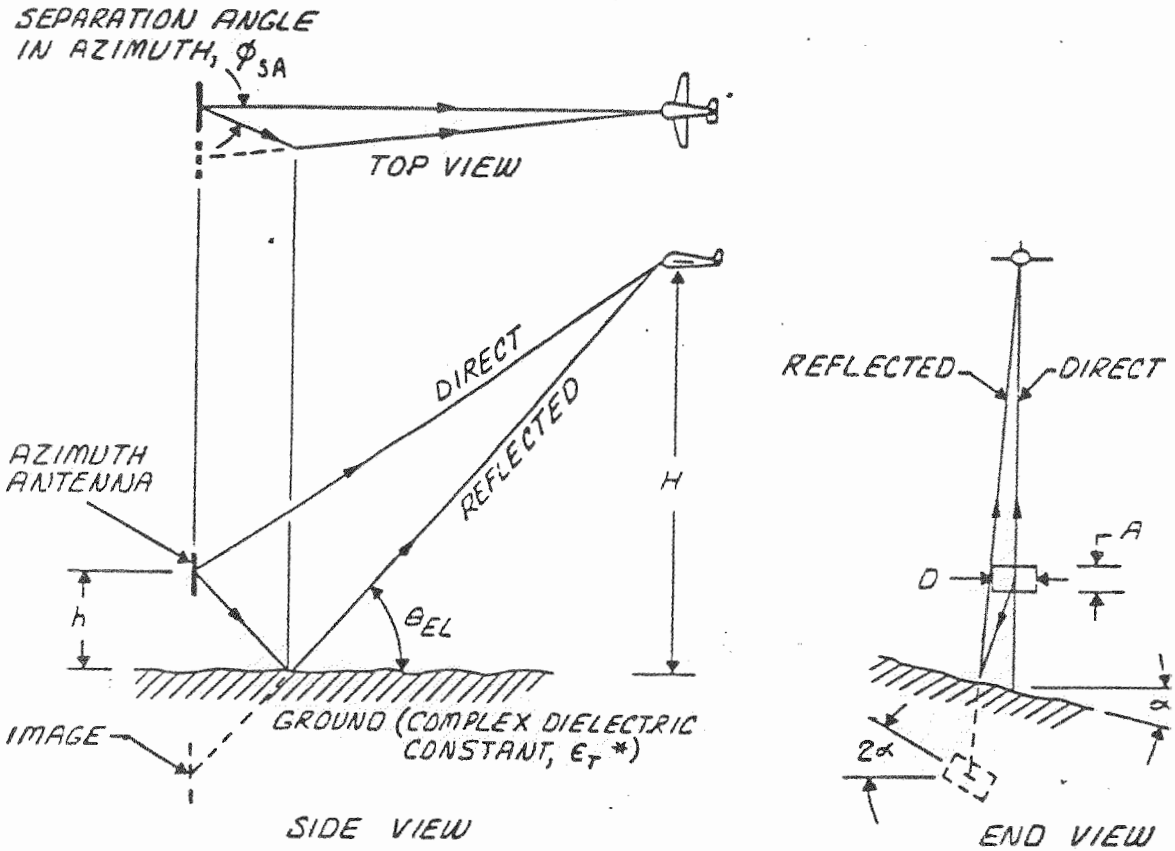

THIS DIAGRAM SHOWS THE SIDE, TOP AND END VIEWS FOR THE GROUND CROSSFALL SITUATION. IT SHOWS THE DIRECT SIGNAL AND THE PATH FOR THE GROUND REFLECTED SIGNAL. THE TOP VIEW SHOWS THAT THE GROUND REFLECTED SIGNAL HAS A CODING DIFFERENT THAN THAT OF THE DIRECT SIGNAL WITH A SEPARATION ANGLE ϕ_{SA}. THE END VIEW SHOWS THAT THE GROUND IMAGE IS ROTATED 2 TIMES THE CROSSFALL ANGLE α. THIS FACTOR OF 2 IS CHARACTERISTIC OF A MIRROR SURFACE.

THE ANGLE CODING OF THE GROUND REFLECTION IS SKEWED AT AN ANGLE OF 2α WITH RESPECT TO THE CODING OF THE DIRECT SIGNAL.

IN-BEAM MULTIPATH ERROR

SEPARATION ANGLE < 1/4 BEAMWIDTH

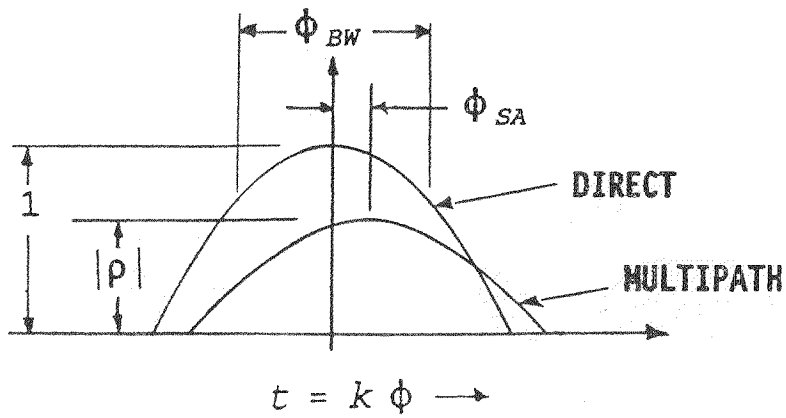

$$\delta\phi = \frac{\pm|\rho|}{1 \pm |\rho|}\,\phi_{SA}$$

$$\phi_{SA} \leq \frac{\phi_{BW}}{4}$$

ERROR IS INDEPENDENT OF BEAMWIDTH

IN-BEAM MULTIPATH

FOR THE AZ ANTENNA GROUND REFLECTION PROBLEM THE PRIMARY CONCERN IS IN-BEAM MULTIPATH FOR AN AIRCRAFT ON FINAL APPROACH. AS THE AIRCRAFT APPROACHES TOUCHDOWN THE MULTIPATH SEPARATION ANGLE IS SMALL COMPARED WITH THE BEAMWIDTH AND THE ERROR BECOMES INDEPENDENT OF BEAMWIDTH. THE RELATIONSHIP OF ANGLE GUIDANCE ERROR, $\delta\phi$, AND MULTIPATH SEPARATIONS ANGLE, ϕ_{SA}, IS PRESENTED ABOVE. THE + SIGN CORRESPONDS TO 0° PHASE FOR THE REFLECTED SIGNAL; THE - SIGN CORRESPONDS TO 180° PHASE.

REDLIEN-KELLY MULTIPATH DIAGRAMS

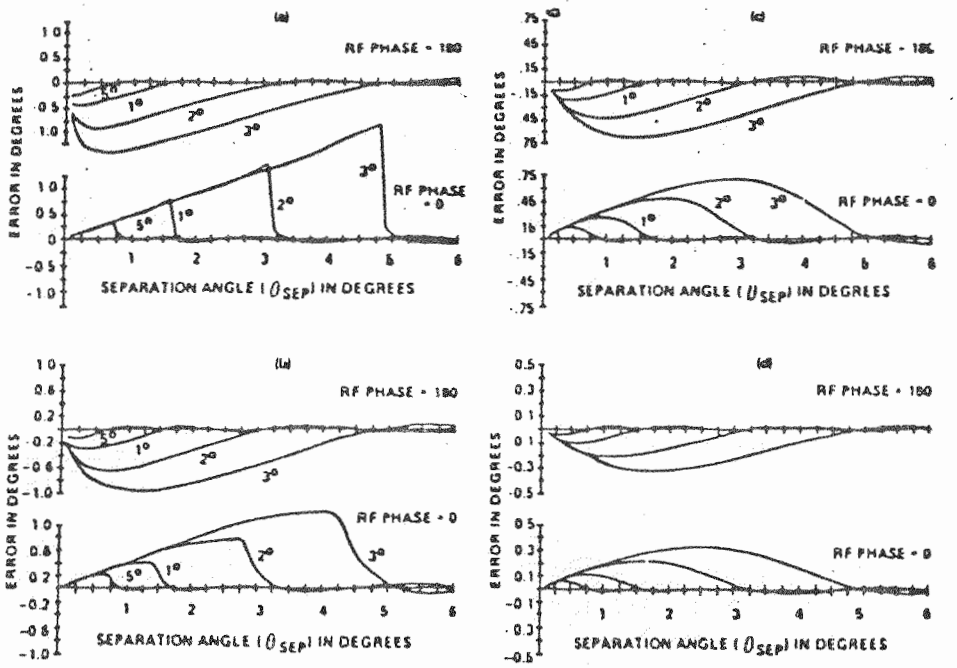

FIG. 36. Dwell gate processor error versus separation angle curves; μ = 1.0 dB (a), 3.0 (b), 6.0 (c), 12.0 (d).

THESE ARE THE REDLIEN-KELLY MULTIPATH DIAGRAMS (REF. "MICROWAVE LANDING SYSTEM: THE NEW INTERNATIONAL STANDARD", ACADEMIC PRESS, ADVANCES IN ELECTRONICS AND ELECTRON PHYSICS, VOL. 57, 1981). THEY SHOW THE INDEPENDENCE OF BEAMWIDTH FOR SMALL SEPARATION ANGLES. THE FORMULA PRESENTED PREVIOUSLY FOR SMALL SEPARATION ANGLE IS IN AGREEMENT WITH THESE DIAGRAMS FOR THE 0° AND 180° RF PHASE CASES.

MEASURED IN-BEAM MULTIPATH ERROR

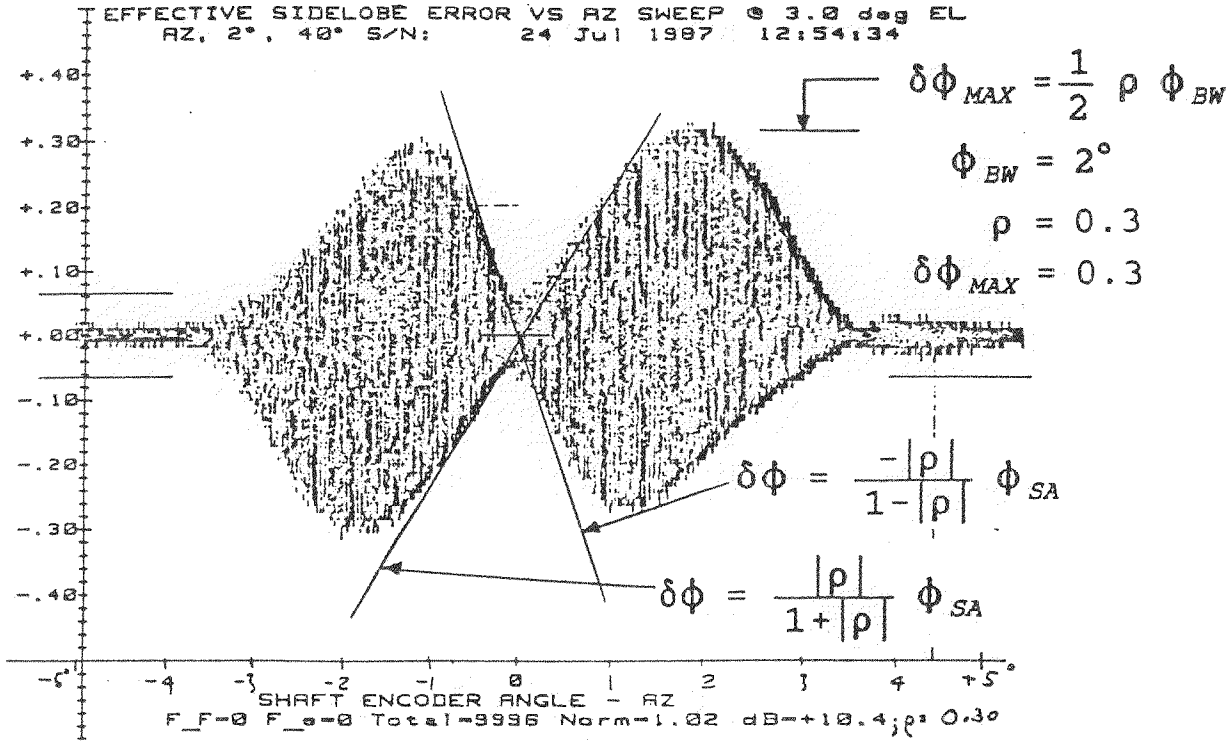

MEASURED IN-BEAM MULTIPATH ERROR IS SHOWN IN THIS ILLUSTRATION. IT IS NOTED THAT THE SMALL SEPARATION ANGLE APPROXIMATIONS ARE IN GOOD AGREEMENT WITH THE MEASUREMENT.

THE IN-BEAM CHARACTERISTICS ARE FUNDAMENTAL. THEY WERE ACTUALLY USED TO VALIDATE AN ANTENNA RANGE CAPABILITY FOR MEASURING EFFECTIVE SIDELOBE ERROR.

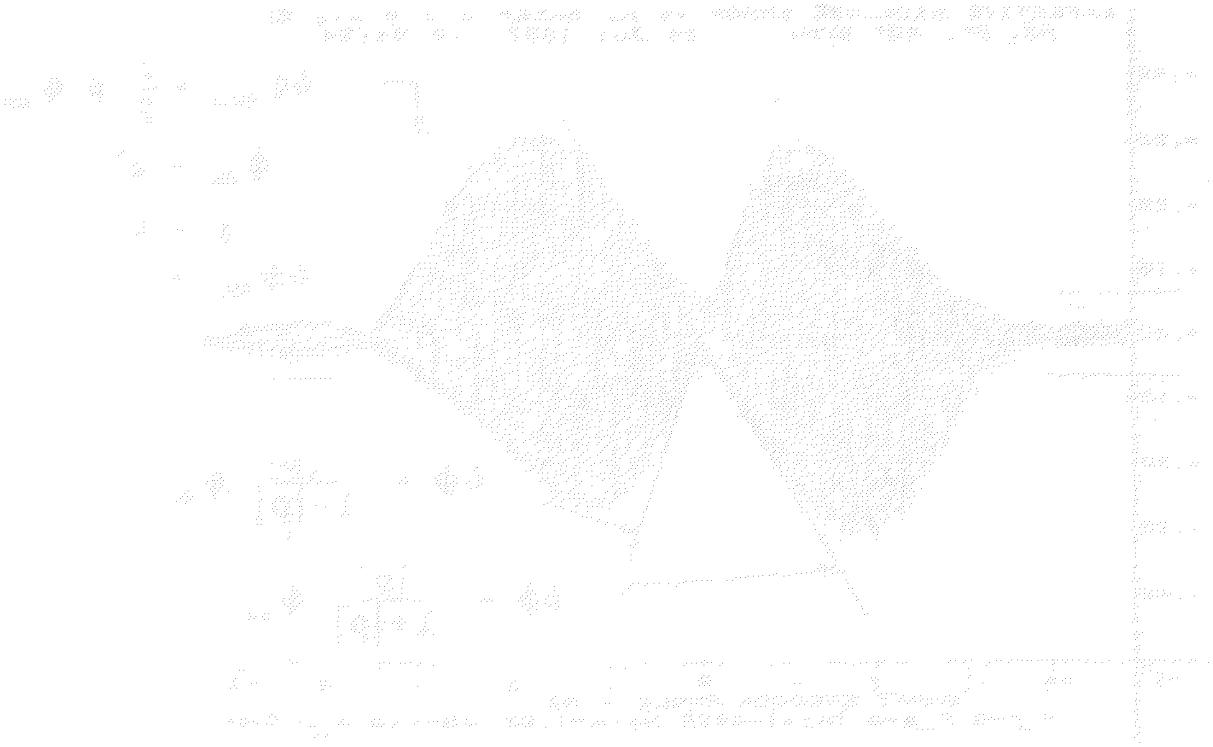

DERIVATION OF $\phi_{SA} = 2\ \alpha\ \theta$

ORTHOGRAPHIC PROJECTION OF DIRECTION HEMISPHERE
("SIN θ" SPACE, "DIRECTION COSINE" SPACE)
A USEFUL TOOL FOR PHASED ARRAY ANALYSIS.

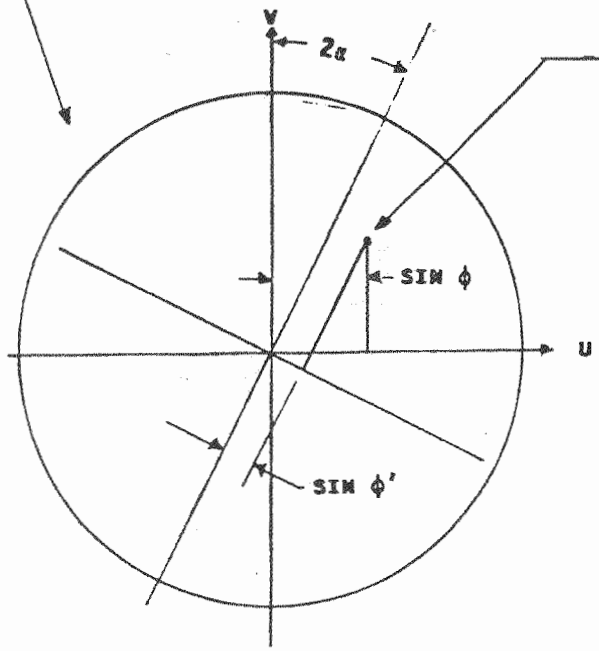

RECEIVER AT U,V

$u = \sin\phi$, ϕ = AZIMUTH CONICAL ANGLE
$v = \sin\theta$, θ = ELEVATION ANGLE

CONSTANT DIRECT SIGNAL ANGLE CODING ARE LINES PARALLEL TO THE "V" AXIS

CONSTANT MULTIPATH SIGNAL ANGLE CODING ARE LINES PARALLEL TO THE LINE AT AN ANGLE OF 2α WITH RESPECT TO THE "V" AXIS

MULTIPATH SEPARATION ANGLE IS GIVEN BY:

$$\sin\phi_{SA} = \sin\phi - \sin\phi'$$

$$\sin\phi' = \sin\phi\cos 2\alpha - \sin\theta\sin 2\alpha$$

$$\sin\phi_{SA} = \sin\phi\,(1 - \cos 2\alpha) + \sin\theta\sin 2\alpha$$

IF $\phi = 0$ AND, θ AND 2α ARE $< \pi/4$, THEN:

$$\phi_{SA} = 2\ \alpha\ \theta$$

MULTIPATH SEPARATION ANGLE

IT WAS NOTED PREVIOUSLY THAT A GROUND CROSSFALL WITH AN ANGLE α CREATES AN IMAGE ROTATED AT AN ANGLE 2α WITH RESPECT TO A HORIZONTAL LINE ARRAY. THE ABOVE ILLUSTRATION PRESENTS A DERIVATION OF THE RELATIONSHIP BETWEEN THE MULTIPATH SEPARATION ANGLE, THE CROSSFALL ANGLE AND THE ELEVATION ANGLE. AN ORTHOGRAPHIC PROJECTION OF THE DIRECTION HEMISPHERE IS USED. ON THIS PROJECTION THE CONSTANT CODING CONTOURS FOR A ONE-DIMENSIONAL PHASED ARRAY ARE STRAIGHT LINES. THIS RESULT IS USED TO FURTHER QUANTIFY THE GROUND CROSSFALL ERROR FORMULA

AZIMUTH GROUND CROSSFALL ERROR FORMULA

$$\delta\phi = \left(\frac{\pm|\rho|}{1\pm|\rho|}\right) 2\ \alpha\ \theta$$

NOTE:

REF: SEYMOUR EVERETT ET. AL., "DESIGN CONSIDERATIONS FOR ACHIEVING MLS CATEGORY III REQUIREMENTS", PROCEEDINGS OF THE IEEE, VOL 77, NO. 11, NOVEMBER 1989.

THE ABOVE REFERENCE INCLUDES THE FORMULA

$$\delta\phi = \left(\frac{\rho}{1-\rho}\right)^2 \alpha\ \theta$$

IT SHOULD BE NOTED THAT THE EXPONENTIAL FACTOR OF 2 WAS INTENDED TO BE A MULTIPLICATIVE FACTOR.

CROSSFALL ERROR FORMULA

THE CROSSFALL ERROR IS RELATED TO CROSSFALL ANGLE AND THE AIRCRAFT ELEVATION ANGLE. IT IS NOTED THAT IN THE LIMIT OF 0° ELEVATION ANGLE THE NUMERATOR AND DENOMINATOR OF THE ERROR FORMULA GO TO 0 VALUE SINCE THE MAGNITUDE AND PHASE OF THE REFLECTED SIGNAL APPROACH UNITY AND 180°. THIS IS AN INDETERMINATE CONDITION. AN APPROXIMATE EXPRESSION FOR THE REFLECTION FACTOR LEADS TO A RESOLUTION OF THE INDETERMINATE CONDITION.

GROUND REFLECTION APPROXIMATION

ASSUMPTIONS: 1. GROUND SURFACE REFLECTIVITY FACTOR = -1
2. A VERTICAL APERTURE, A, IS UTILIZED TO SUPPRESS THE GROUND REFLECTION

$$|\rho| = \frac{1 - .82 \tanh(3.5\, A\, \theta/\lambda)}{1 + .82 \tanh(3.5\, A\, \theta/\lambda)}$$

WHERE

λ = *Freespace wavelenght*

AN EXPRESSION FOR CROSSFALL ERROR, INCLUDING THE DEPENDENCE ON THE PHASE CENTER HEIGHT, h, IS GIVEN BY:

$$\delta\phi = \frac{-2\,\alpha\,\theta(1-.82\tanh(3.5\,A\,\theta/\lambda))\cos(4\pi\,h\sin\theta/\lambda)}{1+.82\tanh(3.5\,A\,\theta/\lambda)-(1-.82\tanh(3.5\,A\,\theta/\lambda))\cos(4\pi\,h\sin\theta/\lambda)}$$

$$\boxed{\delta\phi_{\lim\theta\to 0} = \frac{\alpha\,\lambda}{2.9\,A}}$$

AN APPROXIMATE FORMULA FOR THE MAGNITUDE OF THE REFLECTION COEFFICIENT IS PRESENTED ABOVE. IT RELATES THE REFLECTION COEFFICIENT TO THE VERTICAL APERTURE SIZE IN WAVELENGTHS AND THE ELEVATION ANGLE. THIS RELATIONSHIP, ALONG WITH A PHASE-CENTER-HEIGHT DEPENDENCE FACTOR, ARE SUBSTITUTED IN THE CROSSFALL ERROR FORMULA TO ARRIVE AT RELATIVELY SIMPLE APPROXIMATE EXPRESSION FOR THE CROSSFALL ERROR AS A FUNCTION OF CROSSFALL ANGLE, ELEVATION ANGLE, VERTICAL APERTURE SIZE AND AZ ANTENNA PHASE CENTER HEIGHT. AN EVALUATION OF THIS CROSSFALL ERROR FORMULA AT $\theta = 0°$ LEADS TO A SIMPLE RELATIONSHIP FOR THE CROSSFALL ERROR, CROSSFALL ANGLE AND THE VERTICAL APERTURE SIZE.

CROSSFALL ERROR VERSUS ELEVATION ANGLE

4 Foot Vertical Aperture Size
Alpha = 2 Degrees

Phase Center
Height = 10 feet

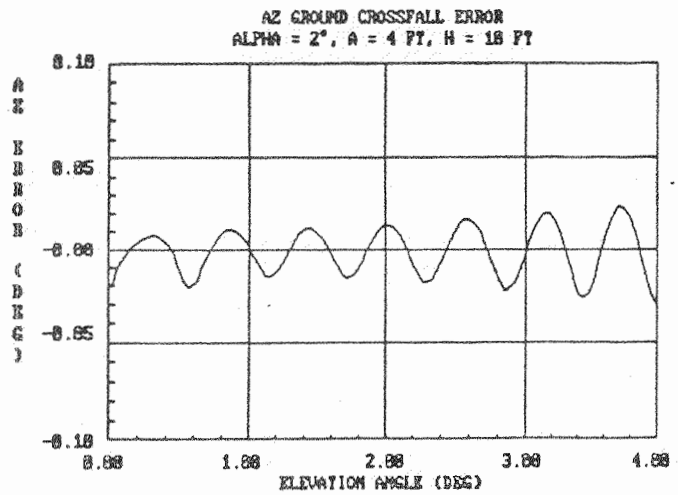

Phase Center
Height = 20 feet

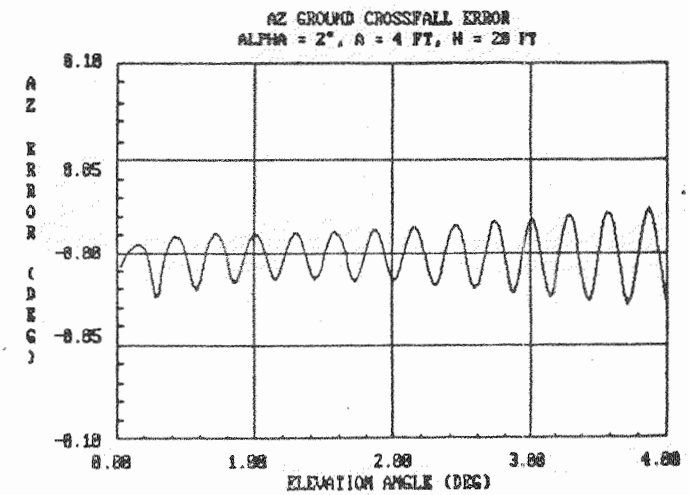

The above illustration shows the predicted crossfall error versus elevation angle for a crossfall angle of 2° for two antenna phase center heights, 10 and 20 feet.

CROSSFALL ERROR VERSUS ELEVATION ANGLE

4 Foot Vertical Aperture Size
Alpha = 4 Degrees

Phase Center Height = 10 feet

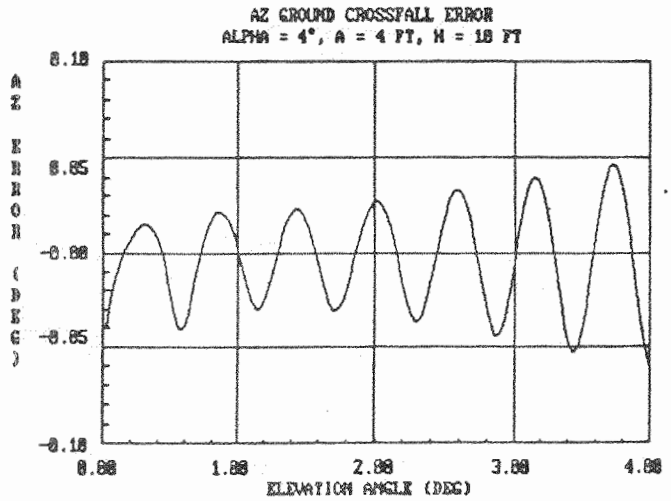

Phase Center Height = 20 feet

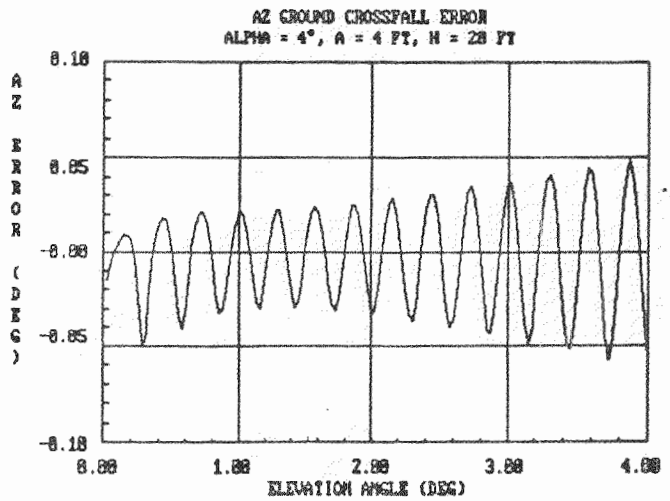

The above illustration shows the predicted crossfall error versus elevation angle for a crossfall angle of 4° for two antenna phase center heights, 10 and 20 feet

CROSSFALL PFE

3 DEGREE GLIDE PATH APPROACH
10000 FOOT ANTENNA TO MLS DATUM POINT DISTANCE
4 FOOT VERTICAL APERTURE SIZE
ALPHA = 2 DEGREES
PHASE CENTER HEIGHT = 10 FEET

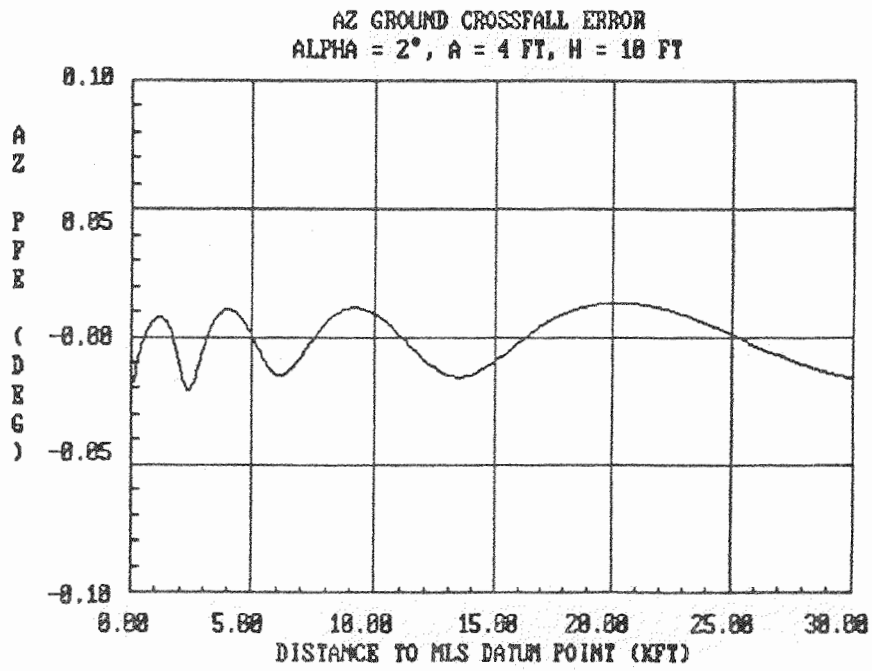

THE CROSSFALL ERROR FORMULA WAS USED TO COMPUTE THE AZ PFE (PFN) ON THE FINAL LEG OF A 3° GLIDE PATH APPROACH TO A RUNWAY WHERE THE AZ ANTENNA WAS AT A DISTANCE OF 10000 FEET FROM THE MLS DATUM POINT, THE CROSSFALL ANGLE = 2° AND THE ANTENNA PHASE CENTER HEIGHT WAS 10 FEET. IT IS NOTED THAT THE ERROR IS SIGNIFICANT.

SUMMARY

- THE BACKGROUND INFORMATION REGARDING AZ ANTENNA GROUND REFLECTION ERROR AND VERTICAL APERTURE SIZE WAS REVIEWED
- THE AZ ANTENNA GROUND CROSSFALL PROBLEM WAS QUANTIFIED
- AN APPROXIMATE GROUND CROSSFALL ERROR FORMULA WAS PRESENTED THAT RELATES THE ERROR TO CROSSFALL ANGLE, ELEVATION ANGLE, ANTENNA VERTICAL APERTURE SIZE, AND PHASE CENTER HEIGHT
- A BASIC RELATIONSHIP, FOR THE LIMIT CASE OF 0 ELEVATION ANGLE, WAS PRESENTED THAT RELATES ERROR TO CROSSFALL ANGLE AND VERTICAL APERTURE SIZE
- IT IS CONCLUDED THAT AZ CROSSFALL CAN CAUSE SIGNIFICANT PFN ON FINAL APPROACH IF THE GROUND DIRECTLY IN FRONT OF THE AZ ANTENNA (REFLECTION ZONE) HAS CROSSFALL THAT EXCEEDS AN ANGLE OF 1°. SPECIAL ATTENTION TO THIS PROBLEM IS WARRANTED FOR THE OFF CENTERLINE AZ SITING SITUATIONS WHERE THE INTERVENING GROUND CAN HAVE SIGNIFICANT CROSSFALL.

KAZUNOBU KOREMURA
E.N.R.I., JAPAN

ELEVATION DIFFRACTION ERROR

Electronics and Communications in Japan, Part 1, Vol. 72, No. 6, 1989
Translated from Denshi Joho Tsushin Gakkai Ronbunshi, Vol. 71-B, No. 3, March 1988, pp. 449-456

Experiments of Diffraction Error on MLS Elevation Guidance

Kazunobu Koremura, Member

Electronic Navigation Research Institute, Ministry of Transport, Mitaka, Japan 181

SUMMARY

In the diffraction region of a microwave landing system (MLS) elevation guidance, the field strength fluctuates due to such objects as buildings and hence the measuring error increases. This paper describes experiments to determine the effect of diffraction caused by the upper edges of a building. The results show that the field has a typical diffraction characteristic which can be calculated by regarding the building as a knife edge. It was found that the diffraction error cannot be ignored when measuring an angle, since the scanning beam is sharp in the vertical direction and flat in the horizontal direction. Hence, both the component proportional to the amplitude of the diffraction wave and that proportional to the partial differentiation of its incident angle (slope diffraction component) increase. It was found also that the measurement error characteristic around the shadow boundary, calculated by using the uniform geometrical theory of diffraction taking account of the slope diffraction, agrees well with the observational results. Generally, this method can be applied to the diffraction field strength and its measuring error estimation such as hangers.

1. Introduction

Microwave landing systems (MLS's) will be used for precision landings at airports after the middle 1990s, replacing the currently used instrument landing systems (ILS's) [1].

The basic angle guidance system in an MLS consists of azimuth guidance equipment and elevation guidance equipment. If there is any object in front of the ground antenna of an MLS, a reflection region and a diffraction region are created, since the coverage of the MLS is large; for example, the area is a fan shape having an azimuth angle of 40°, a distance of 37 km (20 NM), and maximum height of 6000 m. The azimuth-guidance antenna is placed at the end of a runway, and the elevation-guidance antenna is at the approach side of the runway, i.e., the distance between the two antennas is approximately equal to the length of the runway. The reflection area and the diffraction area depend on the locations of buildings at an airport. Although it is possible to avoid directions facing buildings from the beam-scanning for the azimuth guidance, it is not possible to do so for the elevation guidance. Therefore, the latter creates a larger angle-measuring error.

Neither experimental results nor experimental analysis of diffraction characteristic of multipaths have been published. However, those for measuring-angle errors have been published in [2] and [3].

This paper describes the experiment for the diffraction characteristic of the MLS elevation guidance due to such objects as buildings, and presents their results and analysis.

The calculated results of measurement-angle errors agree well with the experimental results when the slope-diffraction waves, in addition to the direct waves and diffraction waves based on "a knife-edge model," are taken into account.

2. Principle of Elevation-Angle Measurement

Figure 1 shows the measurement principle of an elevation angle in the MLS. The beam of a continuous wave is transmitted from a guidance antenna set at the side of a runway. The beam is wide horizontally and vertically narrow as shown in Fig. 1(a). The beam scans vertically, starting from the

ISSN8756-6621/89/0006-0015$7.50/0
© 1989 Scripta Technica, Inc.

89

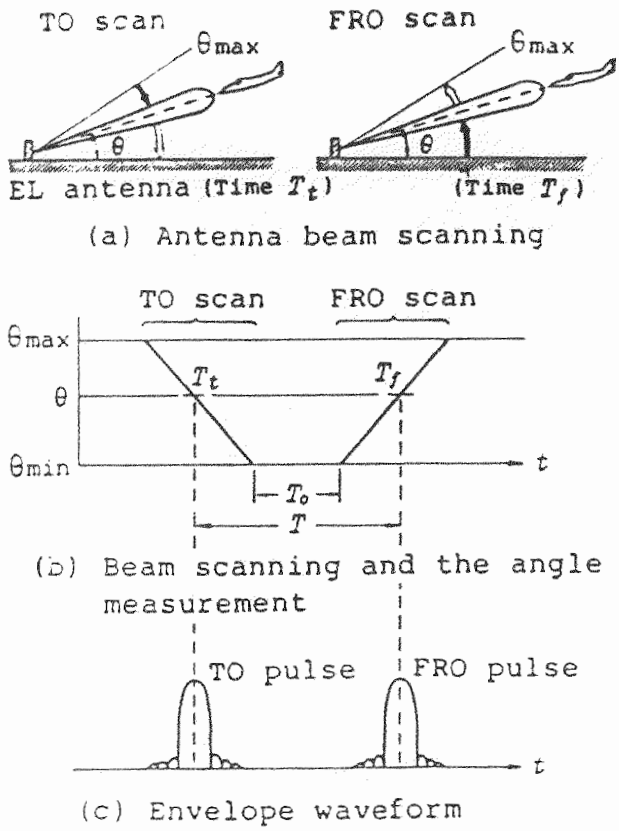

Fig. 1. MLS elevation angle measurement technique.

highest angle (θ_{max}) to the lowest angle (θ_{min}) [TO direction], then from the lowest angle to the highest angle [FRO direction] with a constant angular velocity, as shown in Fig. 1(b). If an airplane is in an elevation angle θ, it will receive the TO pulse and FRO pulse at time T_t and T_f, respectively, which corresponds to θ, as shown in Fig. 1(c). When the interval between the two pulses T is measured, θ is given by

$$\begin{aligned} \theta &= (T - T_0)V/2 + \theta_{min} \\ T_0 &= 3{,}350\,\mu s \\ V &= 0.02^\circ/\mu s \end{aligned} \qquad (1)$$

where T_0 is the interval when the elevation angle is 0°, and V is the scanning velocity of the beam.

To measure times T_t and T_f, some methods are available [4]: for example, the dwell-gate method which measures the interval between the centers of the two pulses (center of each pulsewidth greater than -3 dB); and the split-gate method which uses quantized pulsewidths (two sets of the sum of amplitudes between a peak in a continuous section are made, then the signs of their differences are used). When these methods are used for time-interval measurements and angle conversions, the accuracy of the angle measurement is affected by waveform distortion and shifts due to the multipaths and diffractions.

An accuracy of about 0.1° is required for angle measurements in the elevation guidance system. The multipath error has the greatest effect on the measuring accuracy. For the design of an angle measurement system, this type of error is estimated to be about 0.08°.

Table 1. Data of elevation guidance system

Frequency of transmitter	5064 MHz
Output of transmitter	15 W
Horizontal coverage	±40°
Vertical scanning range	0.9 - 15° (range with proportion 1 - 7.5°)
Width of beam	1.5°
Scanning rate of beam	20°/ms
Step of scanning beam	0.1°
Level of side lobe	less than -20 dB
Accuracy of directivity of beam	0.025° (2σ)
Format of transmission	FAA Phase III

3. Experimental Results

3.1 Experimental apparatus

Table 1 shows the performance of MLS elevation guidance equipment used for the experiment [5]. The main specifications of this equipment are based on the International Standard, the horizontal coverage being ±40°, the vertical beam width is 1.5°, and the frequency of the transmitter is 5064 MHz.

This system was used for both ground and flight experiments. Figure 2 shows the block diagram of the measurement system for the ground experiment. The elevation antenna is used for scanning the beam (power +54 dBm), and transmits the data signal and the sidelobe suppressing signal. The position measurement system consists of a combination

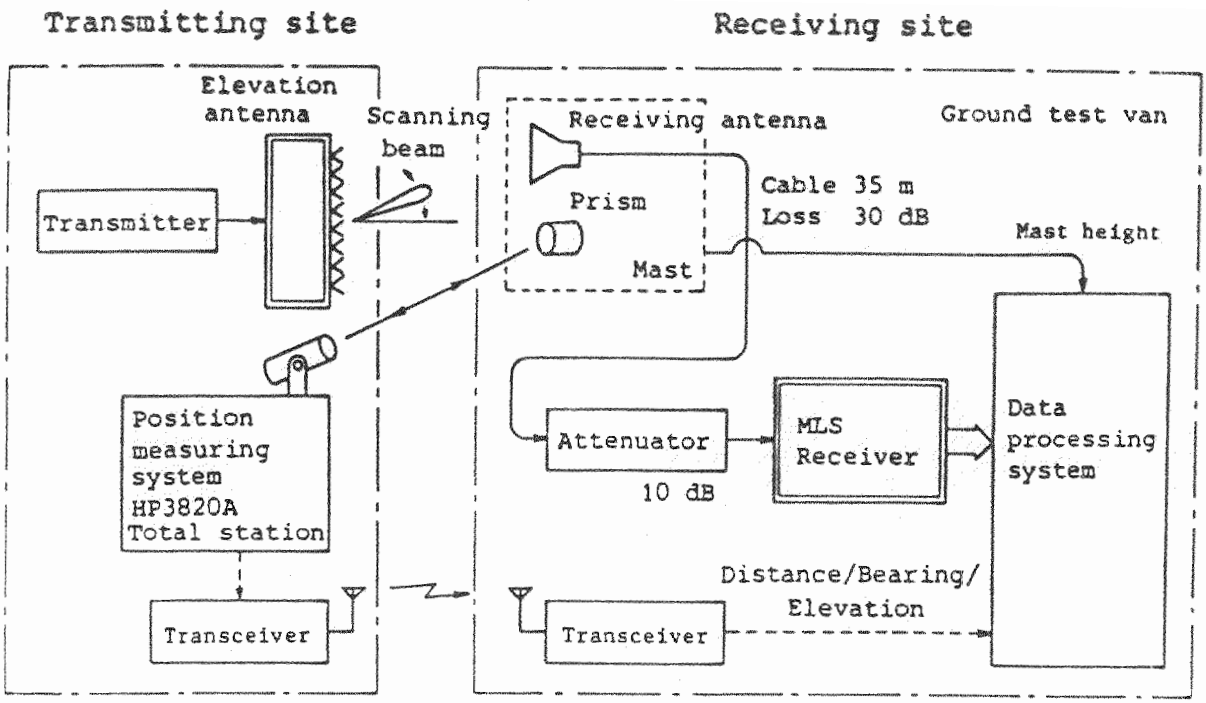

Fig. 2. Block diagram of the measuring system for ground test.

of a transit and a laser distance-meter. This is set at the height of the phase center of the scanning antenna with the optical axis aligned. This system measures the distance between the guidance antenna and the receiving antenna, and the elevation angle and bearing angle. This system also transmits the measured information to the receiving side from which the angle measurement errors are derived. The accuracy of the measurements of the horizontal distance is ±5 mm, that of the elevation angle is ±0.001°, and that of the bearing angle is ±0.006°.

A landing-course test vehicle [6] was developed for tests at the receiving site. This vehicle can set the receiving antenna in a height ranging from 1.5 to 22 m (with reference to ground). The receiving antenna is a horn type. It has a gain of 15 dB, horizontal beamwidth of 36°, and vertical beamwidth of 24°. The field strength and angles of the scanning beam are obtained from a signal received by this antenna and processed by the MLS receiver. The angle error is defined by the difference of angle measured from an elevation angle.

An elevation angle in the shadow of an object (e.g., a building) was calculated based on data of the height of a mast, since the angle cannot be seen from the receiving site. The error of measurement of the

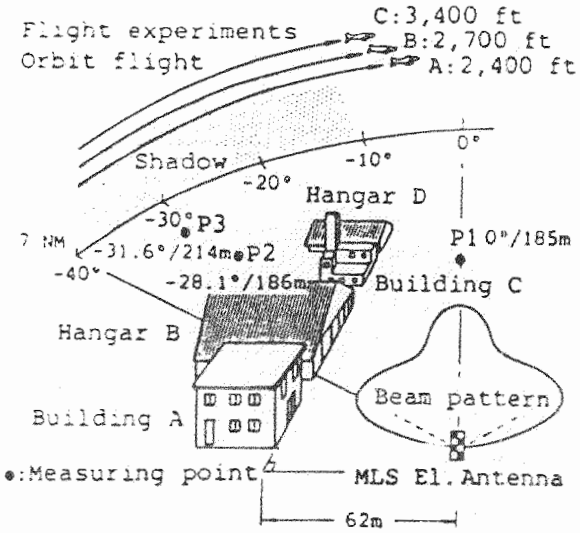

Fig. 3. Measuring point layout.

elevation angle of the height of a mast is within ±0.01°, and this is less than the error of the system under test.

The output signal from the MLS receiver representing the elevation angle during a test flight was recorded by a pen recorder. To obtain the position of the airplane, the

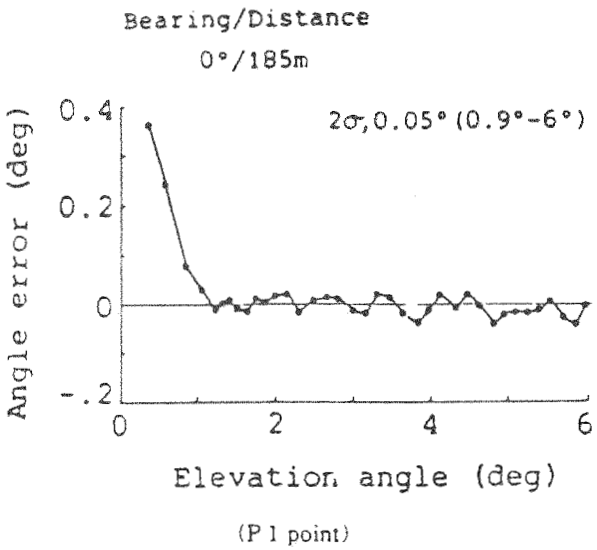

Fig. 4. Elevation angle error.

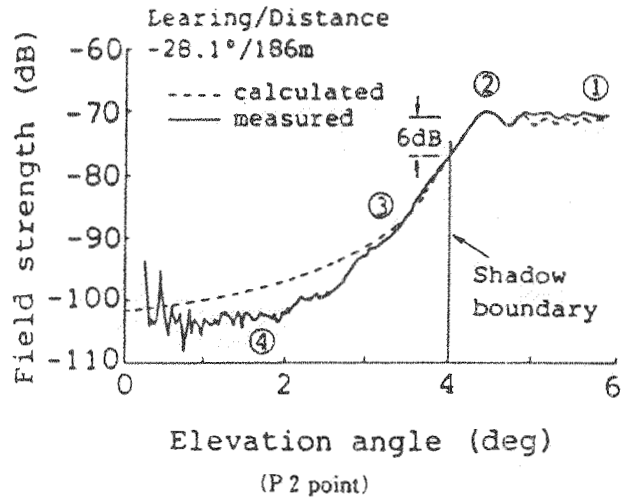

Fig. 5. Field strength in the diffraction area.

bearing signal from a VOR (VHF omnidirectional radio range) and the distance signal from DME (distance measuring equipment) were recorded simultaneously. A dwell-gate method was used for the signal processing on the MLS receiver.

3.2 Method of experiment

The experiment was carried out by using MLS elevation guidance equipment on the apron of Sendai Airport. The central direction of the horizontal scanning beam was set parallel to the front walls of the buildings as shown in Fig. 3. The buildings are situated at the left side of the guidance system keeping distances from 70 to 260 m, and bearings of -10° to -60°. The elevation angles of the tops of the roofs of the buildings are from 2.6° to 4°.

The measuring points on the ground site are situated at the front of the guidance system (P1, 185 m) and in the diffraction area of the hanger B (P2 and Pe); P1 is in a gap of a specular reflection area by building A and hanger B. This is suitable for knowing the inherent characteristics of the system, since almost no reflection and diffraction due to the buildings occur.

To determine the diffraction characteristic at a far distance, horizontal orbit flights were carried out with a radius of 7 NM (13 km) and three different heights.

The ground front of the guidance system is almost flat and covered by concrete,

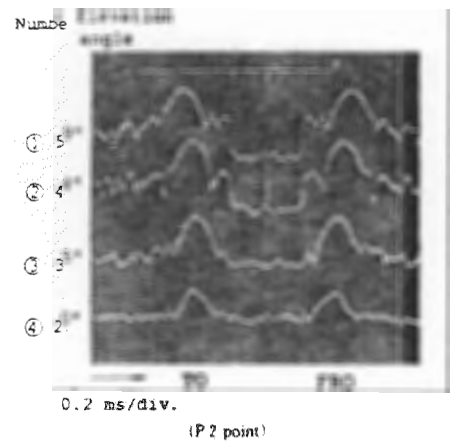

Fig. 6. Beam envelopes received.

except for some parts which are covered by asphalt-concrete.

4. Experimental Results and Discussion

Figure 4 shows the angle error measured at the apron (P1) which is in front of the elevation guidance system (separated from it by 185 m).

2σ of the error between the elevation angle 0.9° to 6° is 0.05°. This value shows that the accuracy of the apparatus is adequate, since this is less than half the internationally specified value.

The elevation angle is about 1° and increases toward the front because the scanning of the beam is stopped at 0°. Hence, there is a cut on the time axis of the receiving beam envelope causing a severe distortion in the waveform. In practice, this is not a problem, since an elevation guidance greater than 0.9° is used according to international regulations.

The fluctuation of the field strength of the scanning beam was small, i.e., within ±0.5 dB, and this was almost constant.

As described in the foregoing, the angle error and field-strength fluctuation in an area surrounded by buildings are adequately small if they cause no reflection and diffraction.

4.2. Diffraction-field strength

Figure 5 shows an example of the field-strength characteristic at P2 (in a diffraction area); the solid line denotes measured values and the broken line the calculated values. Figure 6 shows the beam envelope waveforms with four elevation angles received at P2.

The results show a typical diffraction-field characteristic, i.e., the electrical field strength on a shadow boundary (about 4°) is lower than that at a high elevation angle by 6 dB; and with an elevation angle above the shadow boundary, the waveforms are oscillatory. The calculated values (broken line) were obtained by replacing the hanger with a knife-edge-shaped perfect conductor using the uniform geometrical theory of diffraction [7] (see the Appendix). The calculated values above -90 dB agree with the measured values.

In general, it is known in the calculation of the diffraction electric-field that its discontinuity occurs if high-order diffraction waves (slope diffraction waves) are not taken into account around the unobstructed view-line [8, 9]. The field strength of the slope diffraction waves of the scanning beam of the MLS guidance has little effect on the peak power (field strength) of the scanning beam, since the strength is lower than that of the diffraction wave by about 18 dB according to the calculation. The slope diffraction wave has a significant effect on the angle error around the shadow boundary, as described in the following section.

The numbers indicating the waveforms of the beam-envelopes shown in Fig. 6 correspond to those in Fig. 5. Waveform (1) showing the elevation angle of 5.9° can be

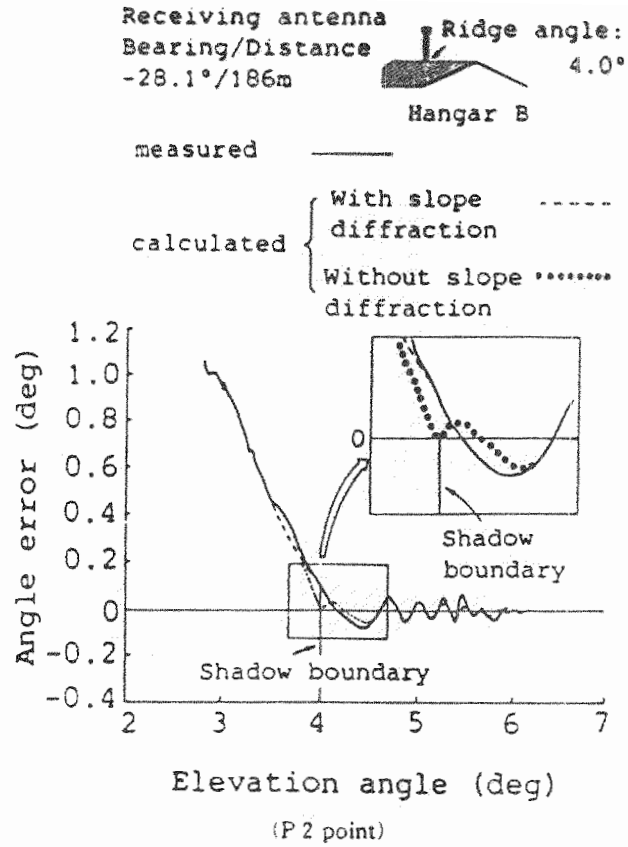

Fig. 7. Diffraction error.

considered as a totally direct wave; (2) is a combined wave of the direct and diffraction waves, above the shadow boundary by 0.4°, although this has no significant difference from (1); (3) and (4) are the diffraction waves alone, and their time intervals are not changed although their elevation angles are reduced.

4.3 Diffraction error

Figures 7 and 8 show the angle errors in the diffraction area, the solid lines denote experimental values, and the broken lines denote calculated values taking into account the slope diffraction waves due to the TUD. The enlarged graph within Fig. 7 shows the computed results derived from the direct and diffraction waves alone (i.e., excluding the slope diffraction wave).

Let us consider the error characteristic shown in Figs. 7 and 8 divided into three regions: above the shadow boundary, on the line, and below the line.

(i) Region above shadow boundary

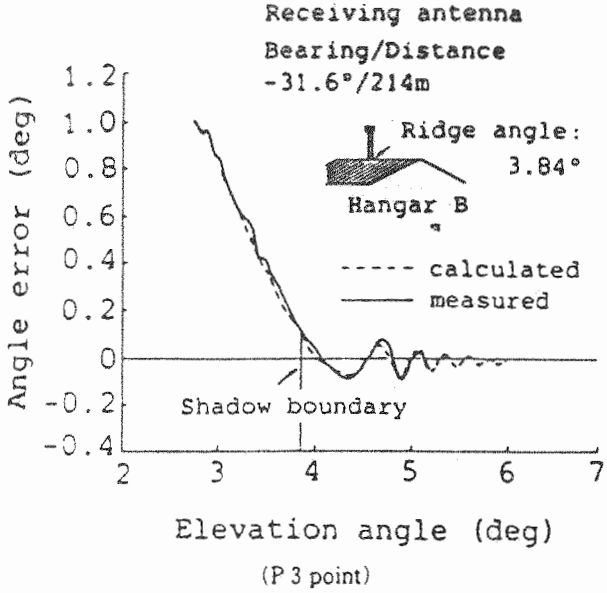

(P 3 point)

Fig. 8. Diffraction error.

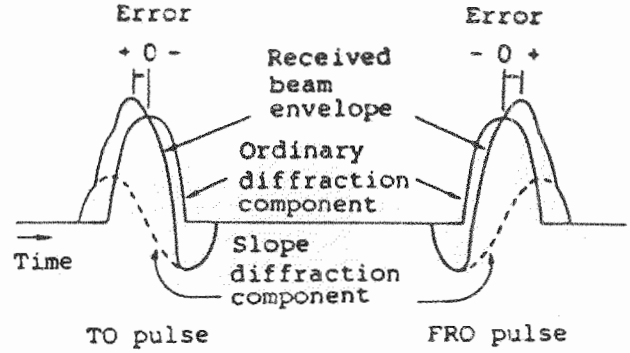

Fig. 9. Occurrence of error on the shadow boundary.

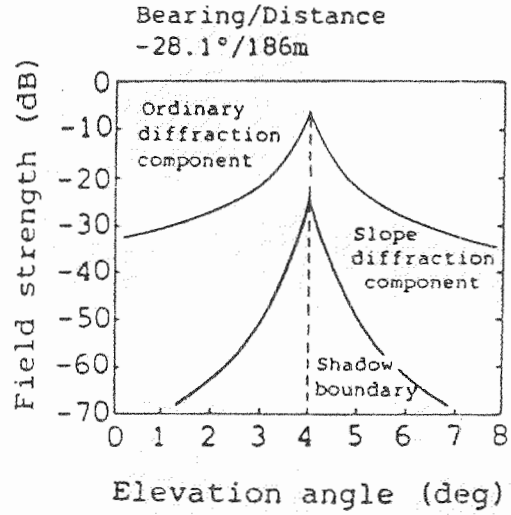

Fig. 10. Field strength of ordinary diffraction component and the slope diffraction component (calculated).

In the region above the shadow boundary, the error fluctuates in both the positive and negative directions, and the fluctuation decreases when the elevation angle increases. In this region, mainly the result of the direct and diffraction waves is received. When the elevation angle of the beam received increases, the relative phase between the direct and diffraction waves rotates, and a distortion which changes periodically occurs in the wave received. The angle measured changes with the same period as that of the relative phase, forming an error as shown in the region above 4° in Fig. 7. The error follows a typical shape of a decaying oscillation since the amplitude of the diffraction wave reduces with the increase of the distance from the shadow boundary (as shown by a thin line in Fig. 10), while the amplitude of the direct wave is almost constant. As described in the foregoing, the mechanism of causing the error is considered to be the same as that in the reflection multipath wave [10].

The maximum error is 0.08°; this is the same order as that of the acceptable multipath for the system design specification, i.e., a small margin.

According to the calculation derived from a simulation (in which a hanger is replaced by a knife-edge shape conductor), this value does not change significantly with a beamwidth of 1 or 2° which is usually employed for most elevation guidance equipment. The calculation of the diffraction error above the shadow boundary depends on the distances between the transmission antenna, knife edge and the receiving point, and the beamwidth. It was found that the beamwidth notably affects the damping rate of the error (e.g., the rate reduces to one-half when the beamwidth is doubled), and the range of the oscillation increases.

(ii) Region around shadow boundary

The error fluctuation in an elevation angle around a shadow boundary (above or below about 0.5°) is slightly less than an inclination of -1, and this is about +0.1° on the angle of the shadow boundary. The results of angle error calculated without the slope diffraction wave agree well with the results observed, except for around the

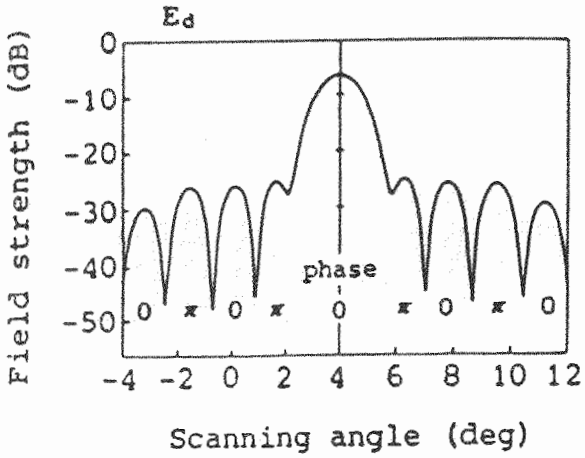

Fig. 11. Beam envelope of ordinary diffraction wave at 4°.

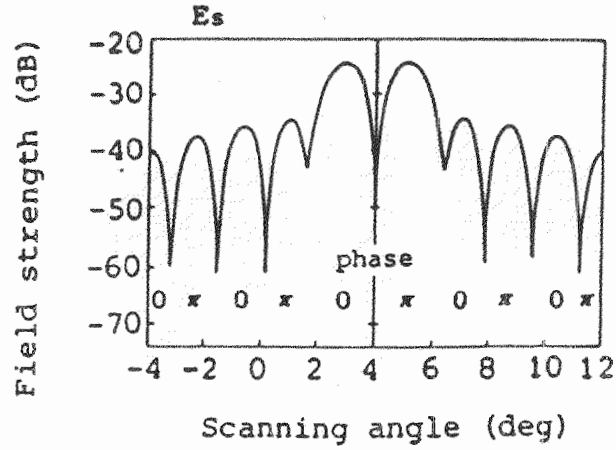

Fig. 12. Slope beam envelope at 4°.

shadow boundary. These values differ significantly around the shadow boundary as shown by the dotted line in Fig. 7.

Let us examine the effect of the slope diffraction wave. Figure 9 shows a model of the occurrence of error on the shadow boundary taking into account the slope diffraction wave; the thin line is the diffraction wave, the broken line, the slope diffraction wave, and thick line, the resultant wave. Two receiving pulses (the resultant wave) distort toward the positive angle error as shown in the figure, since the slope diffraction wave is symmetrical to the center of the scanning point. This is why the angle error is not zero but a positive value.

Let us examine quantitatively the characteristics of the diffraction and slope diffraction around the shadow boundary using simulations. The directivity of the scanning antenna (beamwidth 1.5°, sidelobe level -20 dB) was calculated, and the field strength of the diffraction wave and slope diffraction wave with the geometrical conditions at P2 and the receiving elevation angle was also calculated by using Eqs. (A4) and (A8) in the Appendix. Figure 10 shows the results with reference to the direct wave. The maximum value occurs at an elevation angle of 4° above the shadow boundary, and the slope diffraction wave is lower than the diffraction wave by about 18 dB.

Figures 11 and 12 show the beam envelopes of the diffraction waves and slope diffraction wave with the foredescribed elevation angle. The beam envelope of the slope diffraction wave which is derived from the partial differentiation $\partial E(\theta)/\partial\phi_s$ makes a bimodal shape having a relatively high level, and its phase is asymmetrical, as shown in Fig. 12, since the directivity of the scanning beam is as narrow as 1.5° and the slope of the field strength is sharp. These cause a distortion and angle error in the resultant wave of the diffraction wave and slope diffraction wave.

The effect of the slope diffraction wave on the angle error reduces when the receiving elevation angle is separated from the shadow boundary either above or below it, since the decay of the slope diffraction wave is greater than that of the diffraction wave, as shown in Fig. 10.

This shows that the calculated results agree well with the experimental results even around the shadow boundary, if the slope diffraction wave is taken into account (Fig. 7).

(iii) Region below shadow boundary

The error increases simply with the reduction of the elevation angle with a slope of -1 as far as the measurement is possible (the measure is limited by the reduction of the field strength). The waveform of envelope of the scanning beam received at the shadow region is constant having information of the angle of the shadow boundary, independently of the elevation angle of the receiving antenna. The waveform of its envelope is stable [(3) and (4) in Fig. 6], while the amplitude changes (e.g., as shown by the solid line in Fig. 5 for P2).

In this region, therefore, the angle error is inversely proportional to an elevation angle. This creates a false signal in an airplane command indication to reduce its

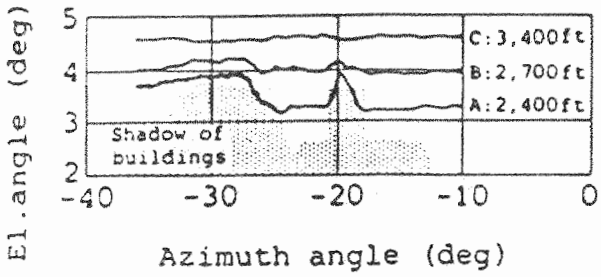

(7 NM orbit flight, Az-40°-0°)

Fig. 13. Elevation angle measured by flight experiments.

flying height; in the worst case, the same command indication continues even if the airplane already has reduced its height. The elevation error on the shadow boundary is about 0.1° in this case.

If the elevation angle of the top of a building is within the beam scanning range, the error has the same shape around the elevation angle, even in the case of another building which has different elevation angle. This is confirmed by measurements of the diffraction errors due to other hangars.

4.4 Result of experimental flights

Diffraction errors in a far region were obtained by using actual flights. Figure 13 shows the results of flight experiments (radios 7 NM, MLS bearing -40° to 0°), taking a flight height as a parameter. The projection of buildings at radios of 7 NM is shown in the same figure.

When the airplane entered the shadows of buildings, the measured angles indicate the elevation angle of the top of the buildings (A: 2400 ft), despite the fact that the airplane flew at almost constant height. When a flight occurred around the shadow boundary (B: 2700 ft), the angle measured increased by 0.1 or 0.2° in the bearing range of -30 to -20°. This is considered to be the effect of the slope diffraction wave. At a higher flight (C: 3400 ft) the variation of the angle measured is small, this is only recognizable around -30°.

The flight experiments show almost the same results as those of the ground experiments.

5. Conclusions

The characteristics of diffraction of the MLS elevation guidance caused by such objects in an airport as large buildings were analyzed experimentally.

The results show the characteristics of the electric field strength and measuring angle errors. It was found that the diffraction of the field strength due to large buildings has a typical pattern which can be modelled by a knife-edge shape.

The following points concerning the measuring angle errors also were found:

The magnitude of the error is oscillatory above the shadow boundary, the maximum error is 0.08°, and this reduces when the elevation angle increases. It is necessary to consider the slope diffraction wave in addition to the ordinary diffraction wave. A value of angle measured below the shadow boundary is higher than the real value, since the measured value is constant even if the receiving elevation angle changes.

It was also found that the angle errors calculated by using the UTD agree well with the experimental values. The proposed method of calculation will be useful for making the standard rules of setting the MLS and the MLS operational procedures, since the method can obtain the field strength and measuring angle errors in a diffraction region caused by large objects such as hangars.

Acknowledgement. The author wishes to express his thanks to the members of Sendai Airport Office, Sendai Air Base of the Maritime Safety Agency, and Iwanuma Branch of Electronic Navigation Research Institute for their cooperation in this experiment; to Mr. Matsumoto and Mr. Asakura, Senior Specialist, Electronic Navigation Research Department who assisted in the experiment and data processing; to Mr. Yamamoto, Senior Specialist, for his advice on the UTD analysis method; and to Dr. Katano, Deputy Director, E. N. Research Institute.

REFERENCES

1. ICAO. Aeronautical telecommunications. Annex 10, Vol. 1 (April 1985).
2. J. Capon. Multipath parameter computation for MLS simulation computer program. DOT-FA74W-AI-461 (April 1976).
3. H. W. Dedlien and R. J. Kelly. Microwave landing system: The new international standard. Ad. Electron. & Electron. Phys., 57, Academic Press, pp. 311-410 (1978).

4. J. Beneke, C. W. Wightman, A. M. Offet, and C. B. Vallone. Time reference scanning beam multimode digital processor. FAA-RD-78-84, Final Report (April 1978).
5. Katano, Matsumoto, Asakura, and Koremura. Construction of a prototype MLS elevation guidance and its measurements. Report of Electronic Navigation Research Institute, No. 49 (1985).
6. Matsumoto, Asakura, Koremura and Katano. Ground experiment of the MLS elevation guidance system. Report of Electronic Navigation Research Institute, No. 53 (1986).
7. R. G. Kouyoumjian and P. H. Pathak. A uniform geometrical theory of diffraction for an edge in perfectly conducting surface. Proc. IEEE, 62, 11, pp. 1448-1461 (Nov. 1974).
8. R. Tiberio and R. G. Kouyoumjian. Calculation of the high-frequency diffraction by two nearby edges illuminated at grazing incidence. IEEE Trans. Antennas & Propag., AP-32, 11, pp. 1186-1196 (Nov. 1984).
9. Norio Yamamoto. Method of representing multidiffraction including slope diffraction wave. Papers of Technical Group on Antennas and Propagation, I.E.C.E., Japan, AP98-71 (1986).
10. Asakura, Katano and Matsumoto. Reduction of multipath error in TRSB microwave landing system. Report of Electronic Navigation Research Institute, No. 37 (1982).

APPENDIX

CALCULATION OF DIFFRACTION FIELD

Let us calculate a diffraction field caused by an adequately long building (e.g., a hangar), by replacing it with a knife-edge shape. Assuming a geometrical relationship as shown in Fig. A1, the electric field strength above the shadow boundary (region I) and that below it (region II, or shadow region) are given, respectively, as follows:

(a) Region I

$$E_{t_1} = E_i + E_d + E_s \tag{A1}$$

(b) Region II

$$E_{t_2} = E_d + E_s \tag{A2}$$

where

E_{t_1}: electric field strength in region I

E_{t_2}: electric field strength in region II

E_i: electric field strength of direct wave

E_d: electric field strength of diffraction wave

E_s: electric field strength of slope diffraction wave

For simplicity, reflection waves from ground are ignored.

i) Component of direct wave

$$E_i = E(\theta)\cdot[\exp(-j\cdot k\cdot \rho_i)]/\rho_i \tag{A3}$$

where

$E(\theta)$: directivity of beam

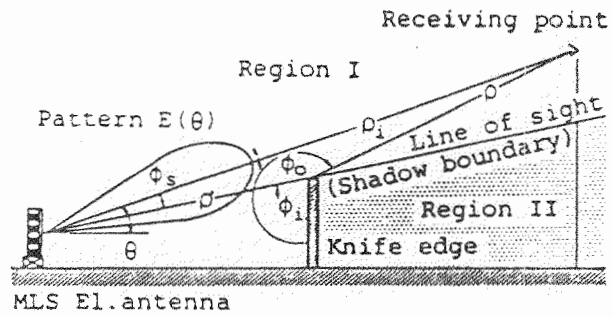

Fig. A1. Diffraction geometry.

$k = 2\pi/\lambda$ (λ being wavelength)

ii) Component of diffraction wave

$$E_d = E(\theta)\cdot\{[\exp(-j\cdot k\cdot \rho')]/\rho'\}\cdot D_{s,h} \cdot \sqrt{\rho'/\rho(\rho-\rho')}\,[\exp(-j\cdot k\cdot \rho)] \tag{A4}$$

where $D_{s,h}$ is the UTD diffraction function, and given by

$$D_{s,h} = -\frac{\exp(-j\cdot\pi/4)}{2\sqrt{2}\cdot\pi\cdot k} \cdot\left[\left\{F\left[2\cdot k\cdot L\cdot\cos^2\frac{(\phi_0-\phi_i)}{2}\right]\Big/\cos\frac{(\phi_0-\phi_i)}{2}\right\} - \left\{F\left[2\cdot k\cdot L\cdot\cos^2\frac{(\phi_0+\phi_i)}{2}\right]\Big/\cos\frac{(\phi_0+\phi_i)}{2}\right\}\right] \tag{A5}$$

transformation function is given by

$$F(X) = 2\cdot j\sqrt{X}\cdot\exp(j\cdot X)\int_{\sqrt{X}}^{\infty}\exp(-j\cdot\tau^2)\,d\tau \tag{A6}$$

and L is given by

$$L=\rho'\cdot\rho/(\rho'+\rho) \tag{A7}$$

iii) Component of slope diffraction wave

$$E_s=\frac{1}{j\cdot k\cdot\rho'}\cdot\frac{\partial D_{s,h}}{\partial_{\phi i}}\cdot\frac{\partial E(\theta)}{\partial\phi_s}\cdot\frac{\exp(-j\cdot k\cdot\rho')}{\rho'}\cdot\sqrt{\frac{\rho'}{\rho(\rho+\rho')}}\cdot\exp(-j\cdot k\cdot\rho) \tag{A8}$$

where partial differentiation of $D_{s,h}$ is given by

$$\frac{\partial D_{s,h}}{\partial\phi_i}=\frac{k\cdot L\cdot\exp(j\cdot 4/\pi)}{\sqrt{2\cdot\pi\cdot k}}\cdot\{[\sin\frac{(\phi_0-\phi_i)}{2}[1-F[2\cdot k\cdot L\cdot\cos^2\frac{(\phi_0-\phi_i)}{2}]]]\pm[\sin\frac{(\phi_0+\phi_i)}{2}[1-F[2\cdot k\cdot L\cdot\cos^2\frac{(\phi_0+\phi_i)}{2}]]]\} \tag{A9}$$

JESSE JONES
FAA TECHNICAL CENTER

THE DME/P MODEL

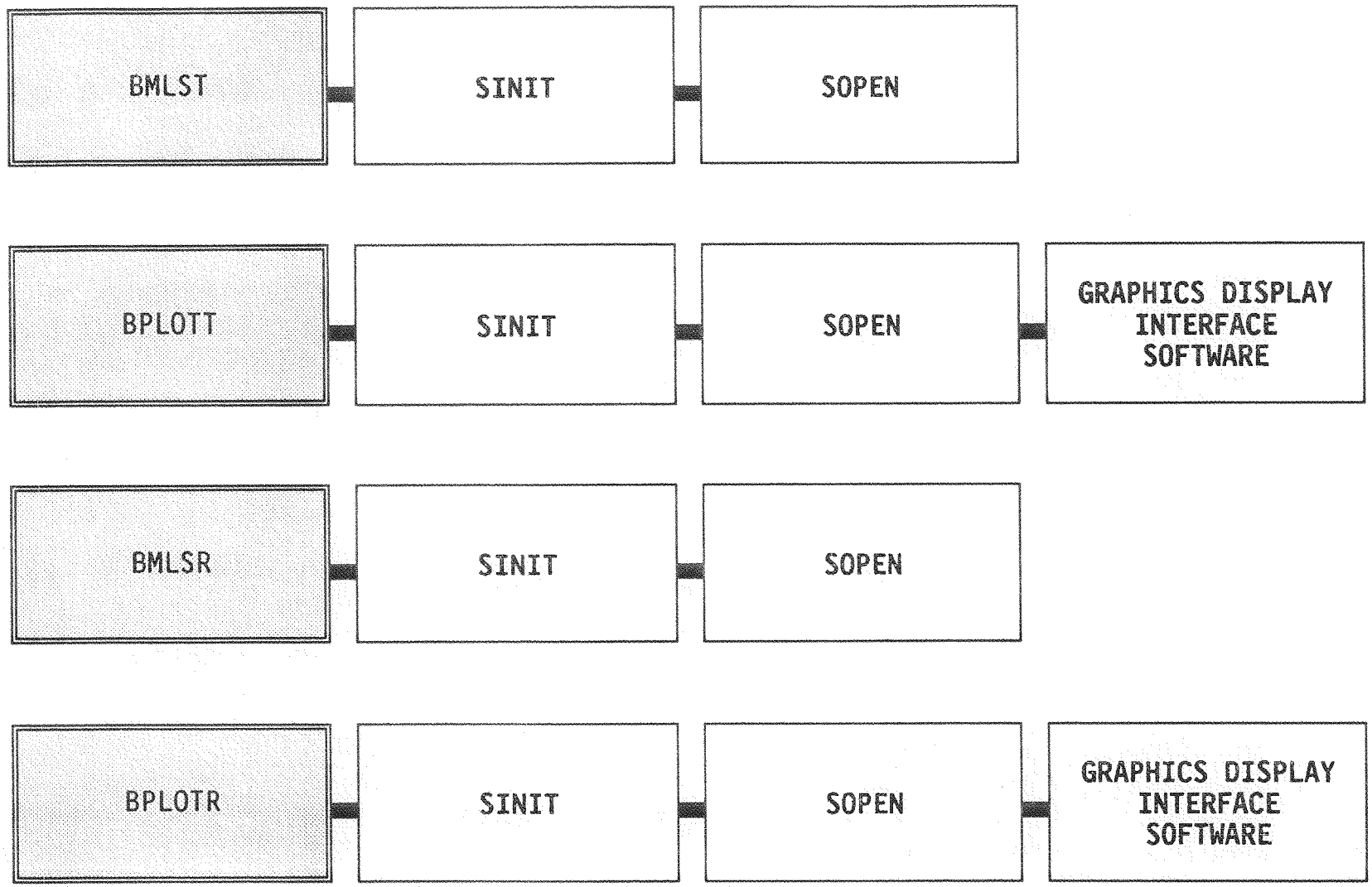

FORTRAN-77 STANDARD SOURCE CODE - CHECK COMPILER IF ANY PROBLEMS	SUBROUTINES SINIT & SOPEN ALONG WITH GRAPHICS DRIVER SUBROUTINES (SIPLOT, SNPLOT, SAXIS, SNUMBR, STITLE, SLINE, SSYMBL, EXTPLT, SCALIU, SCALUI) ARE WRITTEN BY THE USER TO ACCOMMODATE THE SPECIFIC OPERATING ENVIRONMENT IN WHICH THE MODEL IS INSTALLED. SAMPLE SUBROUTINES PROVIDED WILL BE ADAPTED TO OPERATING SYSTEM AND AVAILABLE GRAPHICS SOFTWARE BY THE USER.

STEPHAN KRUGER
OHIO UNIVERSITY

VALIDATION OF THE DME/P MODEL

MLS MATH MODEL VALIDATION: DME/P MODULE

Presented to
MLS MATH MODEL USERS GROUP MEETING
FAA TECHNICAL CENTER
ATLANTIC CITY, N.J.
NOVEMBER 6-7, 1991

by

STEPHAN J. KRUGER
AVIONICS ENGINEERING CENTER
OHIO UNIVERSITY
ATHENS, OHIO 45701

PROGRAM OBJECTIVE

VALIDATION OF THE (DME/P) MODULE OF THE (MLS) MATHEMATICAL MODEL

PROGRAM OF ACTIVITIES

- DEFINITION OF VALIDATION OBJECTIVES
- SELECTION OF TEST SITES
- TEST PLAN DEVELOPMENT
- COLLECTING FIELD DATA AND COMPARISON OF COLLECTED DATA WITH MODEL RESULTS
- MODEL REFINEMENT AS REQUIRED

- MODERN REGULATORY VS ENFORCED
- COMPLIANCE NEED ONLY AND CONVERSION OF CONTROLLED ONLY MULTI MODE BRANDS
- LEGAL NEW DRAFTSMANSHIP
- SELECTION OF LEGAL SUITE
- DERIVATION OF AVOIDANCE OBJECTIVES

PROGRAM OF VALIDATION

MULTIPATH ERROR PARAMETERS

- M/D RATIO
- TIME DELAY
- RELATIVE PHASE OF MULTIPATH PULSE
- RATE OF CHANGE OF RELATIVE PHASE (SCALLOPING RATE)

MODULAR ERROR EXAMINER

- WID RATIO
- LINE DELAY
- RELATIVE LAPSE OF MODULATION NOISE
- RATE OF CHANGE OF RELATIVE NOISE

(CONTROLLING RATE)

MULTIPATH SOURCES

- AIRCRAFT
- BUILDINGS
- RUNWAY HUMPS
- TERRAIN PLATES (RECTANGULAR AND TRIANGULAR)

NONTRADITIONAL SOURCES

- VIDEOTAPE
- BUSINESS
- ELEMENTARY SCHOOLS
- JEWISH AFFAIRS (BRANCHAVER AND TRIANGULAR)

VALIDATION OBJECTIVES

VERIFY THE CORRECT ESTIMATION OF THE MULTIPATH ERROR PARAMETERS FOR THE FOLLOWING PHENOMENA, ALL MULTIPATH SOURCES

A. PROPAGATION PORTION

- SHADOWING AND DIFFRACTION
- REFLECTION (SCATTERING)
- MULTIPATH EDITING

VALIDATION OBJECTIVES

(CONTINUED)

B. RECEIVER PORTION

- VERIFY THRESHOLDING FOR IA/FA MODES
- VERIFY PROPER GENERATION OF COMPOSITE PULSE
- VERIFY MODELING OF INTERMEDIATE FREQUENCY (IF) FILTER
- CONFIRM TRUE PULSE TOA DETERMINATION WITH AND WITHOUT MULTIPATH

A. EXCESSIVE NOISE

- AREAS UNACCEPTABLE FOR ANY NOISE
- AREAS NOISE CERTAIN TO COMPLAINT
- AREAS NOISE OR INTERMITTENT

NOISE (D) LEVEL

- AREAS NOISE JOY DESIRABLE INFORMATION

NOISE

- AREAS NOISE NOT LEGAL

B. EXCEPTIONAL NOISE

(CONTINUED)

AVIATION OBJECTIVES

VALIDATION OBJECTIVES

(CONTINUED)

C. PERFORMANCE ANALYSIS PORTION

- CMN FILTER
- PFE FILTER
- TOLERANCE BRACKETS

VALIDATION PHASE I

- DETERMINE AVAILABILITY OF DME/P DATA COLLECTED WITH PRECISION TRACKING
- TEST SITE SELECTION
- VALIDATION OF SCATTERING - SHADOWING FROM AIRCRAFT FOR SUPPORT OF CRITICAL AREA DEVELOPMENT
- VALIDATION FOR REFLECTIONS FROM BUILDINGS FOR SUPPORT OF CRITICAL AREA DEVELOPMENT

VERY DEAFTONNEAL
ROUTINES NON SIGNOUT OR CONLICYT
- AVIDVION NON INTERCHONS NOW

VERY DEAFTONNEAL
NON VIBCEVIL NON SONOUT OR CONLICYT
- AVIDVION OR ROVIEWING - SIVNONYNE

- LEXI BUS ANNCION

COTTECARD AUN MEDCION LOVCHNE
- DELIEWINE VAVIVBINLA OR INNEL DVLY

AVIDVION BIVSET

AIRPORT DIAGRAM

SAN JOSE INTL (SJC)
SAN JOSE, CALIFORNIA

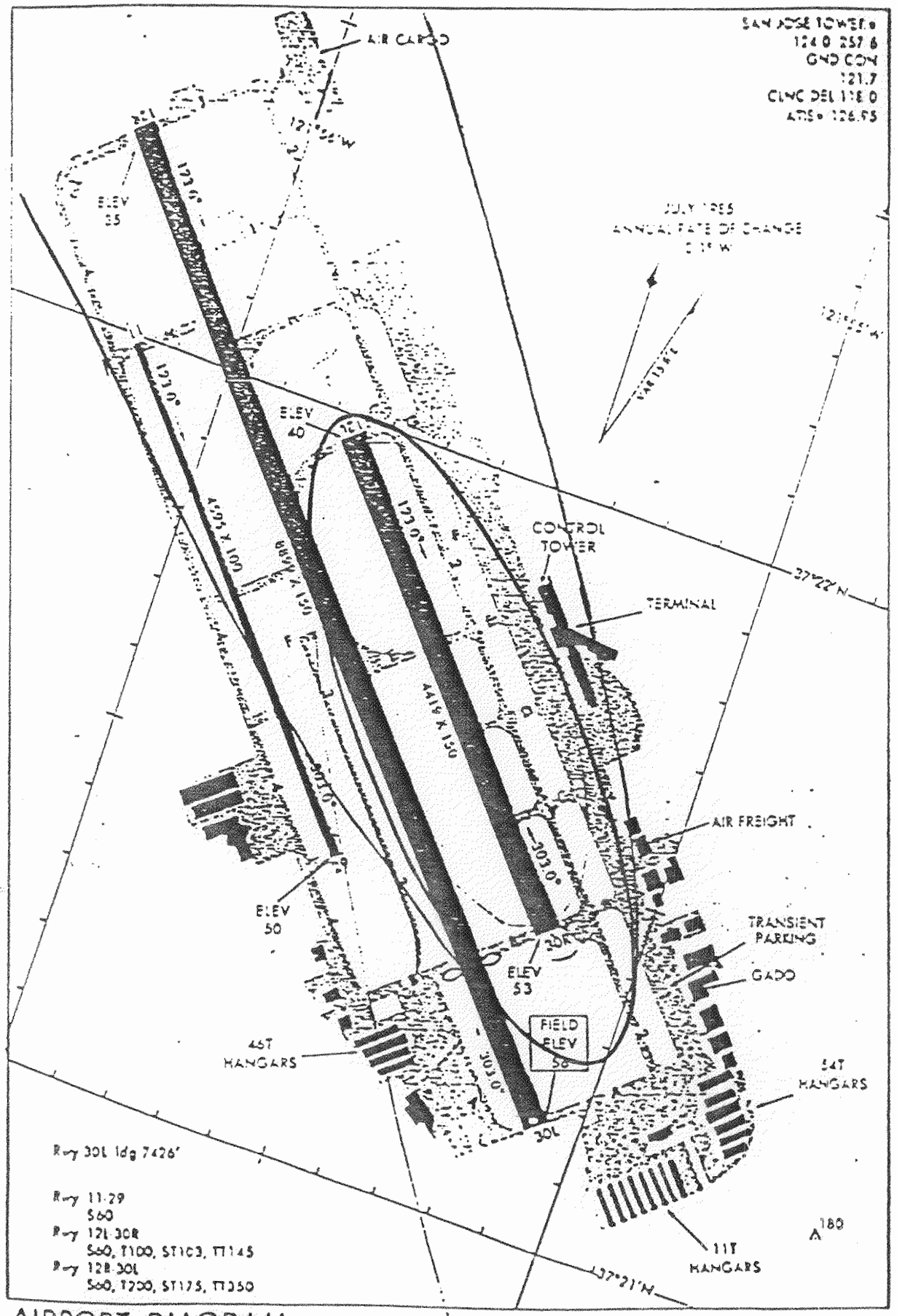

AIRPORT DIAGRAM

SAN JOSE, CALIFORNIA
SAN JOSE INTL (SJC)

VALIDATION PHASE II

- VALIDATE SHADOWING FROM BUILDINGS
- VALIDATE RUNWAY HUMP EFFECT (CAT II, CAT III)
- VALIDATE EFFECTS OF TERRAIN PLATES
- REFINE MODEL AS REQUIRED BY VALIDATION PROCESS

JAIKISHAN RAJENDRAN
OHIO UNIVERSITY

DME/P CRITICAL AREAS

STUDY OF DME/P CRITICAL AREAS

Presented at
MLS MATH MODEL USERS GROUP MEETING
FAA TECHNICAL CENTER
ATLANTIC CITY, N.J.
NOVEMBER 6-7, 1991

by
JAIKISHAN RAJENDRAN
AVIONICS ENGINEERING CENTER
OHIO UNIVERSITY
ATHENS, OHIO 45701

PROGRAM OBJECTIVES

- STUDY CAPABILITY OF AZIMUTH CRITICAL AREA TO PROTECT DME/P SIGNAL
  - COLLOCATED SITING
  - OFFSET SITING

- TO ENSURE DME/P SIGNAL QUALITY FOR ADVANCED PROCEDURES

PROGRAM PHASES

PHASE I: DETERMINATION OF SIMULATION PARAMETERS

PHASE II: DEVELOPMENT OF DME/P CRITICAL AREA CRITERIA FOR BASIC APPROACH PROCEDURES

PHASE III: DEVELOPMENT OF DME/P CRITICAL AREA CRITERIA FOR ADVANCED APPROACH PROCEDURES

PHASE I: DETERMINATION OF SIMULATION
PARAMETERS

PHASE II: DEAUTOMORPHIC OR DWEN OBJECT
VERY CHEERY FOR BASIC UNKNOWN
PROCEDURES

PHASE III: DEAUTOMORPHIC OR DWEN OBJECT
VERY CHEERY FOR ADVANCED UNKNOWN
PROCEDURES

PROGRAM PHASES

PHASE I

- DME/P CRITICAL AREA ERROR ALLOCATION
- MODIFICATION OF UTILITY ROUTINES FOR DME/P ERROR CONTOUR GENERATION
- DETERMINATION OF GRID SIZE AND OPTIMAL GRID SPACINGS
- DETERMINATION OF WORST CASE AIRCRAFT ORIENTATION
- VERIFY GRID SPACING FOR RUNWAY LENGTH EXTREMES

PHASE II

- SELECT SCENARIOS FOR SIMULATIONS
- GENERATE ERROR CONTOUR DATA AND PFE/CMN ERROR CONTOUR PLOTS FOR THE SCENARIOS IDENTIFIED ABOVE
- DEVELOPMENT OF DME/P CRITICAL AREA CRITERIA FROM ANALYSIS OF ERROR CONTOUR PLOTS
- VALIDATION OF CRITERIA THROUGH FLIGHT TESTS

- APPLICATION OF CRITERIA THROUGH HIGH LEVEL
  FLOW ANALYSIS OF ERROR CONTOUR MAPS
- DEVELOPMENT OF DATA CRITICAL VIEW CRITERIA
  IDENTIFIED AREAS
  ERROR CONTOUR MAPS FOR THE SCENARIOS
- GENERATE ERROR CONTOUR DATA AND LENGTH
- SELECT SCENARIOS FOR SIMULATIONS

PHASE II

PHASE III

- OUTLINE SIMULATION METHODOLOGY FOR DEVELOPING ADVANCED PROCEDURE DME/P CRITICAL AREA CRITERIA
- SELECT SCENARIOS FOR SIMULATIONS
- GENERATE SIMULATION DATA FOR SCENARIOS SELECTED.
- DEVELOPMENT OF CRITICAL AREA CRITERIA FOR ADVANCED PROCEDURES
- VALIDATION OF CRITERIA THROUGH FLIGHT TESTS.

- A STUDY OF CRUDDY THROUGH HIGH LEVEL ADVANCED PROCEDURES
- DEVELOPMENT OF CRITICAL VERY CRUDDY FOR CERTIFIED
- GENERATE SIMULATION DATA FOR SCENARIOS
- SENSITIVE SCENARIOS FOR SIMULATIONS
- CRITICAL VERY CRUDDY DEVELOPING ADVANCED PROCEDURE DATA
- OUTLINE SIMULATION METHODOLOGY FOR

PHASE III

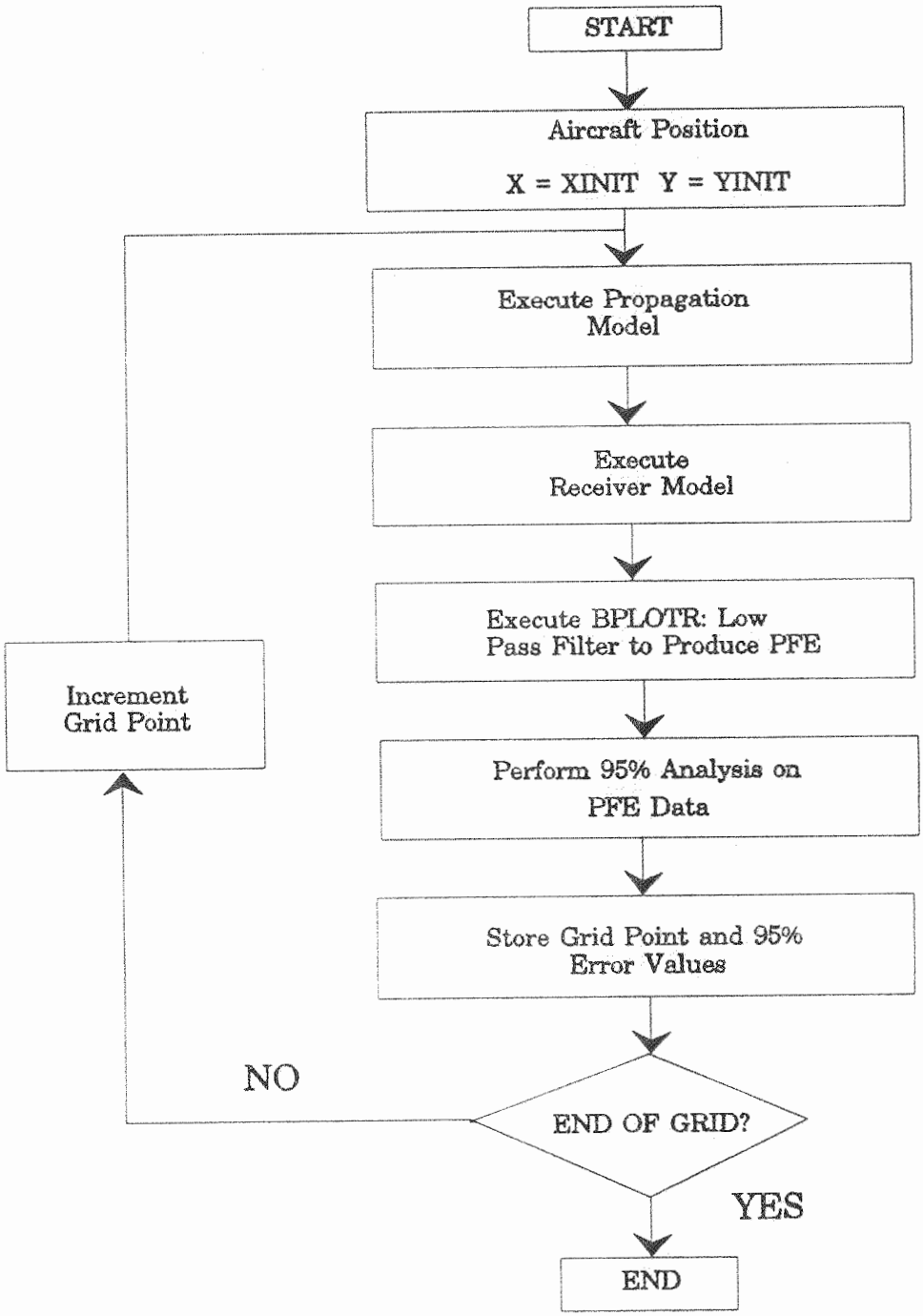
START
Aircraft Position
X = XINIT Y = YINIT
Execute Propagation Model
Execute Receiver Model
Execute BPLOTR: Low Pass Filter to Produce PFE
Perform 95% Analysis on PFE Data
Store Grid Point and 95% Error Values
END OF GRID?
NO
YES
Increment Grid Point
END

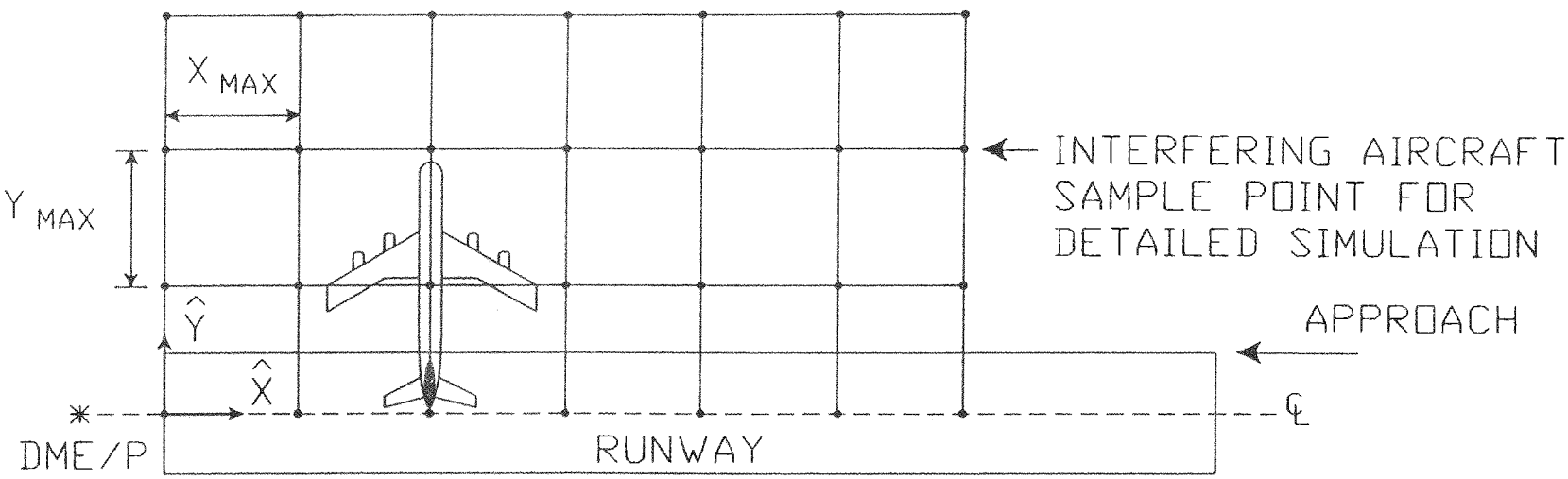

X_{MAX} ≡ MAXIMUM GRID SPACING IN X-DIRECTION

Y_{MAX} ≡ MAXIMUM GRID SPACING IN Y-DIRECTION

0040044

SAMPLE PFE PLOT FOR DME/P SUBSYSTEM

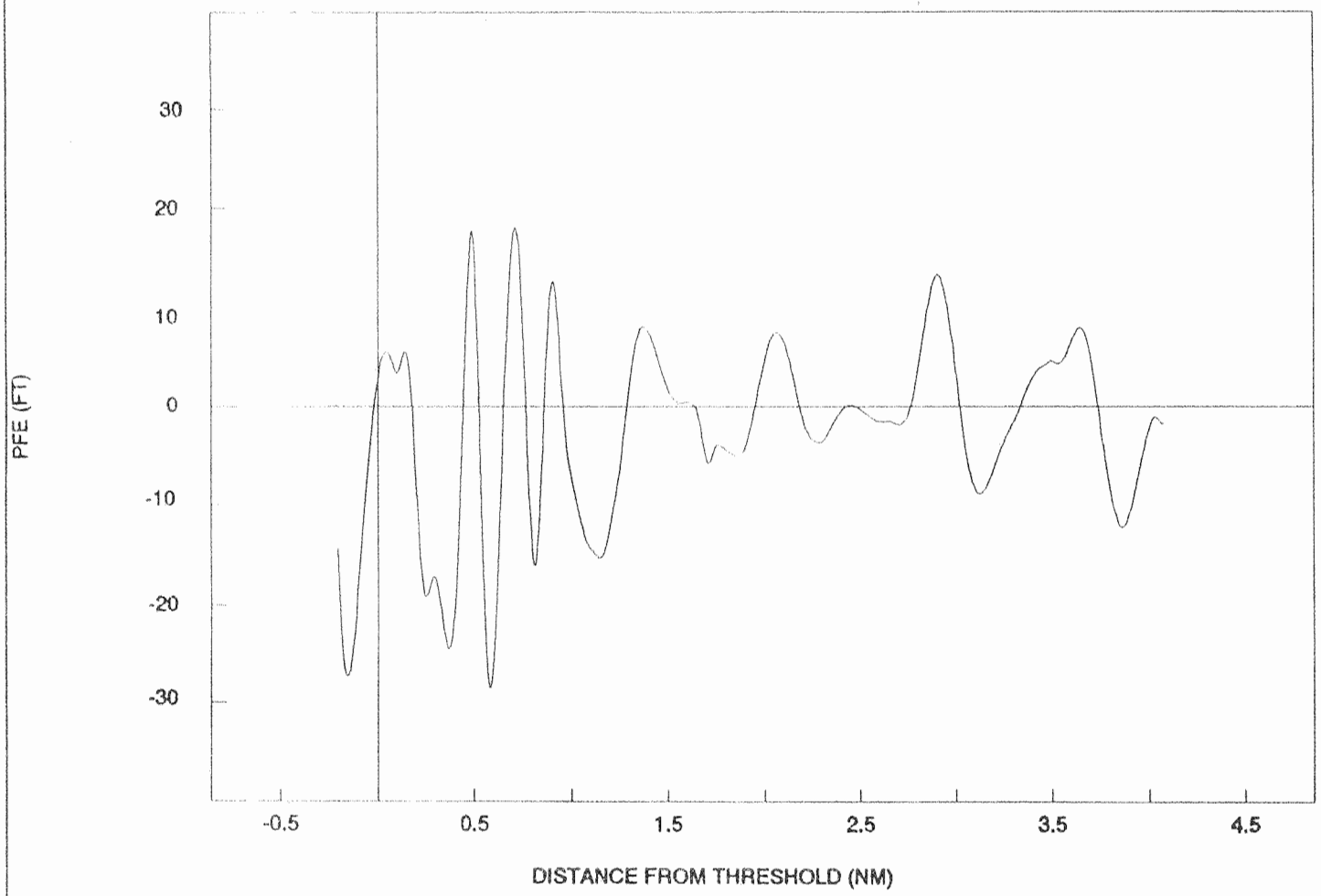

SAMPLE CONTOUR DATA

XPOS	YPOS	PFE	STWIN	ENWIN
-500.000	200.00	0.5000	2.268430	2.635036
-400.000	200.00	7.5000	0.000000	0.374273
-300.000	200.00	7.5000	0.000000	0.374273
-200.000	200.00	10.0000	0.000000	0.374273
-100.000	200.00	10.0000	0.954757	1.329000
0.000	200.00	5.0000	0.000000	0.374273
100.000	200.00	2.5000	0.908931	1.283175
200.000	200.00	1.0000	0.840193	1.214437
300.000	200.00	0.5000	2.268430	2.635036
400.000	200.00	0.5000	2.589210	2.955816
500.000	200.00	1.0000	0.000000	0.374273
600.000	200.00	1.0000	0.000000	0.374273
700.000	200.00	1.0000	0.000000	0.374273
800.000	200.00	1.0000	0.000000	0.374273
900.000	200.00	1.0000	0.565229	0.939482

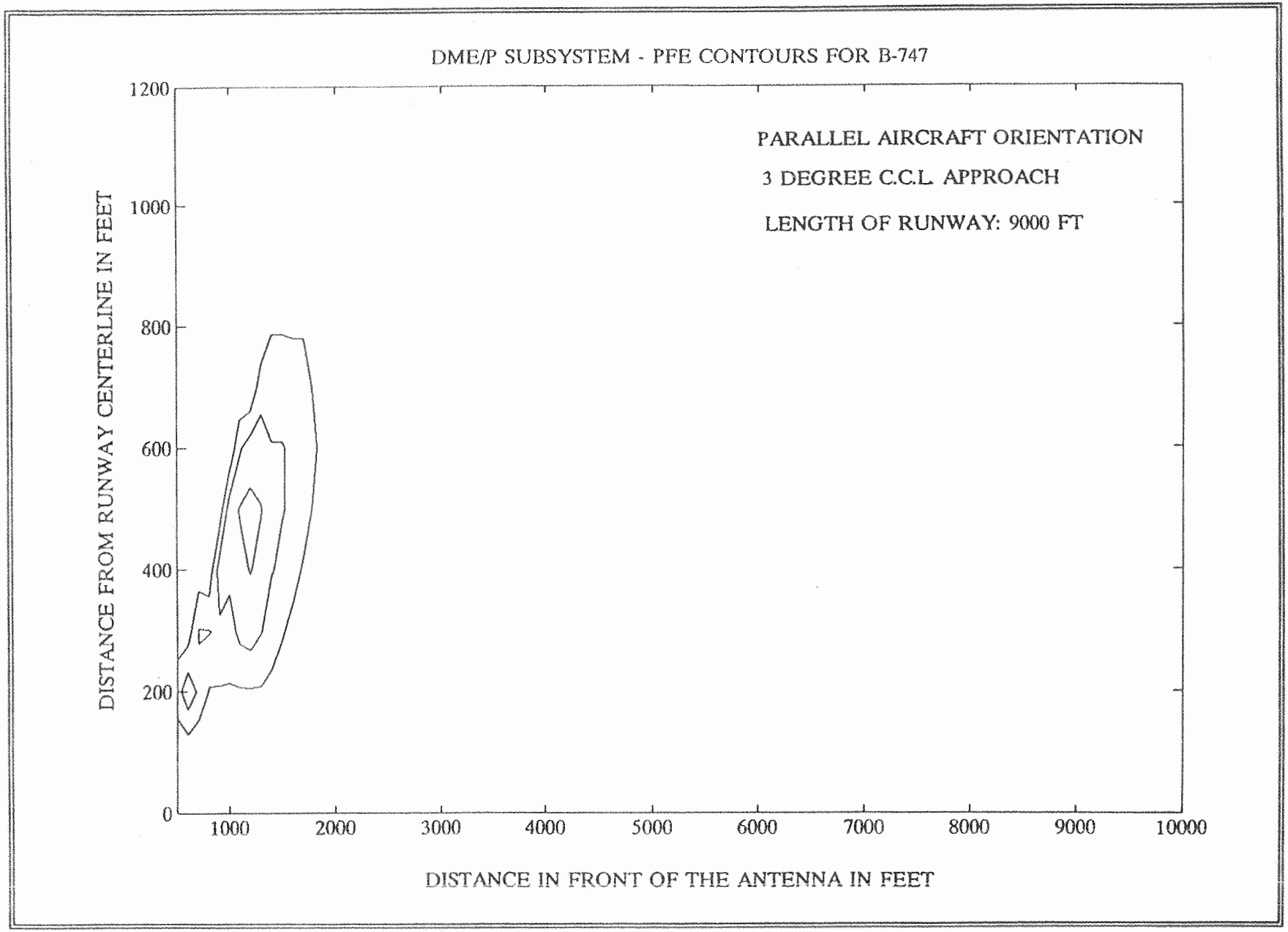
DME/P SUBSYSTEM - PFE CONTOURS FOR B-747
PARALLEL AIRCRAFT ORIENTATION
3 DEGREE C.C.L. APPROACH
LENGTH OF RUNWAY: 9000 FT
DISTANCE FROM RUNWAY CENTERLINE IN FEET
0
200
400
600
800
1000
1200
1000
2000
3000
4000
5000
6000
7000
8000
9000
10000
DISTANCE IN FRONT OF THE ANTENNA IN FEET

GRID SIZE DETERMINATION

- GRID SIZE IS A FUNCTION OF TRANSMITTER -OBSTACLE-RECEIVER GEOMETRY

- MINIMUM GRID SIZE IS OBTAINED BY EXCLUDING GEOMETRIES FOR WHICH:
  - (i) TIME DELAY $\leq$ 20 ns
  - (ii) TIME DELAY $\geq$ 300 ns
  - (iii) SCALLOPING FREQUENCY $\geq$ 10 RAD/SEC
  - (iv) SPECULAR POINT LOCATION ABOVE AIRCRAFT

- HIGH RESOLUTION GRID CAN BE USED SINCE CALCULATIONS ARE NOT COMPUTATIONALLY INTENSIVE

ESTIMATING GRID SIZE

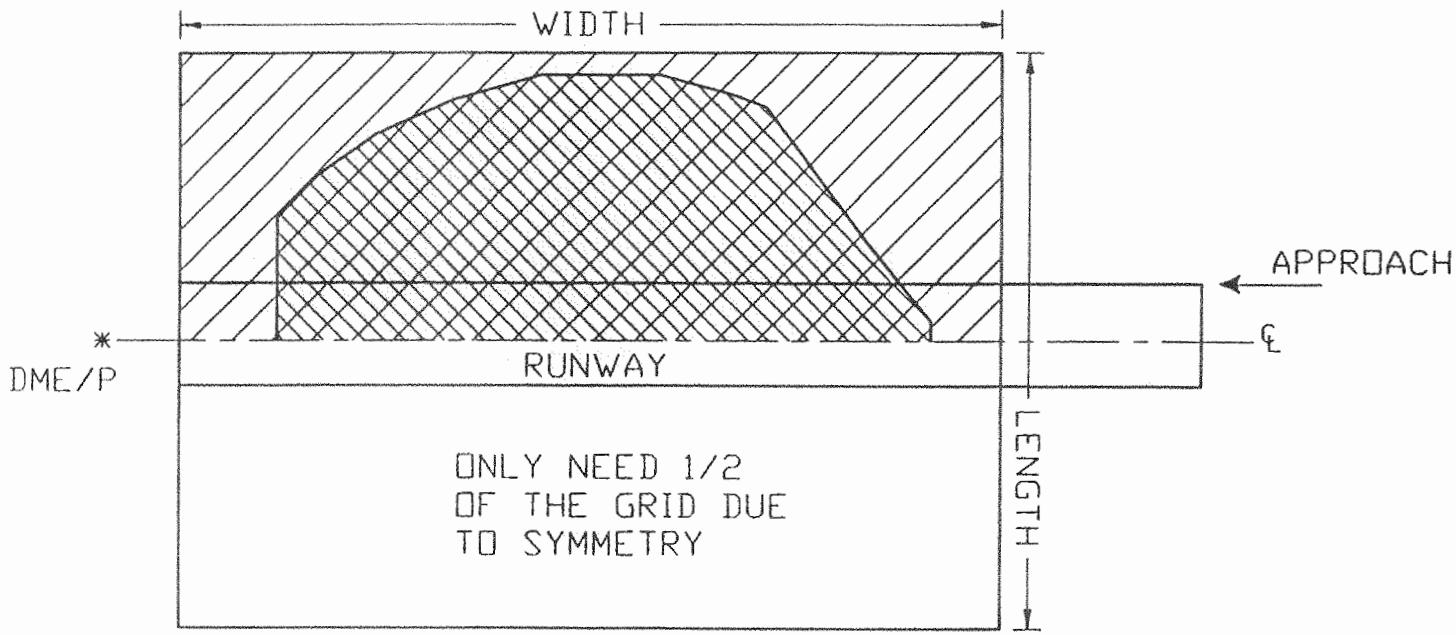

BOUNDS THE GEOMETRIES
THAT SATISFY 1,2,3

1) TIME-DELAYS < 300 NSEC
2) SCALLOPING FREQUENCIES < 10 RAD/SEC
3) SPECULAR REFLECTION POINT LOCATED
ON THE AIRCRAFT

GRID SPACING DETERMINATION

- GENERATE ERROR CONTOUR PLOT (MEAN RUNWAY LENGTH)
- LOCATE REGION OF MAXIMUM RATE OF CHANGE OF ERROR IN A LOCAL WINDOW
- GENERATE HIGH RESOLUTION CONTOUR IN THE LOCAL WINDOW
- DETERMINE 2-D FFT OF ERROR CONTOUR PLOTS
- LOW PASS FILTER OUTPUT OF FFT
- RECONSTRUCT ERROR CONTOUR PLOTS

GRID SPACING DETERMINATION

(CONTINUED)

- COMPARE RECONSTRUCTED CONTOUR TO ORIGINAL CONTOUR TO DETERMINE RECONSTRUCTION ERROR
- DECREASE FILTER BANDWIDTH UNTIL RECONSTRUCTION ERROR IS JUST WITHIN ACCEPTABLE LIMITS - PROVIDES MINIMUM BANDWIDTH REQUIRED
- KNOWING MINIMUM BANDWIDTH, APPLY NYQUIST SAMPLING THEOREM TO DETERMINE OPTIMAL GRID SPACING

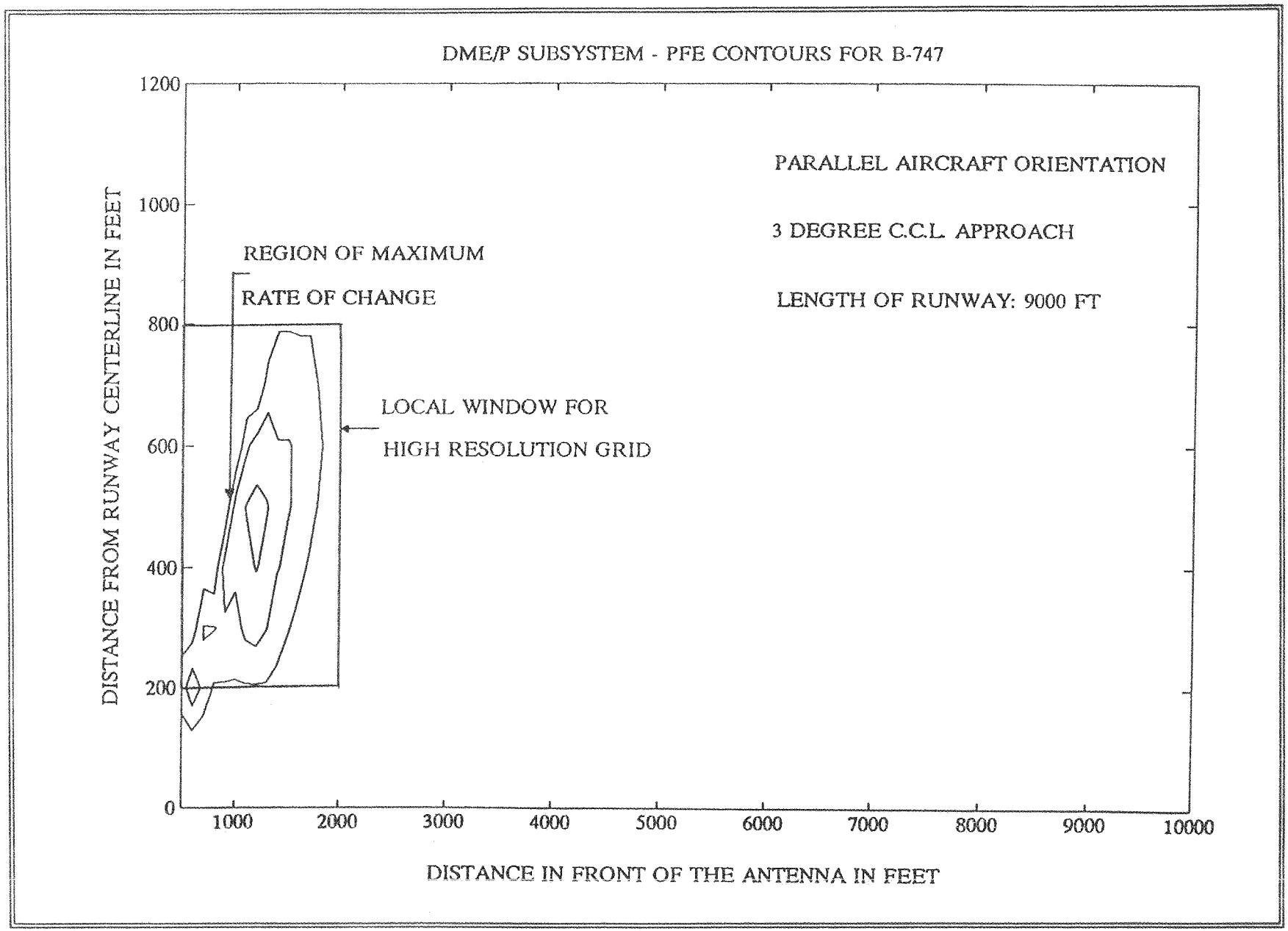
DME/P SUBSYSTEM - PFE CONTOURS FOR B-747
PARALLEL AIRCRAFT ORIENTATION
3 DEGREE C.C.L. APPROACH
LENGTH OF RUNWAY: 9000 FT
REGION OF MAXIMUM
RATE OF CHANGE
LOCAL WINDOW FOR
HIGH RESOLUTION GRID
DISTANCE FROM RUNWAY CENTERLINE IN FEET
DISTANCE IN FRONT OF THE ANTENNA IN FEET
0
200
400
600
800
1000
1200
1000
2000
3000
4000
5000
6000
7000
8000
9000
10000

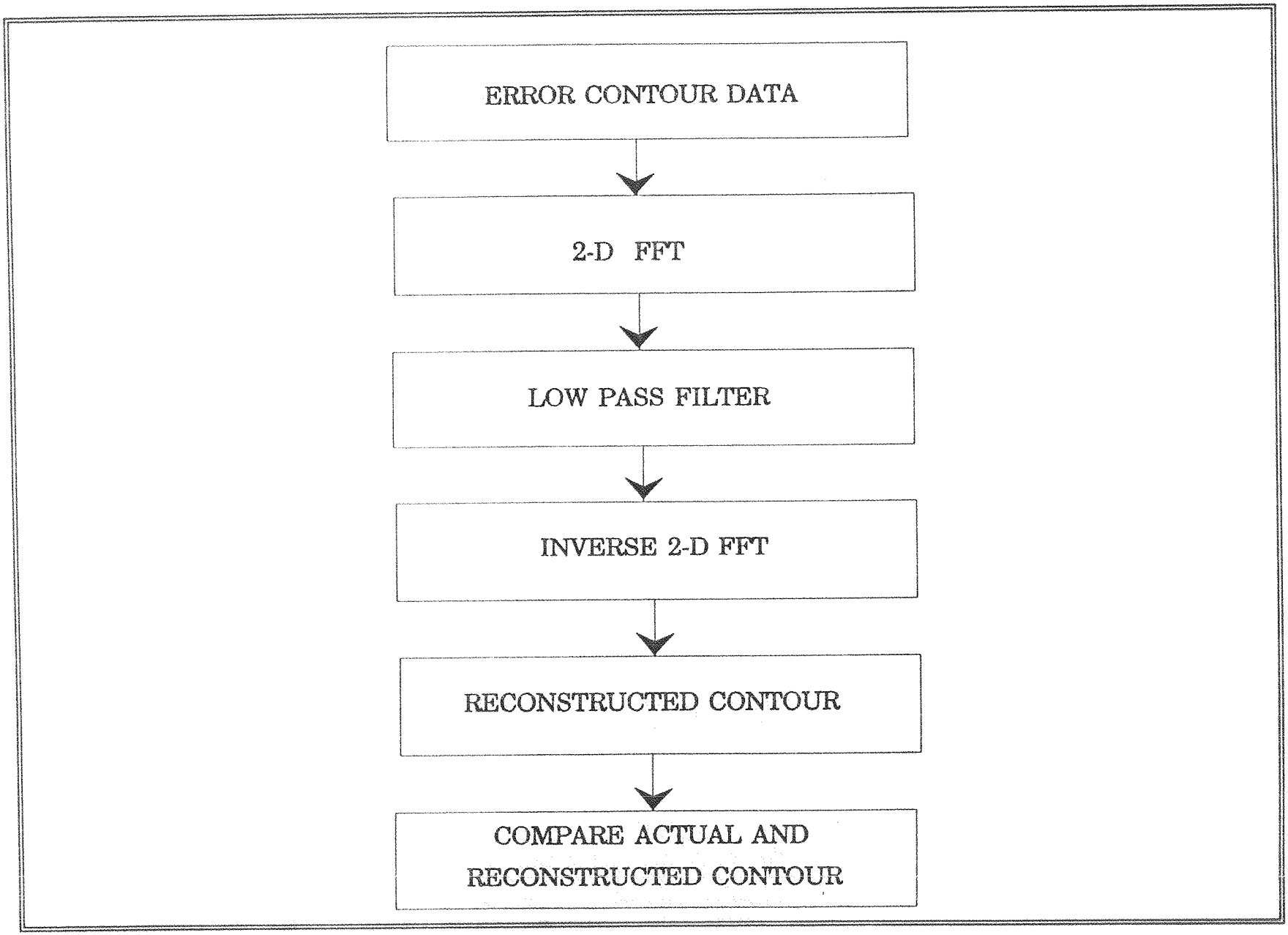
ERROR CONTOUR DATA
2-D FFT
LOW PASS FILTER
INVERSE 2-D FFT
RECONSTRUCTED CONTOUR
COMPARE ACTUAL AND RECONSTRUCTED CONTOUR

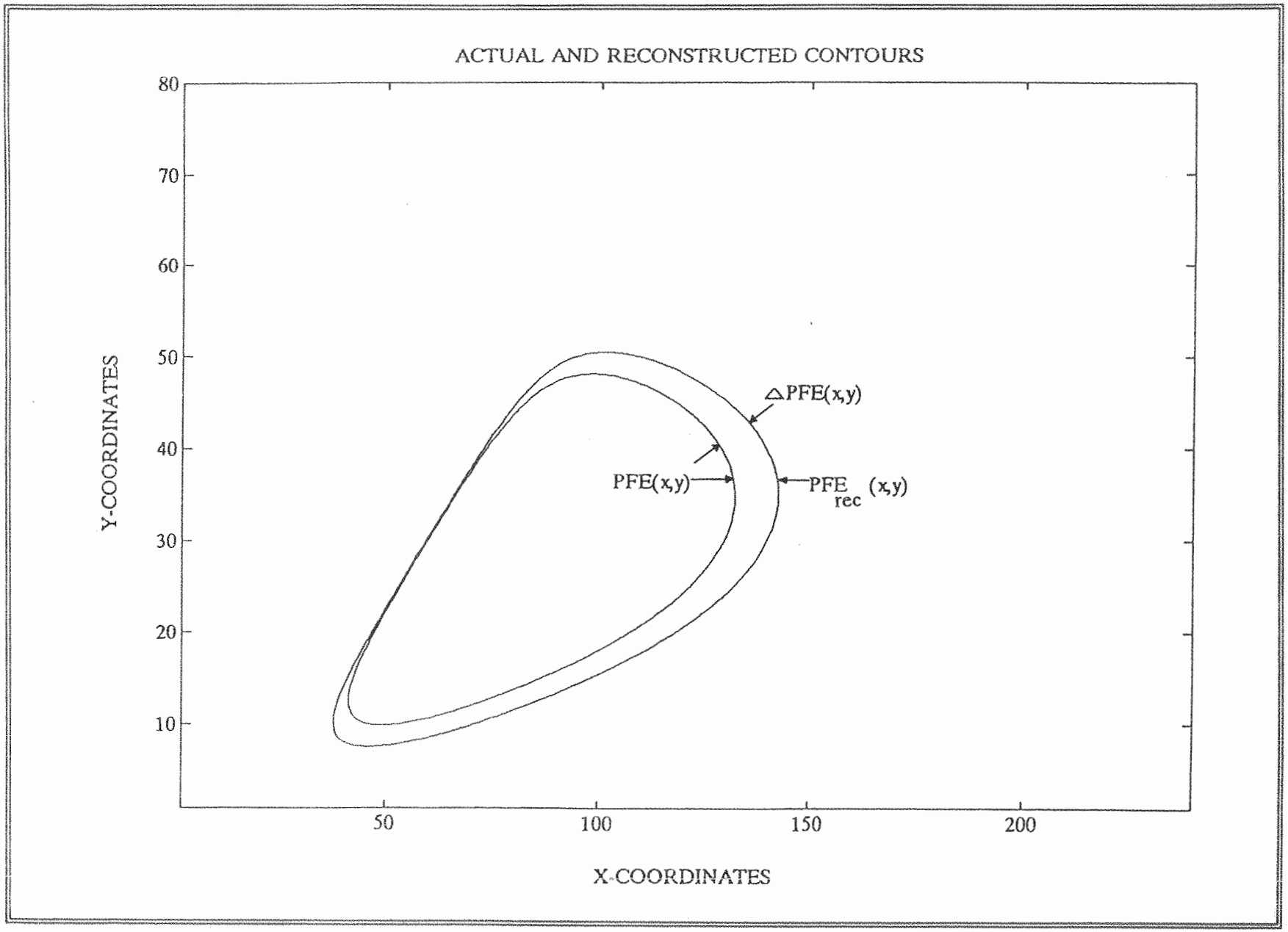
ACTUAL AND RECONSTRUCTED CONTOURS
Y-COORDINATES
X-COORDINATES
80
70
60
50
40
30
20
10
50
100
150
200
△PFE(x,y)
PFE(x,y)
PFE rec (x,y)

131

MICHAEL KLEINTZ
DLR, GERMANY

DIFFRACTION AT A RECTANGULAR PLATE

Diffraction at a Rectangular Plate

MLS-Model of Fresnel-Diffraction and a New Model by DLR

Dipl.-Ing. Michael P. Kleintz
DLR - Institute of Radio Frequency Technology
D-8031 Oberpfaffenhofen

DLR

MLS - Propagation - Model

- Multipath propagation with defined points of
  - Transmitter (XMTR) → fixed at the end of the runway
  - Receiver (RCVR) → variable along the flight path
- Propagation paths
  - Direct path between XMTR and RCVR
  - Reflection paths (e.g.)
    - Buildings
    - Building - Ground
    - Ground - Building - Ground
    - Building - Building
    - Aircraft etc.
  - Diffraction paths by shadowing (e.g.) by
    - Buildings
    - Aircraft
    - Runway humps etc.

SSR - Propagation - Model

- Multipath propagation points of
  - Transmitter (XMTR) → fixed at the periphery of the airport
  - Receiver (RCVR) → distributed over an area of constant height (e.g.)
- Propagation paths
  - Direct path between XMTR and RCVR
  - Reflection- and diffraction paths (e.g.)
    - Buildings
    - Building - Ground
    - Ground - Building - Ground
    - Building - Building etc.

Fresnel Diffraction (New Model)	
Ray Path	XMTR → rectangular plate → diffraction path to the RCVR
Taylor expansion of ray path	Around the middle of the plate (terms of 0 th, 1 st and 2 nd order without mixed term)
Fresnel-Integrals	Separable to factors in x and y
Range of validity	Region of a propagation-error $\leq \lambda/4$ → $\gg$ MLS-Model
Phase-Reference	Middle of the plate

[illegible]	[illegible]
[illegible]	[illegible]
[illegible]	[illegible]
[illegible]	[illegible]
[illegible]	[illegible]
[illegible]	[illegible]

Fresnel Diffraction (MLS-Model)	
Ray Path	Path of specular reflection
Taylor expansion of ray path	Around the specular point in terms of constant and second order (without mixed term)
Fresnel-Integrals	Separable to factors in ξ and η
Range of validity	Limited to the next (3 th ... 4 th) sidelobes around the main beam of specular reflection
Phase	No reference point defined

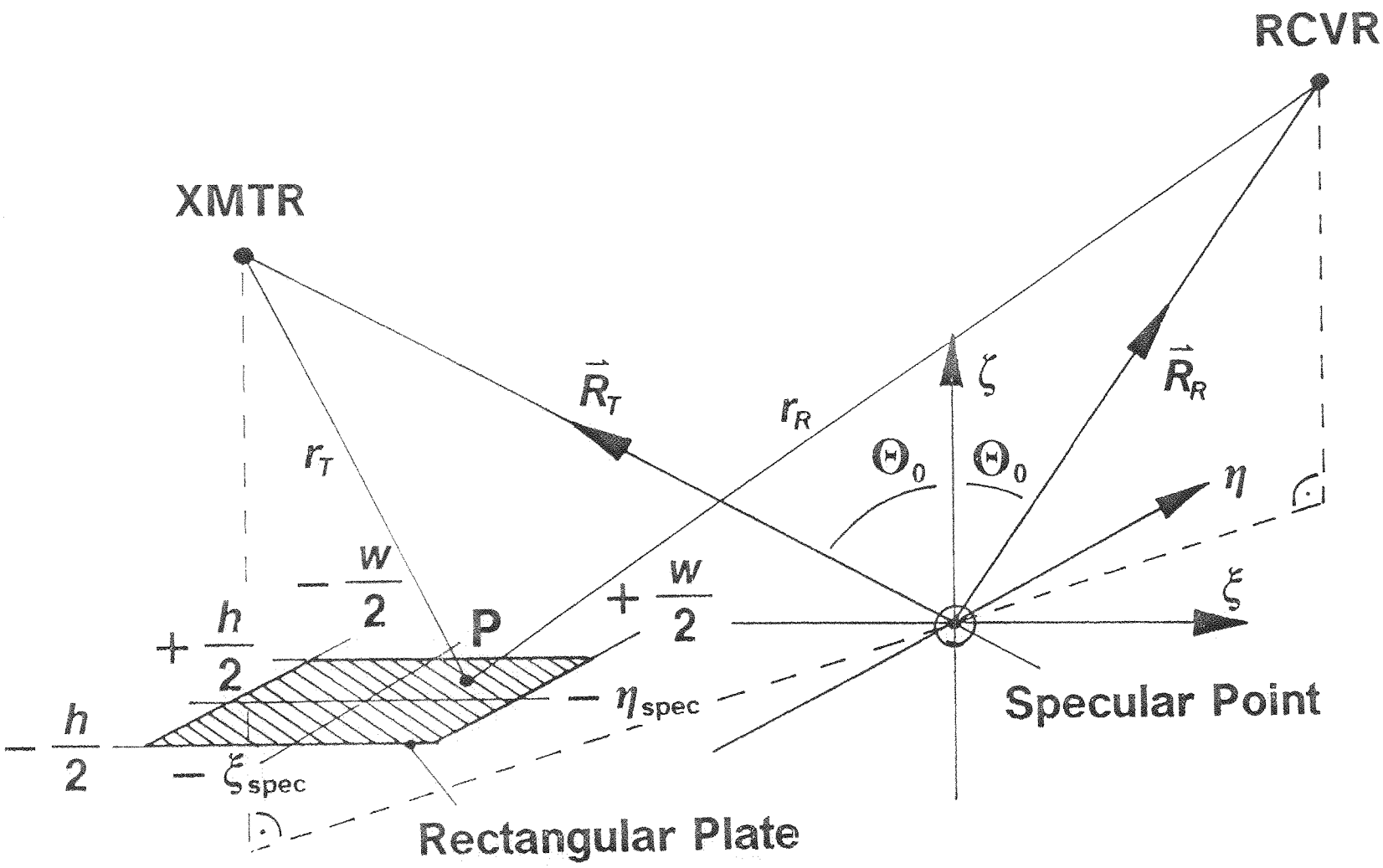

Geometry of Fresnel Diffraction (MLS-Model)

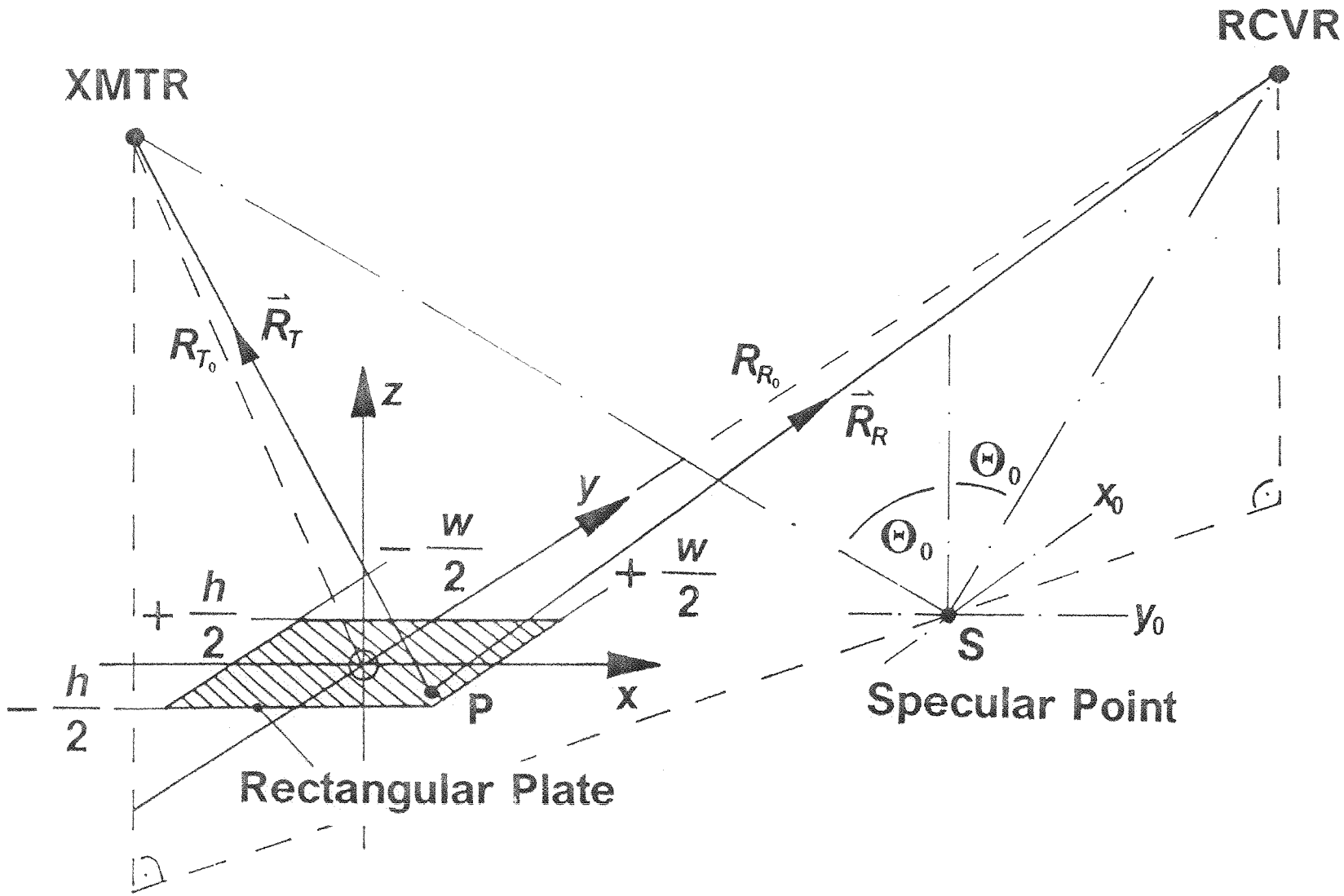

Geometry of Fresnel Diffraction (New Model)

Fresnel Diffraction (MLS-Model)

Specular Point

$$\vec{R}_{\text{spec}} = \frac{1}{z_T + z_R} \begin{pmatrix} x_T z_R + x_R z_T \\ y_T z_R + y_R z_T \\ 0 \end{pmatrix}$$

Fresnel Diffraction (MLS-Model)

Path of Specular Reflection

$$\vec{R}_T = R_T \begin{pmatrix} \alpha \\ \beta \\ \gamma \end{pmatrix} \qquad \vec{R}_R = R_R \begin{pmatrix} -\alpha \\ -\beta \\ \gamma \end{pmatrix}$$

with $\alpha^2 + \beta^2 + \gamma^2 = 1$

$$R(\xi, \eta) = \sqrt{R_T^2 + \xi^2 + \eta^2 - 2R_T(\alpha\xi + \beta\eta)} +$$

$$+ \sqrt{R_R^2 + \xi^2 + \eta^2 + 2R_R(\alpha\xi + \beta\eta)} \approx$$

$$\approx R_T + R_R +$$

$$+ \frac{R_T + R_R}{2 R_T R_R} \left[\xi^2 \left(1 - \alpha^2\right) + \eta^2 \left(1 - \beta^2\right) \right]$$

Fresnel Diffraction (MLS-Model)

Radii of Fresnel Zones

$$R_f = \sqrt{\lambda \frac{R_T R_R}{R_T + R_R}}$$

Projections to ξ- and η-axes

$$R_{f_\xi} = \frac{R_f}{\sqrt{1 - \alpha^2}} \qquad R_{f_\eta} = \frac{R_f}{\sqrt{1 - \beta^2}}$$

Fresnel Diffraction (MLS-Model)

Integration of all phase contributions over the rectangular area of the plate

$$\rho_{\text{geom}} = \text{const} \cdot e^{-jk(R_T + R_R)} \cdot$$

$$\cdot \int_{-\frac{w}{2} - \xi_{\text{spec}}}^{\frac{w}{2} - \xi_{\text{spec}}} e^{-j\pi\left(\frac{\xi}{R_{f_\xi}}\right)^2} d\xi \cdot$$

$$\cdot \int_{-\frac{h}{2} - \eta_{\text{spec}}}^{\frac{h}{2} - \eta_{\text{spec}}} e^{-j\pi\left(\frac{\eta}{R_{f_\eta}}\right)^2} d\eta$$

Fresnel Diffraction (New Model)

Path of Diffraction

$$\vec{R}_{T_0} = \begin{pmatrix} x_T \\ y_T \\ z_T \end{pmatrix} \qquad \vec{R}_{R_0} = \begin{pmatrix} x_R \\ y_R \\ z_R \end{pmatrix}$$

$$R(x, y) = \sqrt{R_{T_0}^2 + x^2 + y^2 - 2(x\,x_T + y\,y_T)} +$$

$$+ \sqrt{R_{R_0}^2 + x^2 + y^2 + 2(x\,x_R + y\,y_R)} \approx$$

$$\approx R_{T_0} + R_{R_0} + \Delta R_{0_x} + \Delta R_{0_y} +$$

$$+ c_x (x - x_0)^2 + c_y (y - y_0)^2$$

Fresnel Diffraction (New Model)

Path of Diffraction (Abbreviations)

Terms for Phase Correction

$$\Delta R_{0_x} = -\frac{1}{2} \cdot \frac{\left(\frac{x_T}{R_{T_0}} + \frac{x_R}{R_{R_0}} \right)^2}{\frac{1}{R_{T_0}} \left(1 - \frac{x_T^2}{R_{T_0}^2} \right) + \frac{1}{R_{R_0}} \left(1 - \frac{x_R^2}{R_{R_0}^2} \right)}$$

$$\Delta R_{0_y} = -\frac{1}{2} \cdot \frac{\left(\frac{y_T}{R_{T_0}} + \frac{y_R}{R_{R_0}} \right)^2}{\frac{1}{R_{T_0}} \left(1 - \frac{y_T^2}{R_{T_0}^2} \right) + \frac{1}{R_{R_0}} \left(1 - \frac{y_R^2}{R_{R_0}^2} \right)}$$

Fresnel Diffraction (New Model)

Path of Diffraction (Abbreviations)

Shift of Integration Boundaries

$$x_0 = \frac{\dfrac{x_T}{R_{T_0}} + \dfrac{x_R}{R_{R_0}}}{\dfrac{1}{R_{T_0}}\left(1 - \dfrac{x_T^2}{R_{T_0}^2}\right) + \dfrac{1}{R_{R_0}}\left(1 - \dfrac{x_R^2}{R_{R_0}^2}\right)}$$

$$y_0 = \frac{\dfrac{y_T}{R_{T_0}} + \dfrac{y_R}{R_{R_0}}}{\dfrac{1}{R_{T_0}}\left(1 - \dfrac{y_T^2}{R_{T_0}^2}\right) + \dfrac{1}{R_{R_0}}\left(1 - \dfrac{y_R^2}{R_{R_0}^2}\right)}$$

Fresnel Diffraction (New Model)

Path of Diffraction (Abbreviations)

Form Factors of Quadratic Terms in Phase

$$c_x = \frac{\lambda}{2\,R_{f_x}^2} =$$

$$= \frac{1}{2} \cdot \left[\frac{1}{R_{T_0}} \left(1 - \frac{x_T^2}{R_{T_0}^2} \right) + \frac{1}{R_{R_0}} \left(1 - \frac{x_R^2}{R_{R_0}^2} \right) \right]$$

$$c_y = \frac{\lambda}{2\,R_{f_y}^2} =$$

$$= \frac{1}{2} \cdot \left[\frac{1}{R_{T_0}} \left(1 - \frac{y_T^2}{R_{T_0}^2} \right) + \frac{1}{R_{R_0}} \left(1 - \frac{y_R^2}{R_{R_0}^2} \right) \right]$$

Fresnel Diffraction (New Model)

Integration of all phase contributions over the rectangular area of the plate

$$\rho_{\text{geom}} = \text{const} \cdot e^{-jk\left(R_{T_0} + R_{R_0} - \Delta R_{0_x} - \Delta R_{0_y}\right)} \cdot$$

$$\cdot \int_{-\frac{w}{2} - x_0}^{\frac{w}{2} - x_0} e^{-j\pi\left(\frac{x}{R_{f_x}}\right)^2} dx \cdot$$

$$\cdot \int_{-\frac{h}{2} - y_0}^{\frac{h}{2} - y_0} e^{-j\pi\left(\frac{y}{R_{f_y}}\right)^2} dy$$

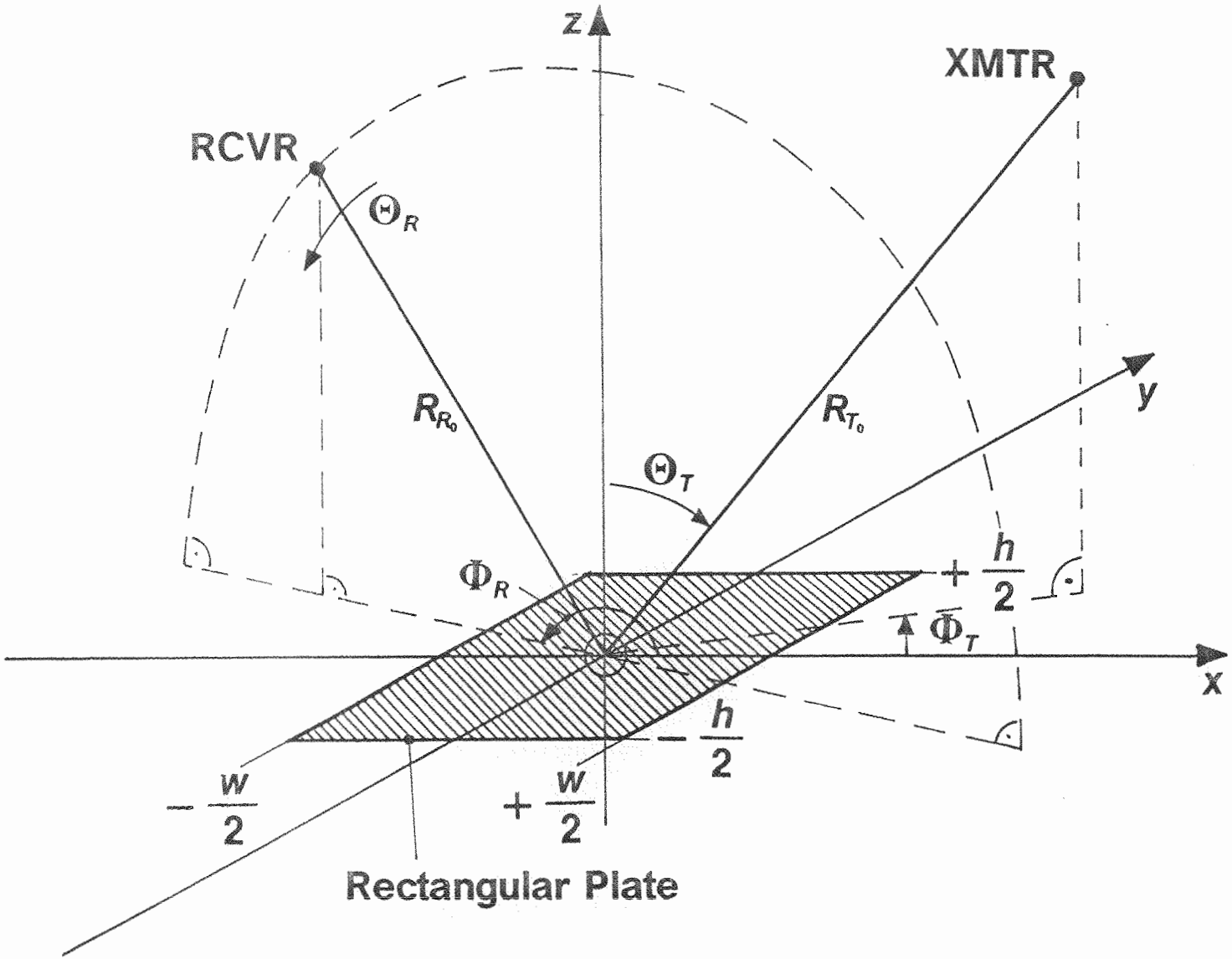

Geometry of Diffraction Diagram (constant azimuth angle)

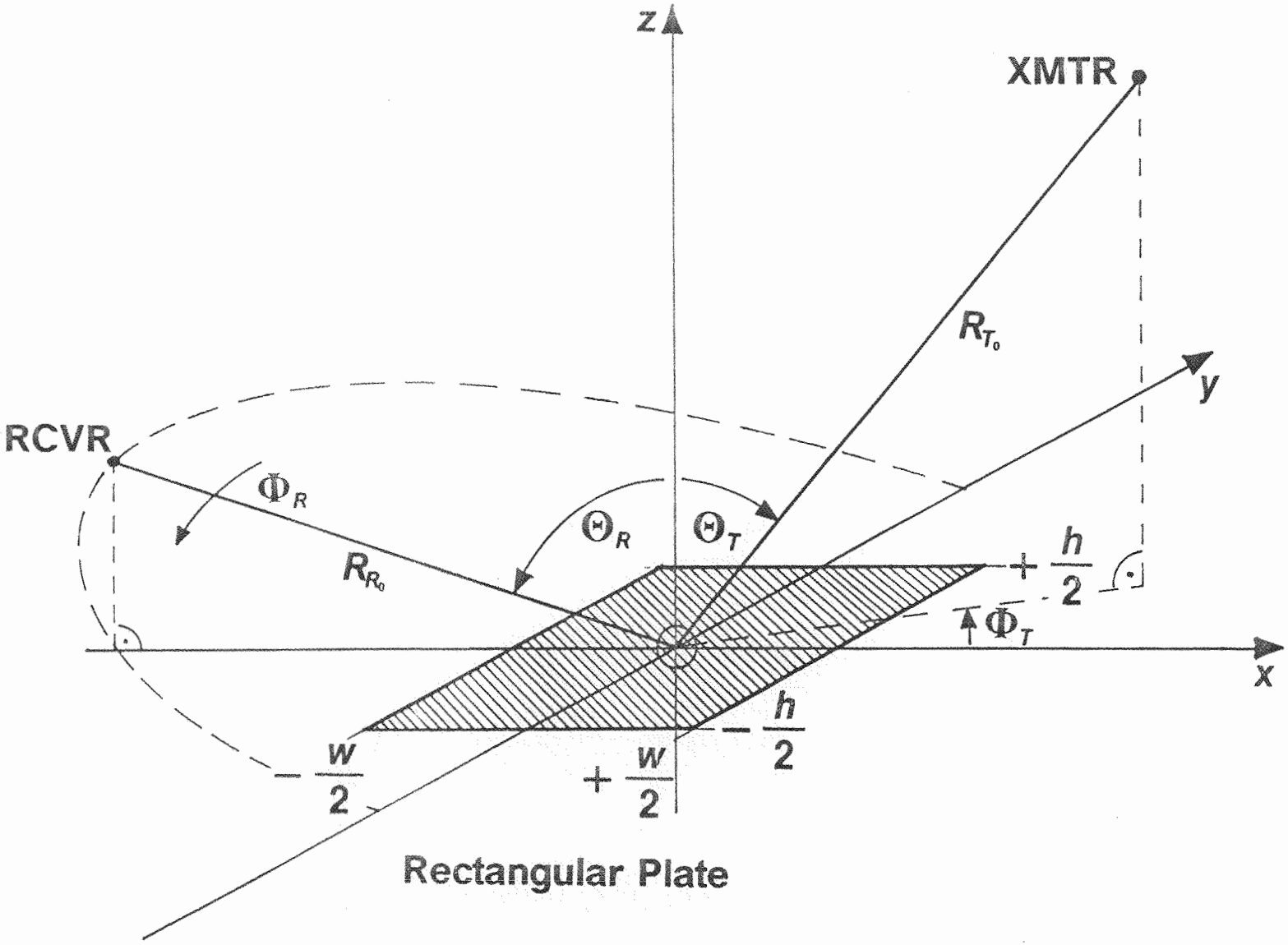

Geometry of Diffraction Diagram (constant elevation angle)

Diffraction Diagram of a Rectangular Plate (constant Azimuth)			
X-Path	$R_{T_0} = 5000.0$ m	$\Phi_T = 0.0°$	$\Theta_T = 60.0°$
R-Path	$R_{R_0} = 5000.0$ m	$\Phi_R = 180.0°$	$\Theta_R = \pm 90.0°$
Plate	Metal	$w = 10.0$ m	$h = 10.0$ m
RF-Par.	$\lambda_0 = 0.30$ m		Pol = H

P.O. MODEL (Far Zone)

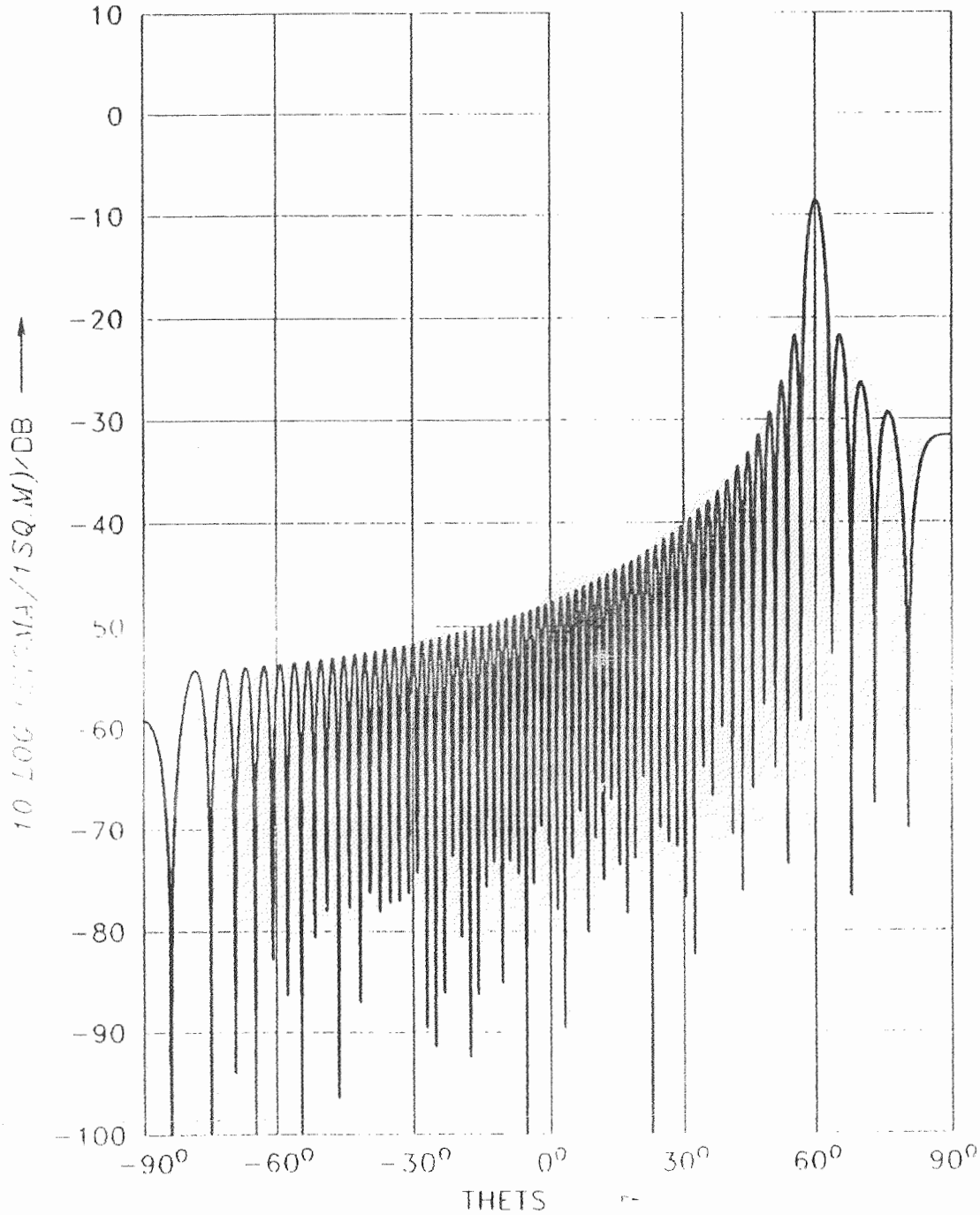

Diffraction Diagram of a Rectangular Plate (constant Azimuth)			
X-Path	$R_{T_0} = 5000.0$ m	$\Phi_T = 0.0°$	$\Theta_T = 60.0°$
R-Path	$R_{R_0} = 5000.0$ m	$\Phi_R = 90.0°$	$\Theta_R = \pm 90.0°$
Plate	Metal	$w = 10.0$ m	$h = 10.0$ m
RF-Par.	$\lambda_0 = 0.30$ m		Pol = H

P.O. MODEL (Far Zone)

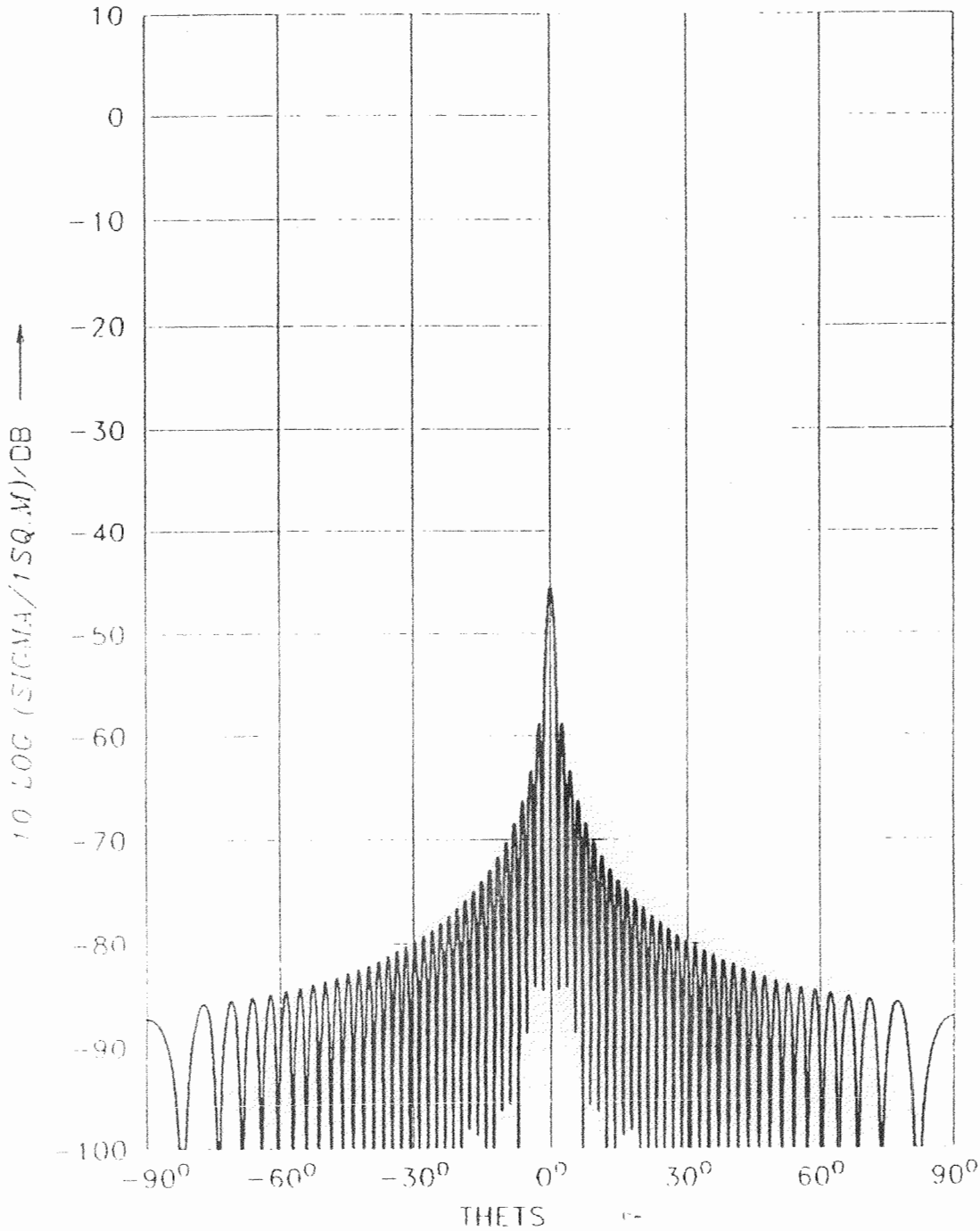

Diffraction Diagram of a Rectangular Plate (constant Azimuth)

X-Path	$R_{T_0} = 5000.0$ m	$\Phi_T = 0.0°$	$\Theta_T = 60.0°$
R-Path	$R_{R_0} = 5000.0$ m	$\Phi_R = 180.0°$	$\Theta_R = \pm 90.0°$
Plate	Metal	$w = 30.0$ m	$h = 0.6$ m
RF-Par.	$\lambda_0 = 0.30$ m	$\lvert\rho_{max}\rvert = -26.72$ dB	Pol = H

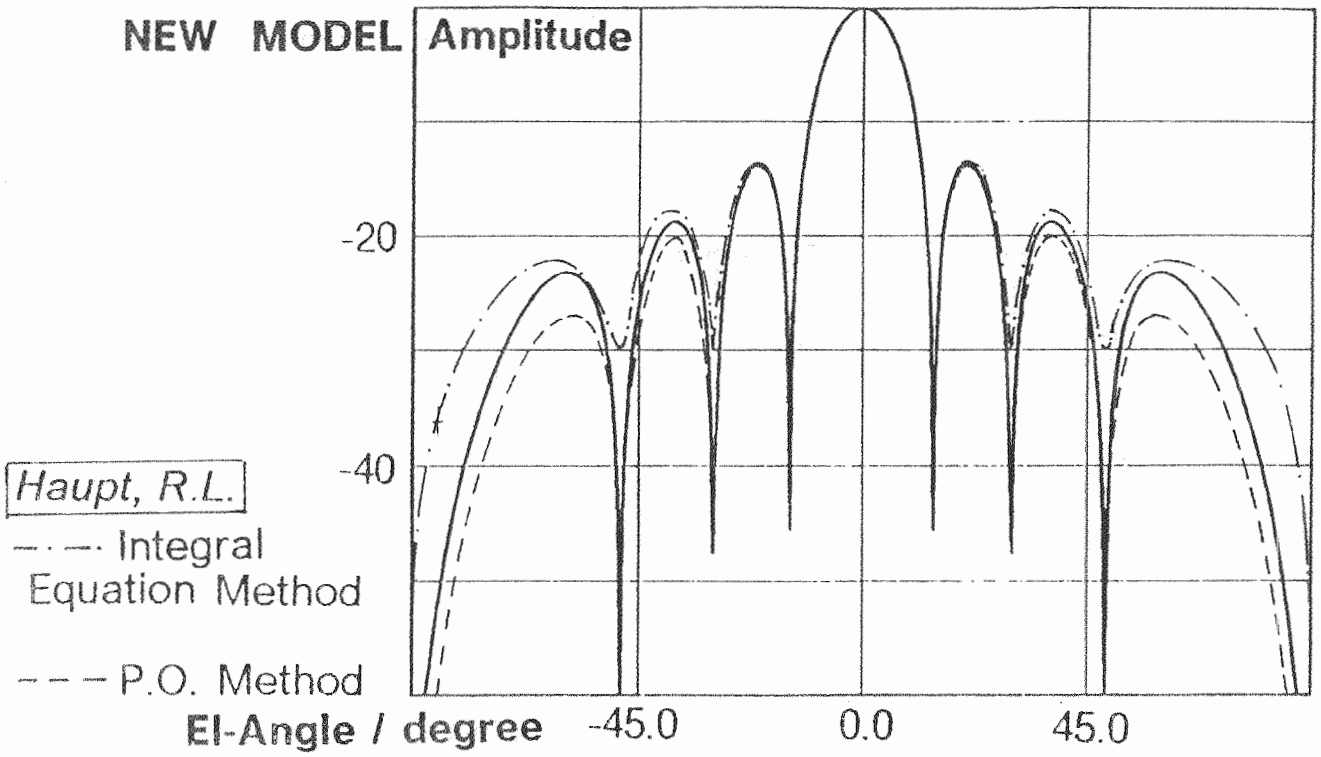

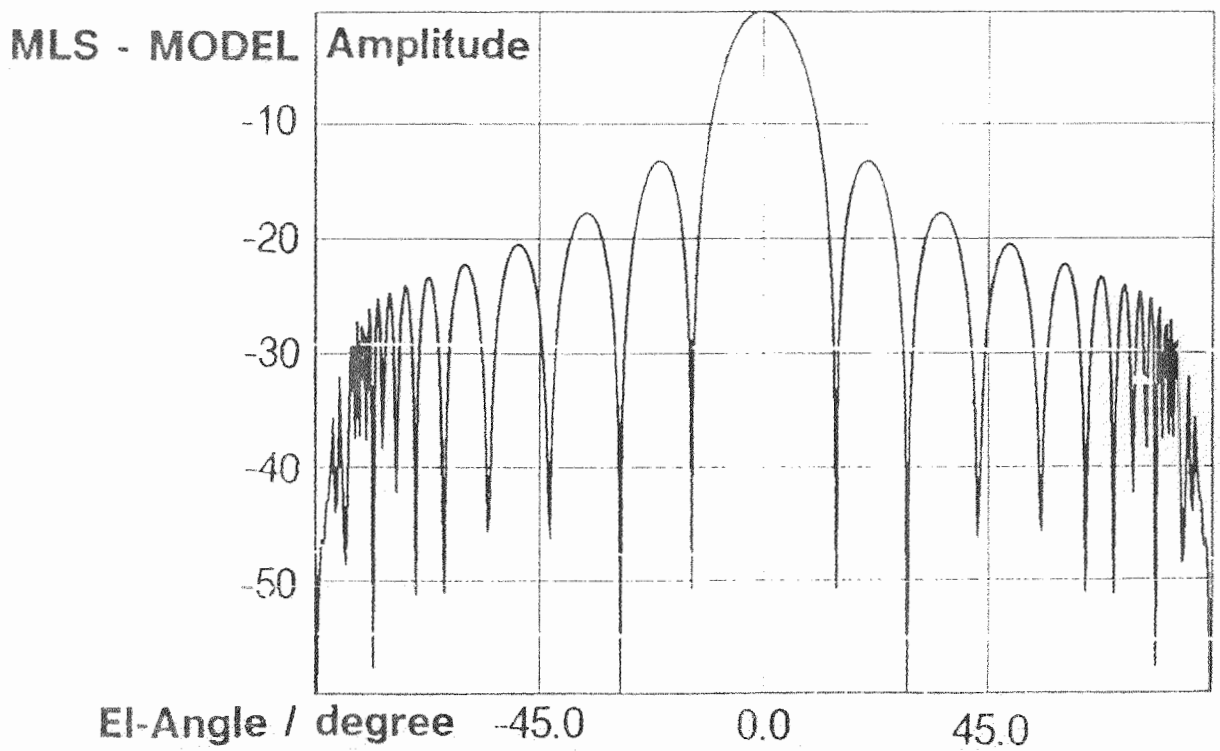

Diffraction Diagram of a Rectangular Plate (constant Azimuth)			
X-Path	$R_{T_0} = 5000.0$ m	$\Phi_T = 0.0°$	$\Theta_T = 60.0°$
R-Path	$R_{R_0} = 5000.0$ m	$\Phi_R = 173.2°$	$\Theta_R = \pm 90.0°$
Plate	Metal	$w = 10.0$ m	$h = 10.0$ m
RF-Par.	$\lambda_0 = 0.30$ m		Pol = H

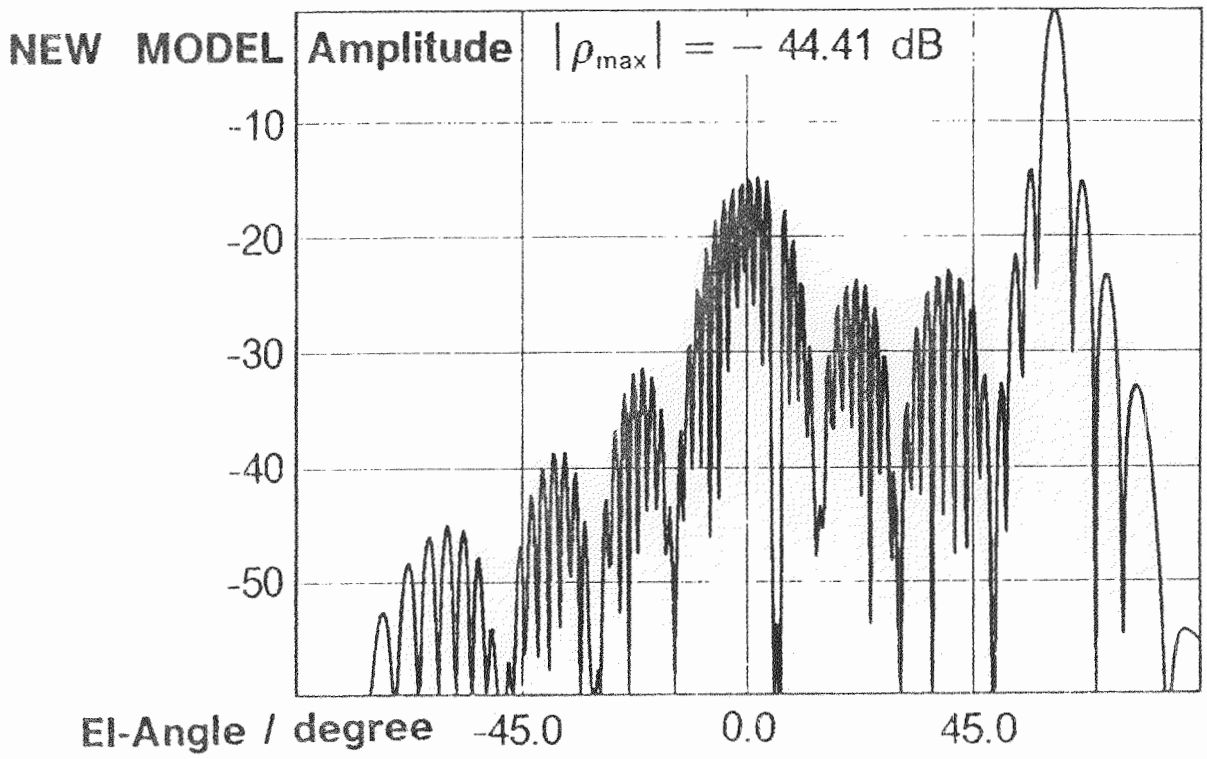

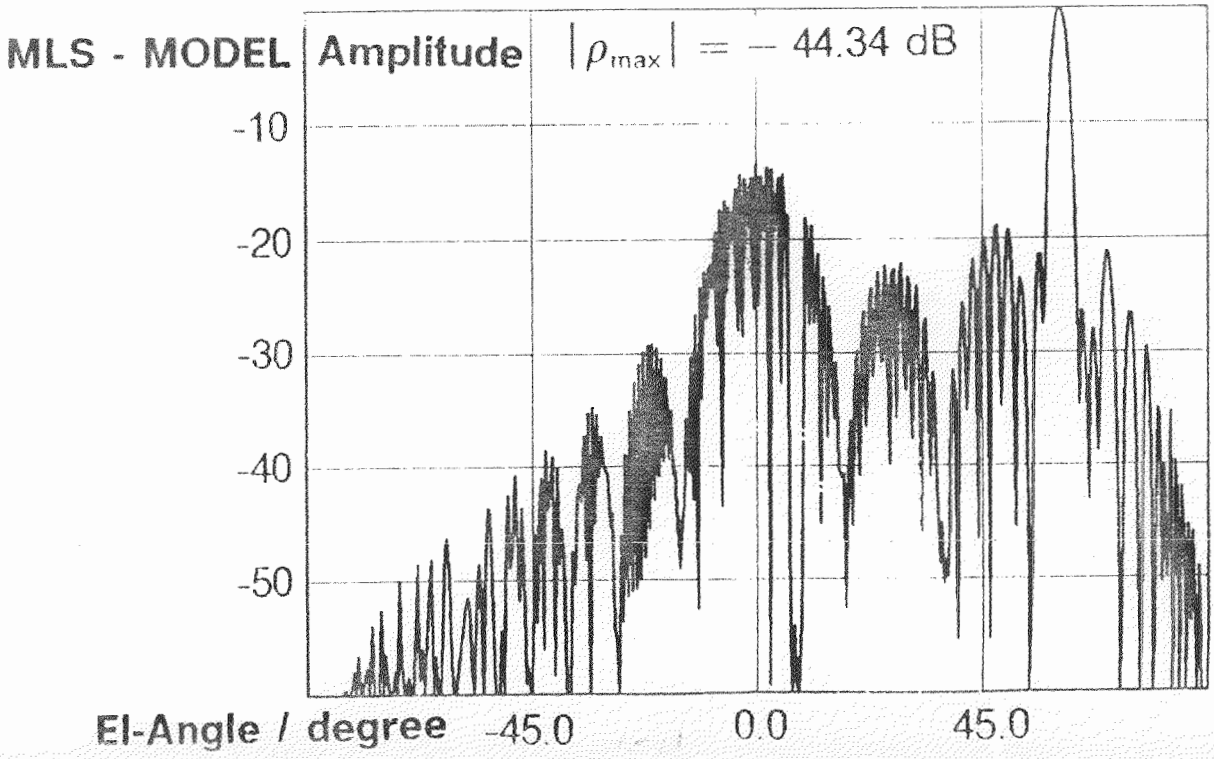

Diffraction Diagram of a Rectangular Plate (constant Azimuth)			
X-Path	$R_{T_0} = 5000.0$ m	$\Phi_T = 0.0°$	$\Theta_T = 60.0°$
R-Path	$R_{R_0} = 5000.0$ m	$\Phi_R = 175.2°$	$\Theta_R = \pm 90.0°$
Plate	Metal	$w = 10.0$ m	$h = 10.0$ m
RF-Par.	$\lambda_0 = 0.30$ m		Pol = H

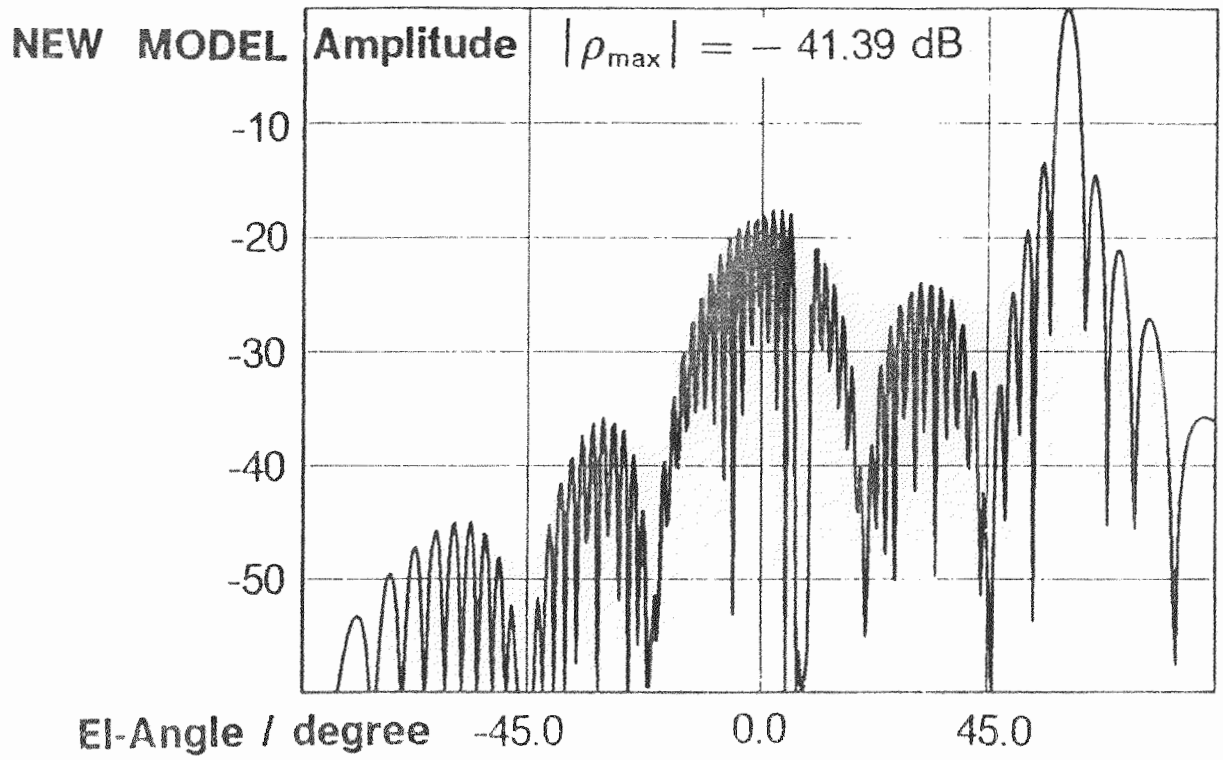

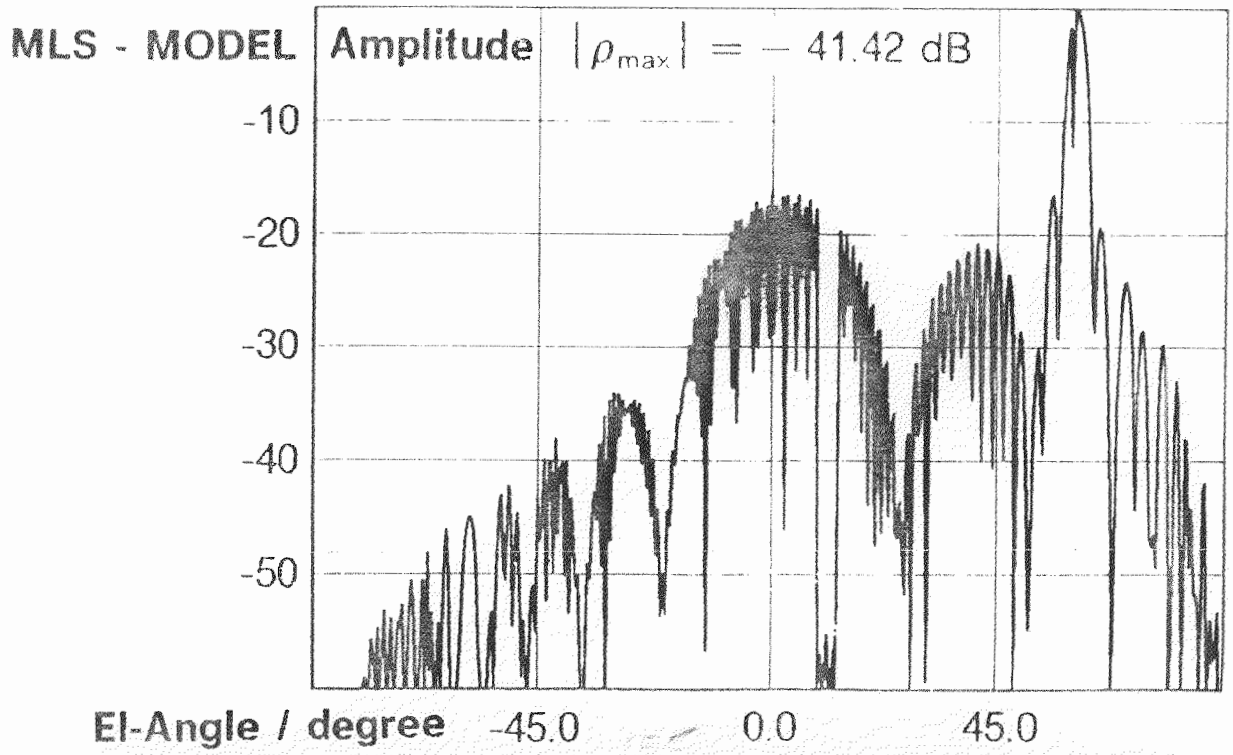

Diffraction Diagram of a Rectangular Plate (constant Azimuth)			
X-Path	$R_{T_0} = 5000.0$ m	$\Phi_T = 0.0°$	$\Theta_T = 60.0°$
R-Path	$R_{R_0} = 5000.0$ m	$\Phi_R = 177.2°$	$\Theta_R = \pm 90.0°$
Plate	Metal	$w = 10.0$ m	$h = 10.0$ m
RF-Par.	$\lambda_0 = 0.30$ m		Pol = H

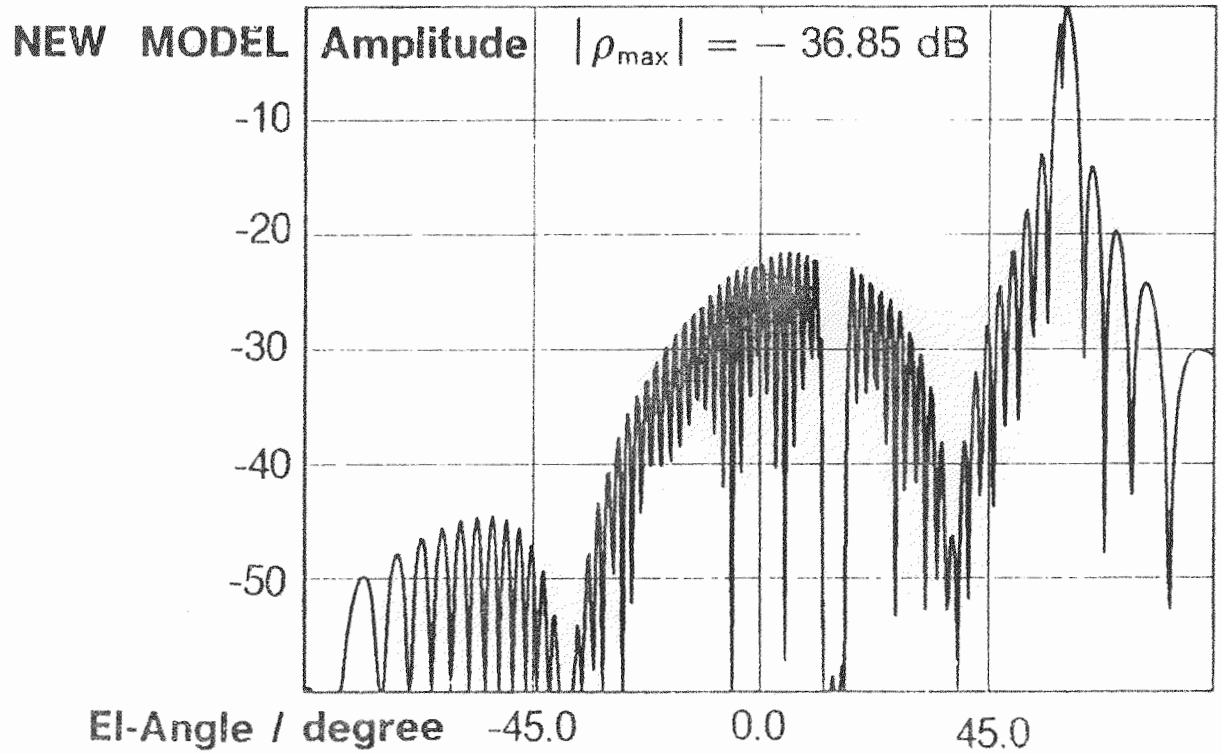

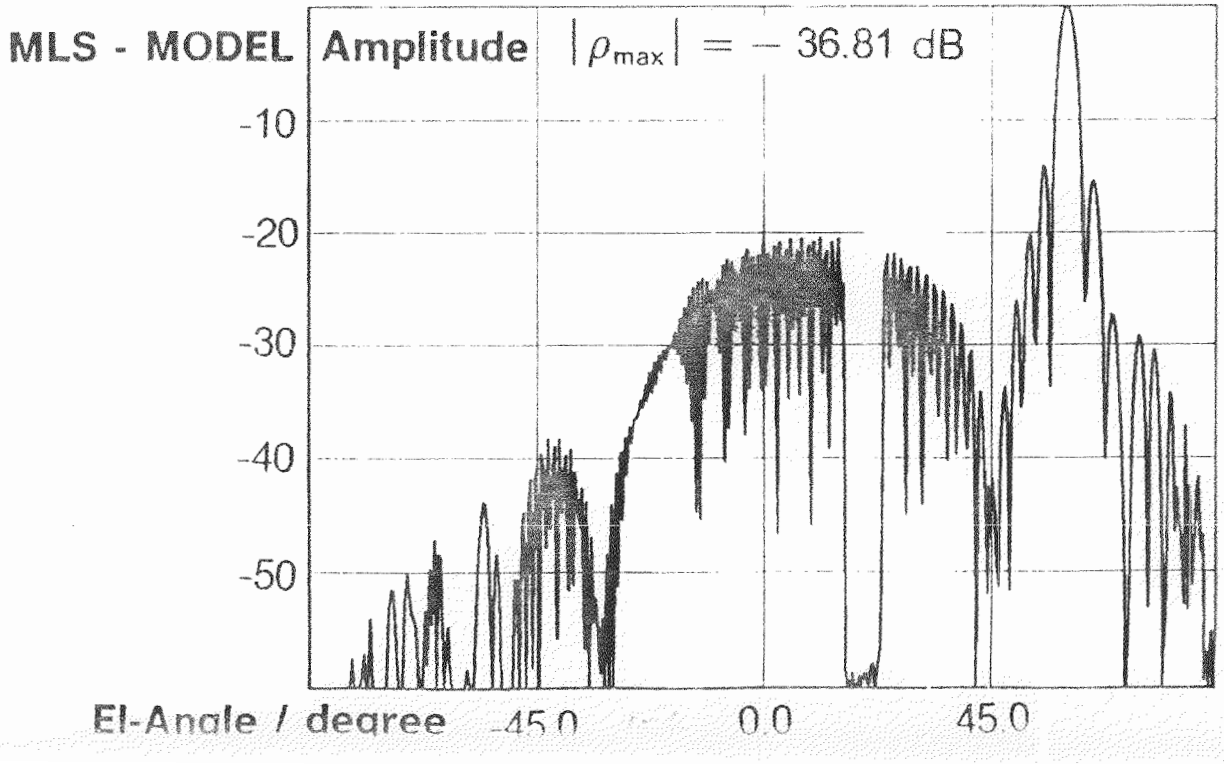

Diffraction Diagram of a Rectangular Plate (constant Azimuth)			
X-Path	$R_{T_0} = 5000.0$ m	$\Phi_T = 0.0°$	$\Theta_T = 60.0°$
R-Path	$R_{R_0} = 5000.0$ m	$\Phi_R = 180.0°$	$\Theta_R = \pm 90.0°$
Plate	Metal	$w = 10.0$ m	$h = 10.0$ m
RF-Par.	$\lambda_0 = 0.30$ m		Pol = H

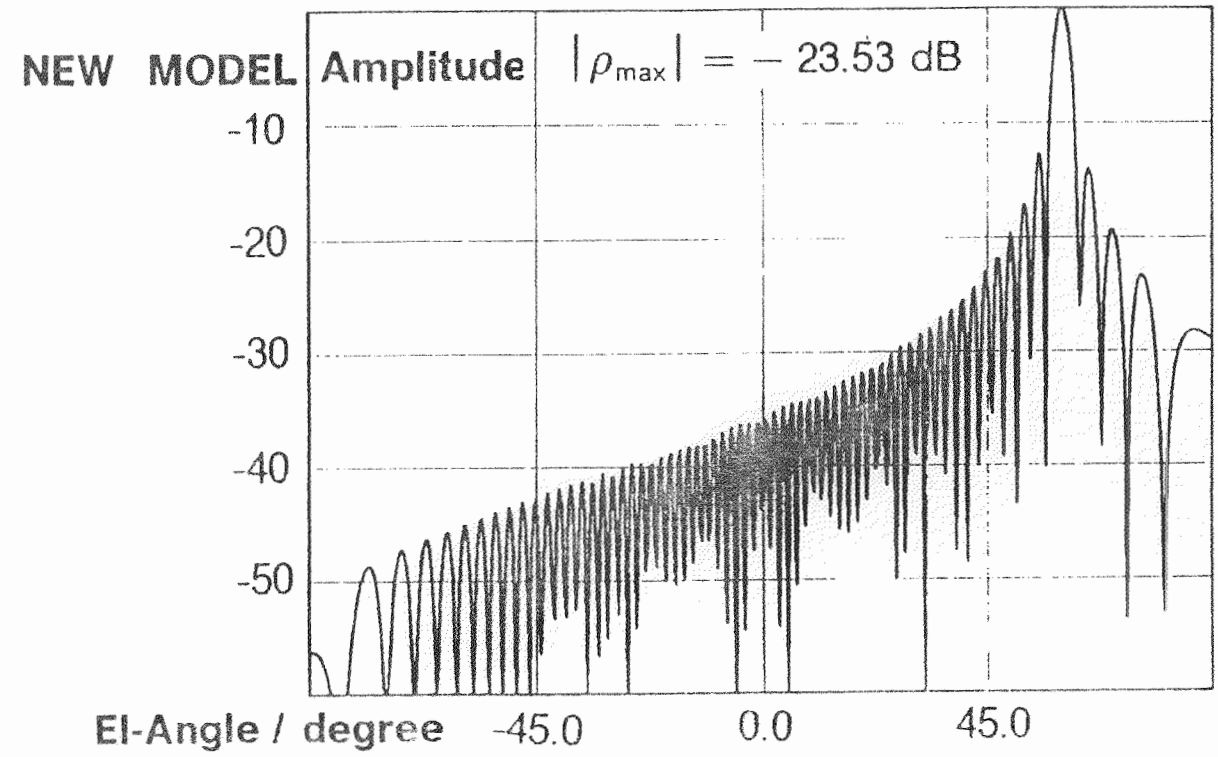

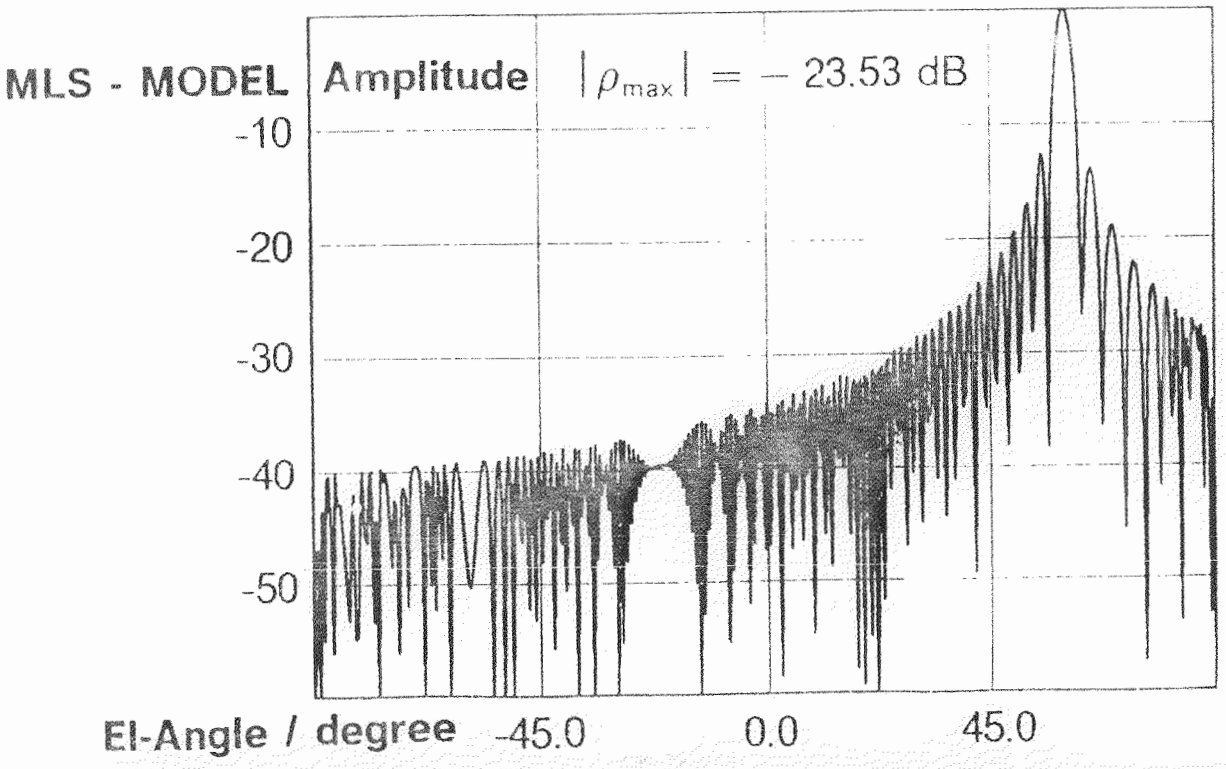

Diffraction Diagram of a Rectangular Plate (constant Elevation)

X-Path	$R_{T_0} = 5000.0$ m	$\Phi_T = 0.0°$	$\Theta_T = 60.0°$
R-Path	$R_{R_0} = 5000.0$ m	$\Phi_R = 180.0° \pm 90.0°$	$\Theta_R = 70.0°$
Plate	Metal	$w = 10.0$ m	$h = 10.0$ m
RF-Par.	$\lambda_0 = 0.30$ m		Pol = H

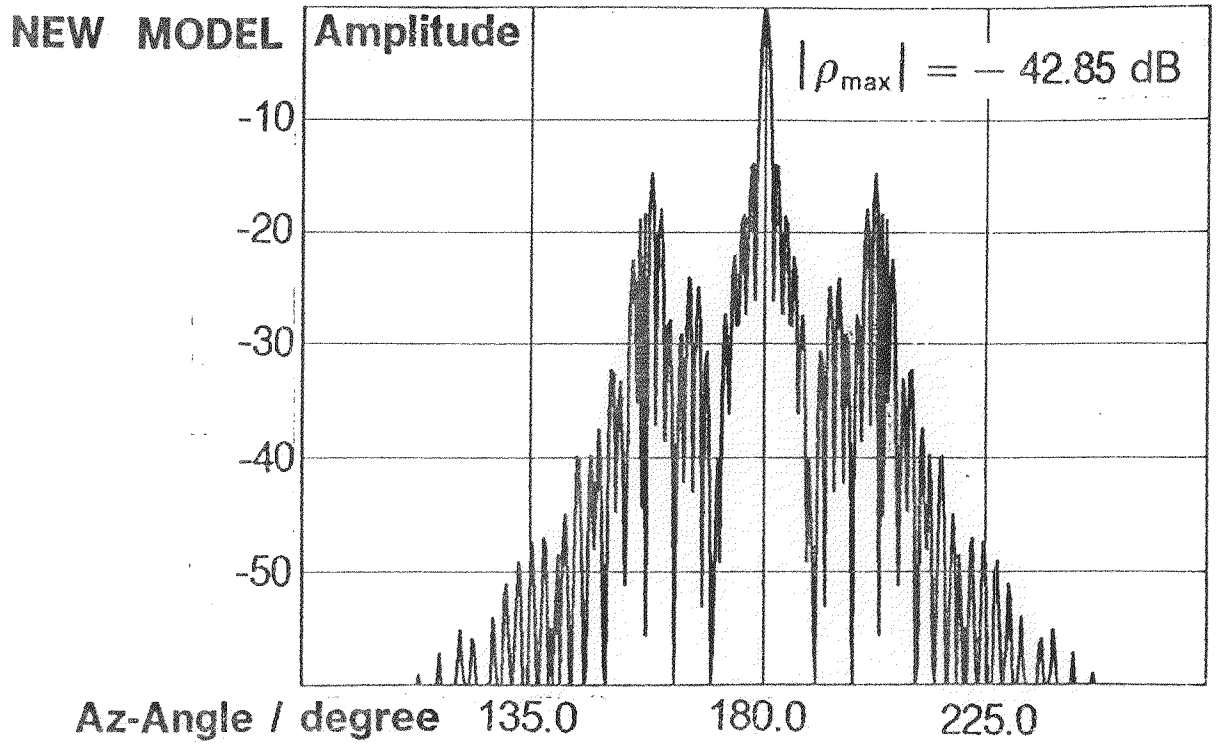

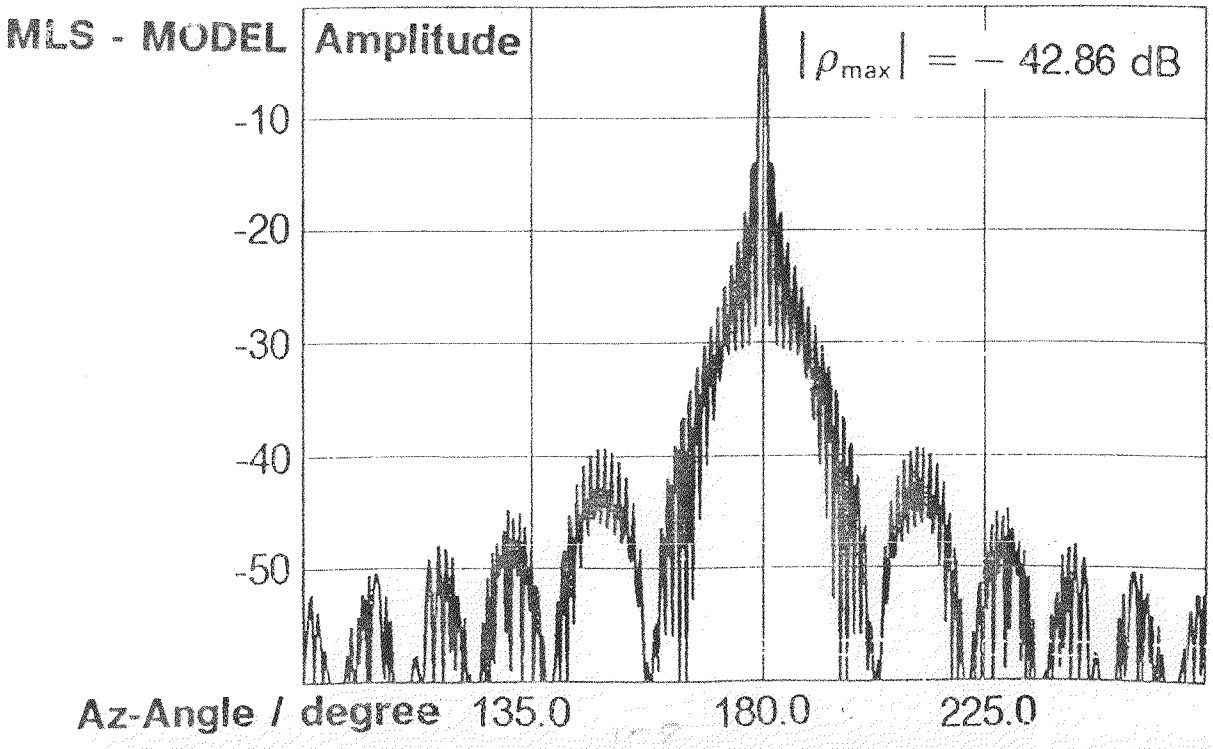

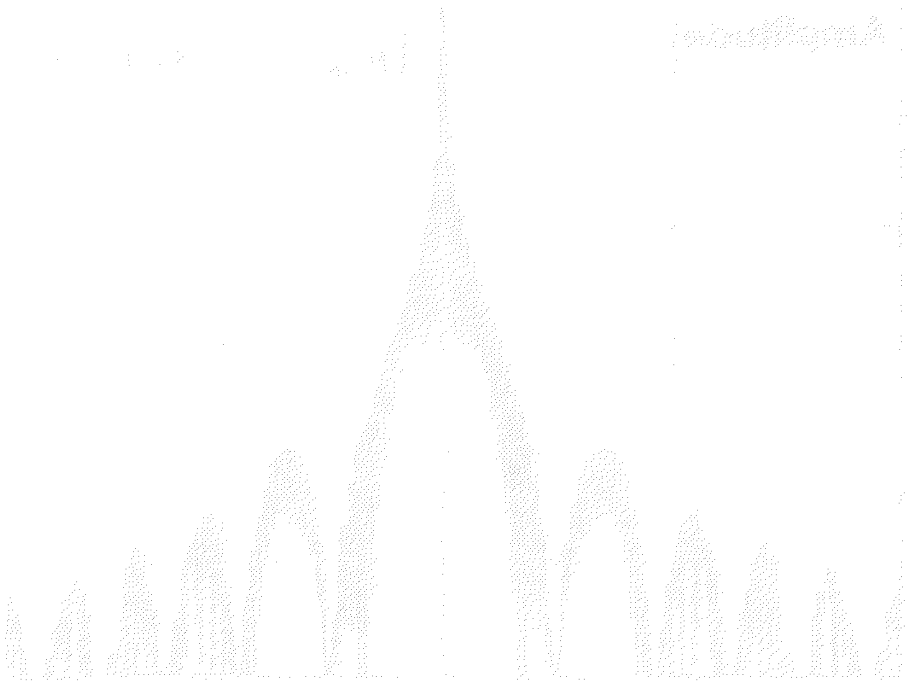

Diffraction Diagram of a Rectangular Plate (constant Elevation)

X-Path	$R_{T_0} = 5000.0$ m	$\Phi_T = 0.0°$	$\Theta_T = 60.0°$
R-Path	$R_{R_0} = 5000.0$ m	$\Phi_R = 180.0° \pm 90.0°$	$\Theta_R = 65.3°$
Plate	Metal	$w = 10.0$ m	$h = 10.0$ m
RF-Par.	$\lambda_0 = 0.30$ m		Pol = H

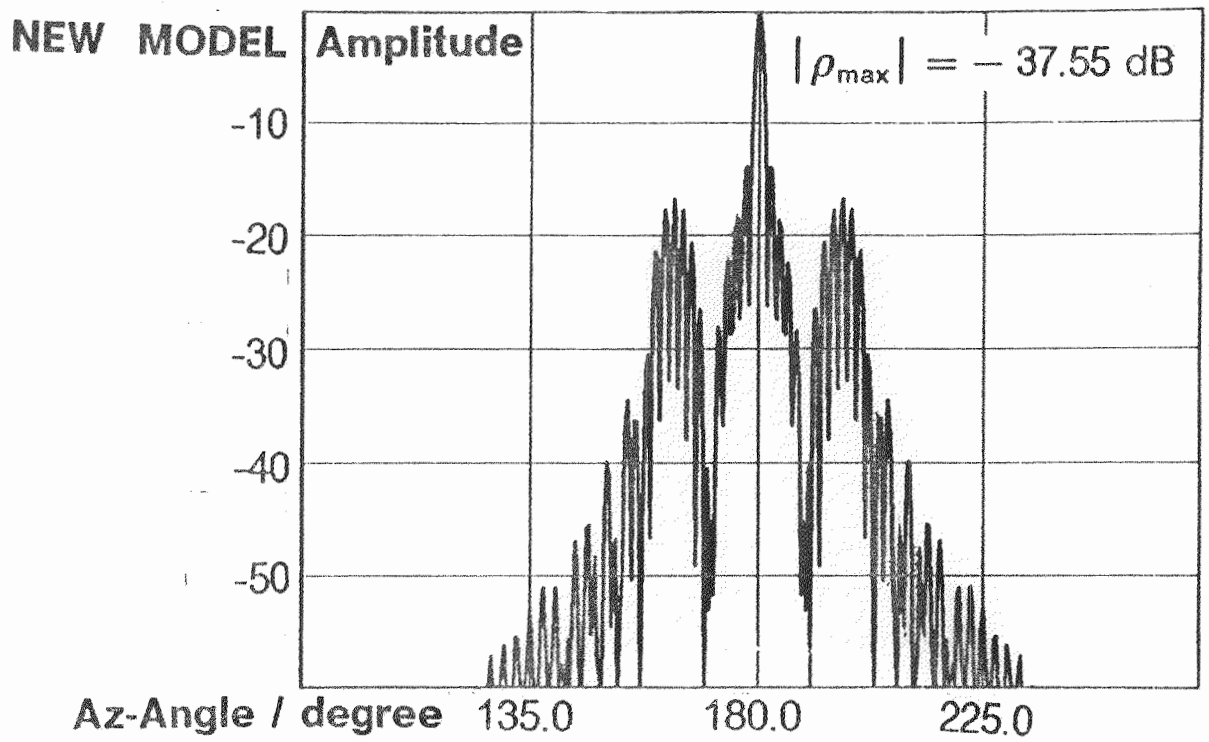

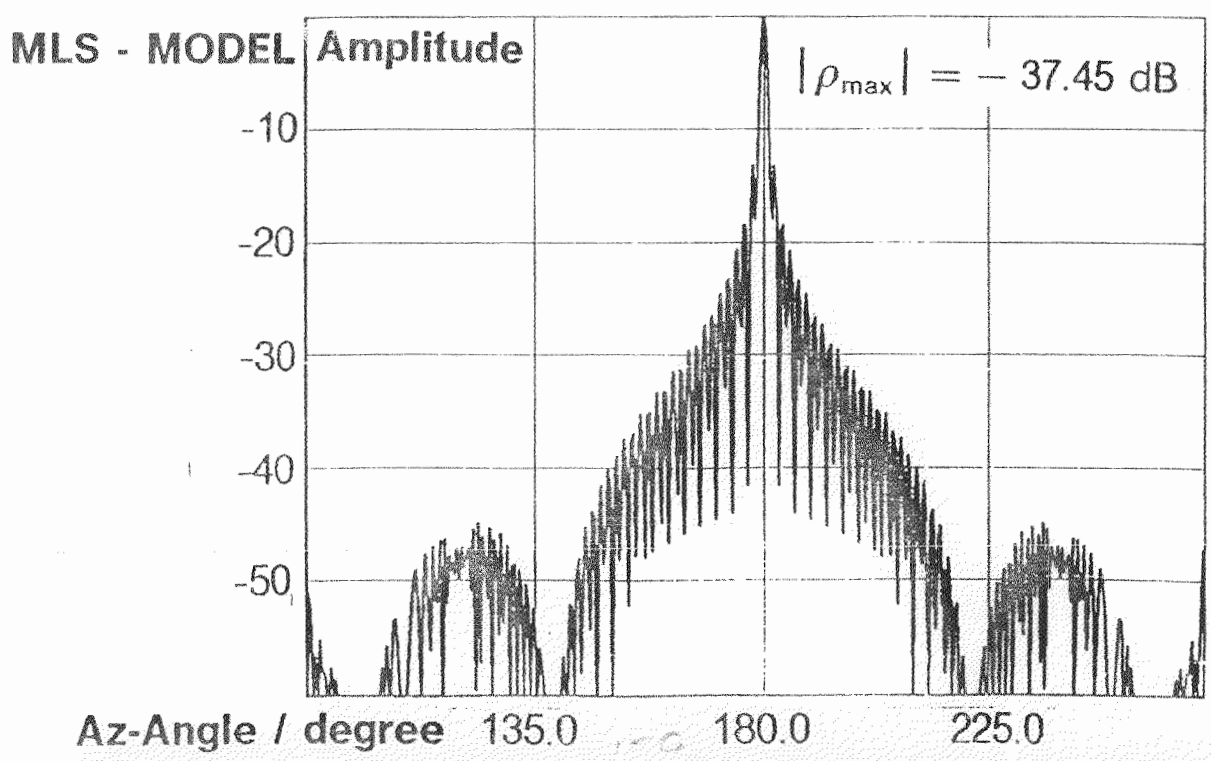

Diffraction Diagram of a Rectangular Plate (constant Elevation)

X-Path	$R_{T_0} = 5000.0$ m	$\Phi_T = 0.0°$	$\Theta_T = 60.0°$
R-Path	$R_{R_0} = 5000.0$ m	$\Phi_R = 180.0° \pm 90.0°$	$\Theta_R = 60.0°$
Plate	Metal	$w = 10.0$ m	$h = 10.0$ m
RF-Par.	$\lambda_0 = 0.30$ m		Pol = H

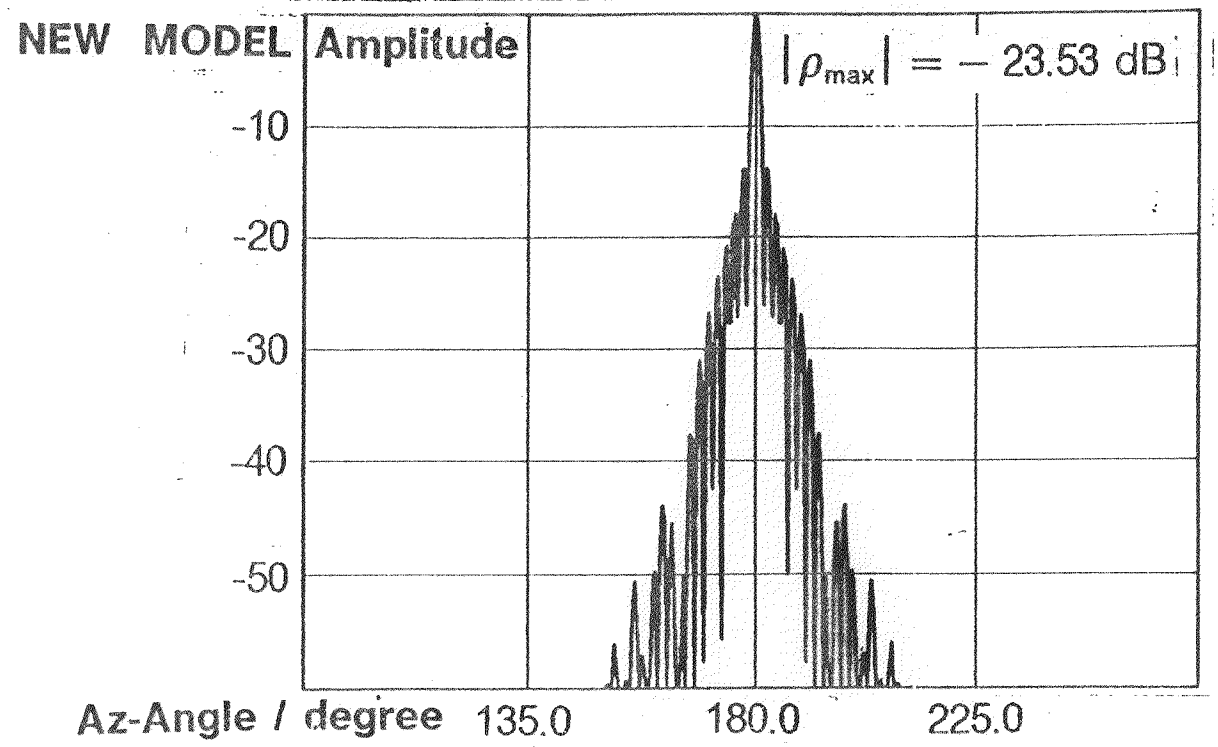

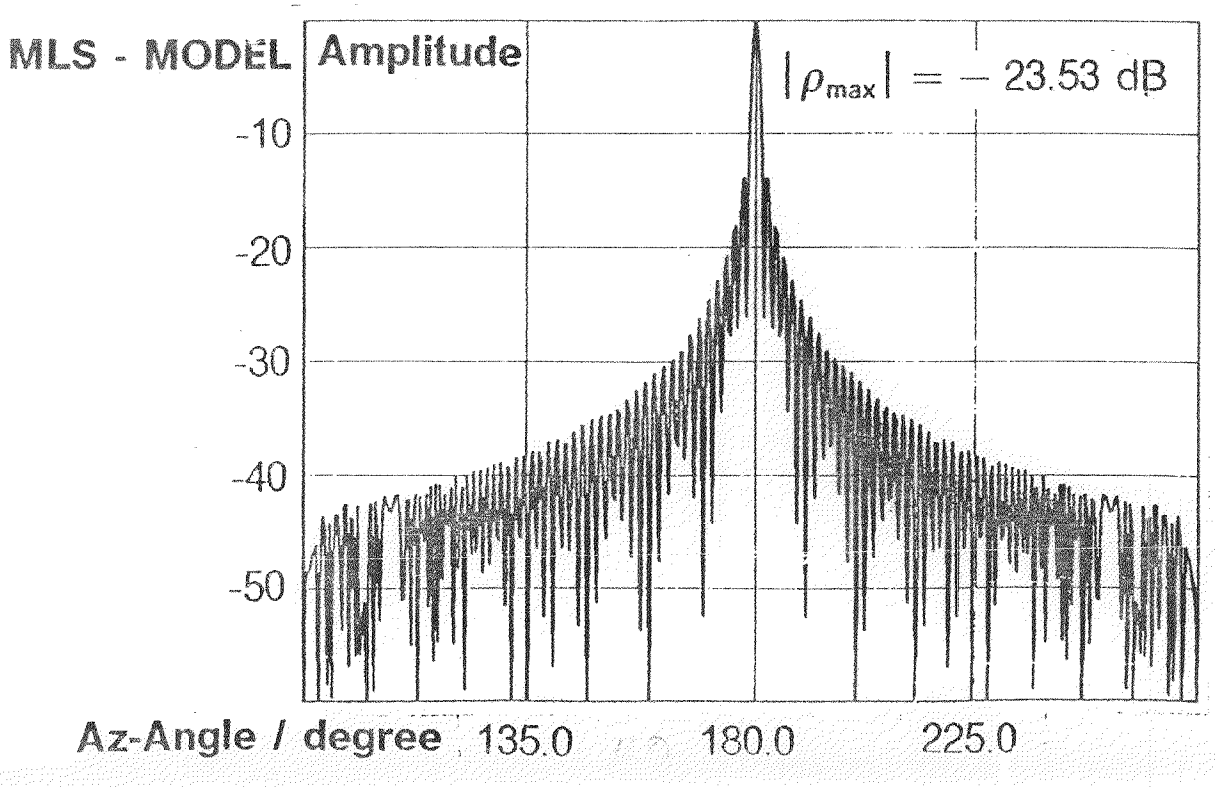

Diffraction Diagram of a Rectangular Plate (constant Elevation)			
X-Path	$R_{T_0} = 5000.0$ m	$\Phi_T = 0.0°$	$\Theta_T = 60.0°$
R-Path	$R_{R_0} = 5000.0$ m	$\Phi_R = 180.0° \pm 90.0°$	$\Theta_R = 55.5°$
Plate	Metal	$w = 10.0$ m	$h = 10.0$ m
RF-Par.	$\lambda_0 = 0.30$ m		Pol = H

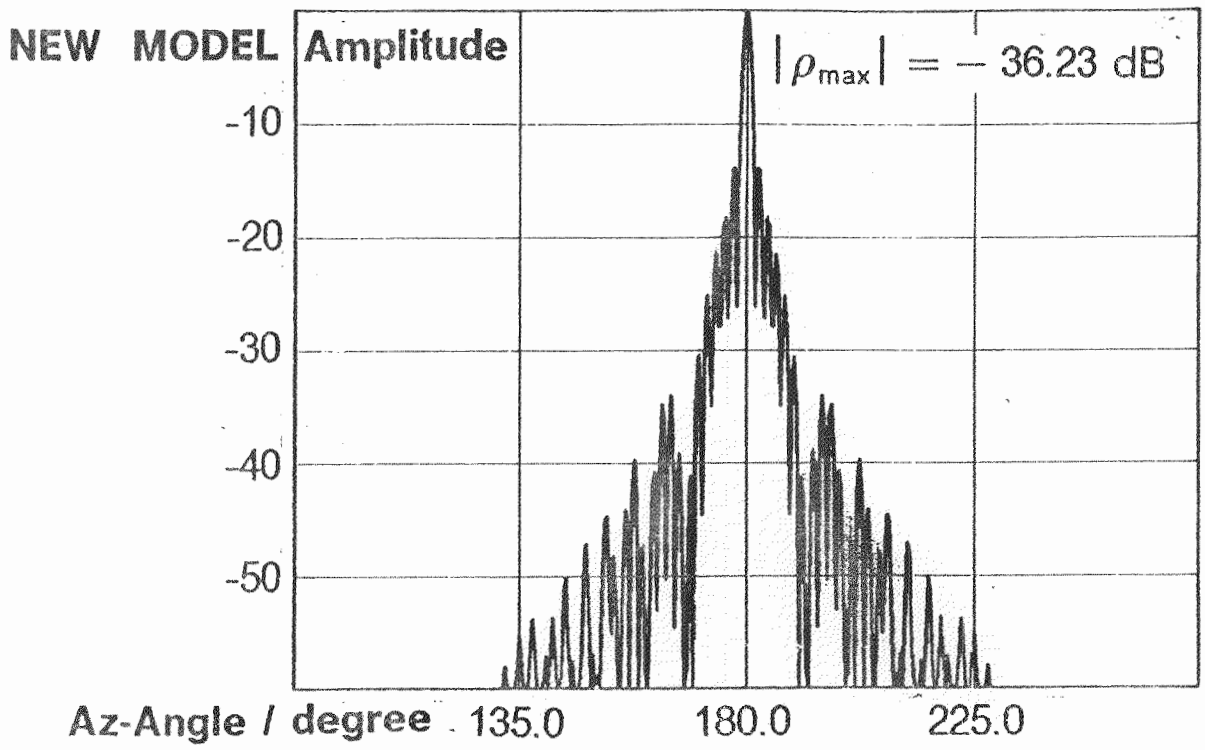

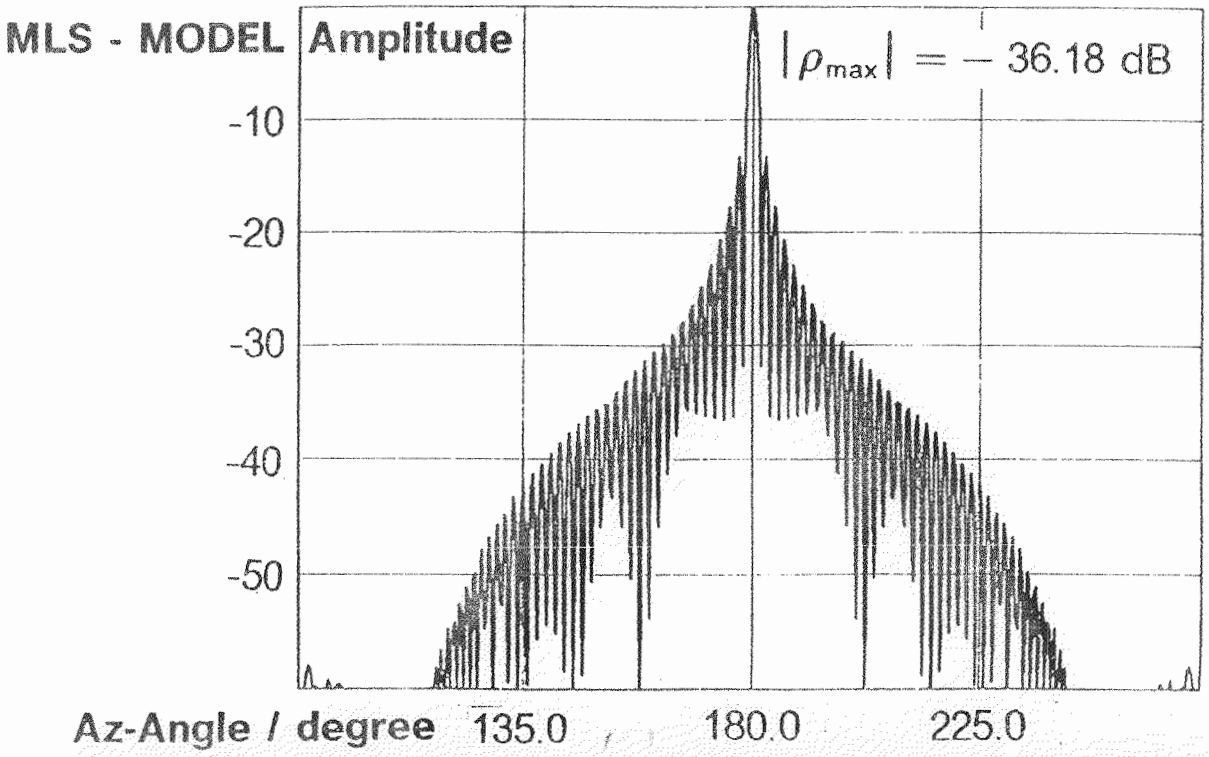

Diffraction Diagram of a Rectangular Plate (constant Elevation)

X-Path	$R_{T_0} = 5000.0$ m	$\Phi_T = 0.0°$	$\Theta_T = 60.0°$
R-Path	$R_{R_0} = 5000.0$ m	$\Phi_R = 180.0° \pm 90.0°$	$\Theta_R = 52.4°$
Plate	Metal	$w = 10.0$ m	$h = 10.0$ m
RF-Par.	$\lambda_0 = 0.30$ m		Pol = H

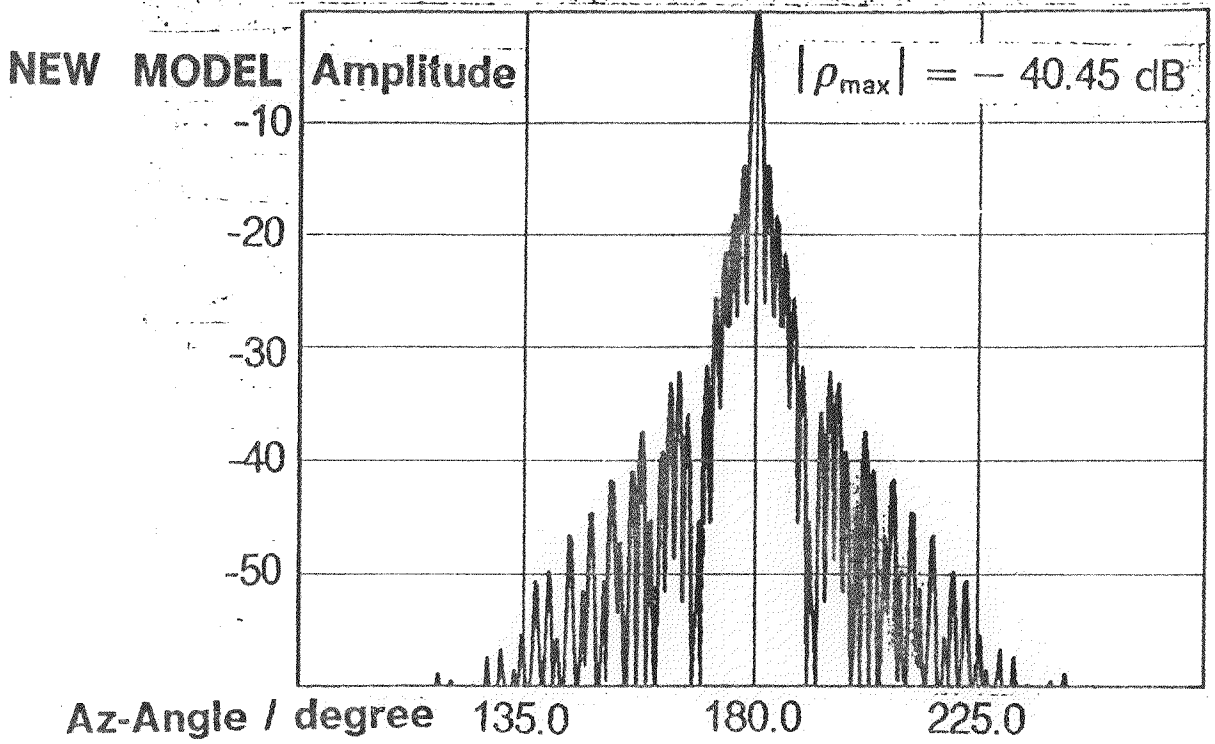

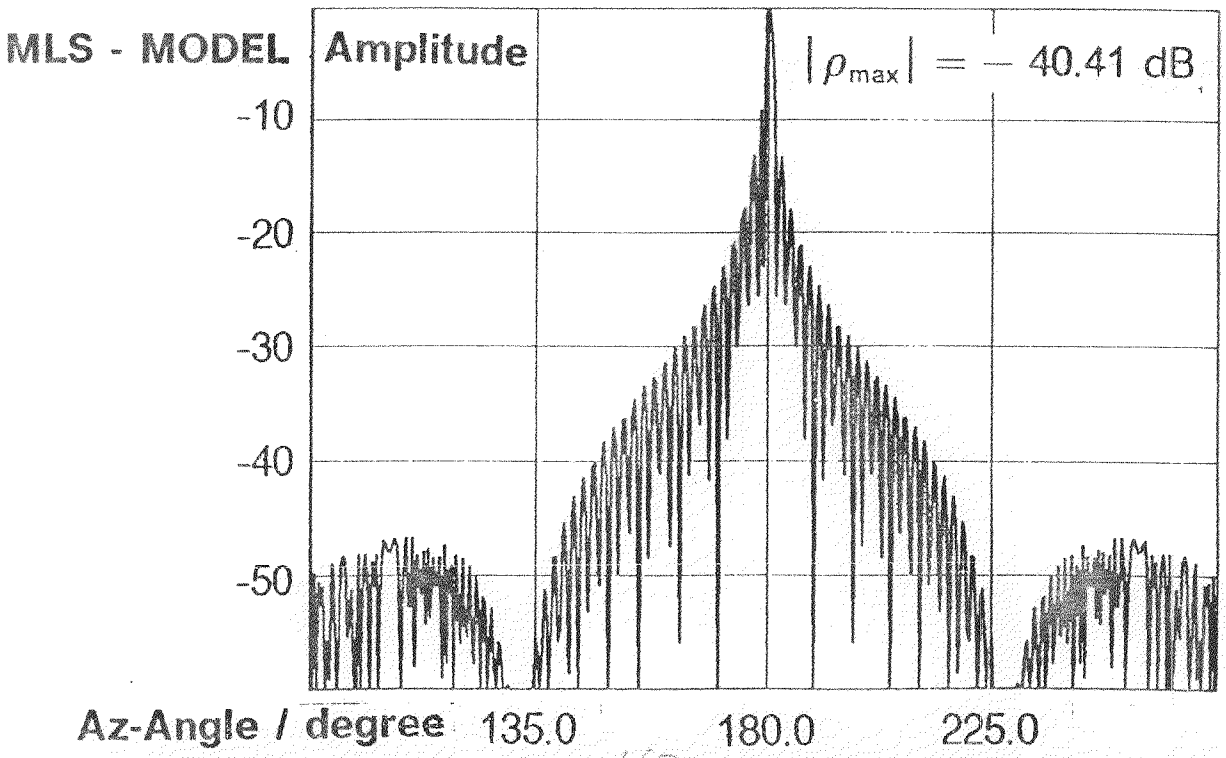

Diffraction Diagram of a Rectangular Plate (constant Elevation)			
X-Path	$R_{T_0} = 5000.0$ m	$\Phi_T = 0.0°$	$\Theta_T = 60.0°$
R-Path	$R_{R_0} = 5000.0$ m	$\Phi_R = 180.0° \pm 90.0°$	$\Theta_R = 0.0°$
Plate	Metal	$w = 10.0$ m	$h = 10.0$ m
RF-Par.	$\lambda_0 = 0.30$ m		Pol = H

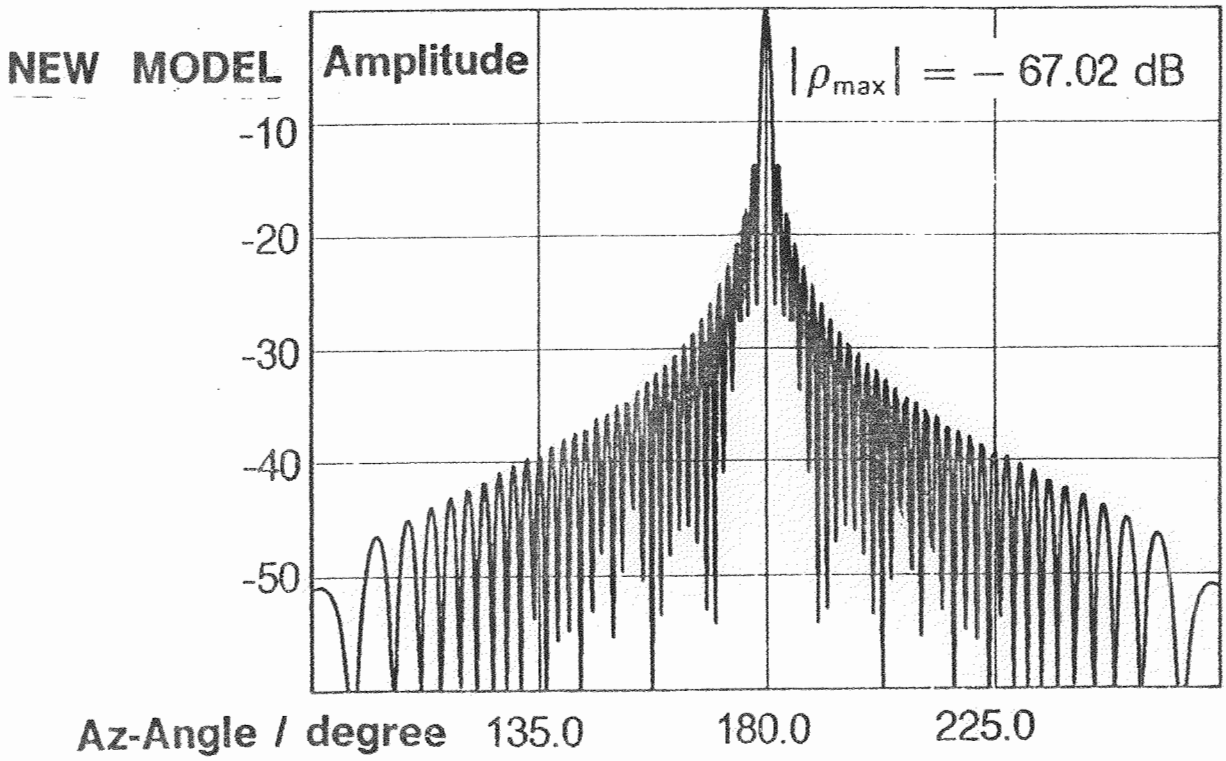

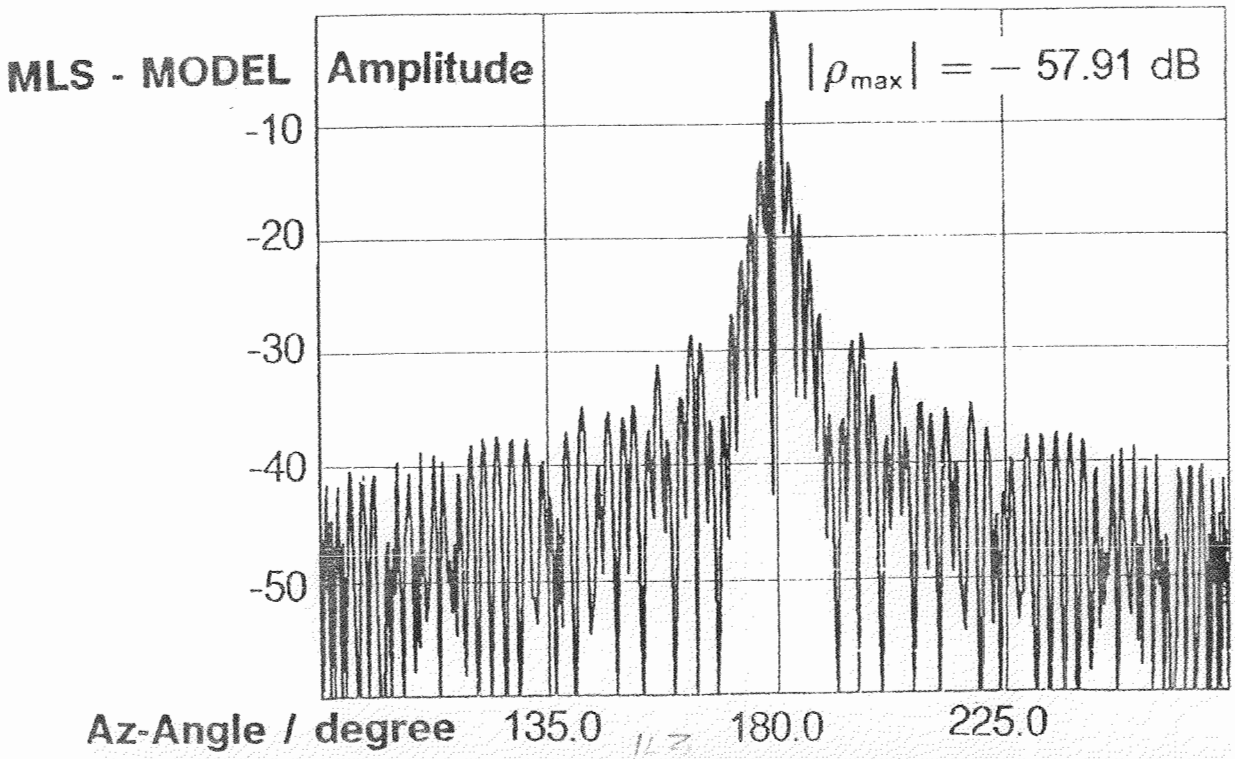

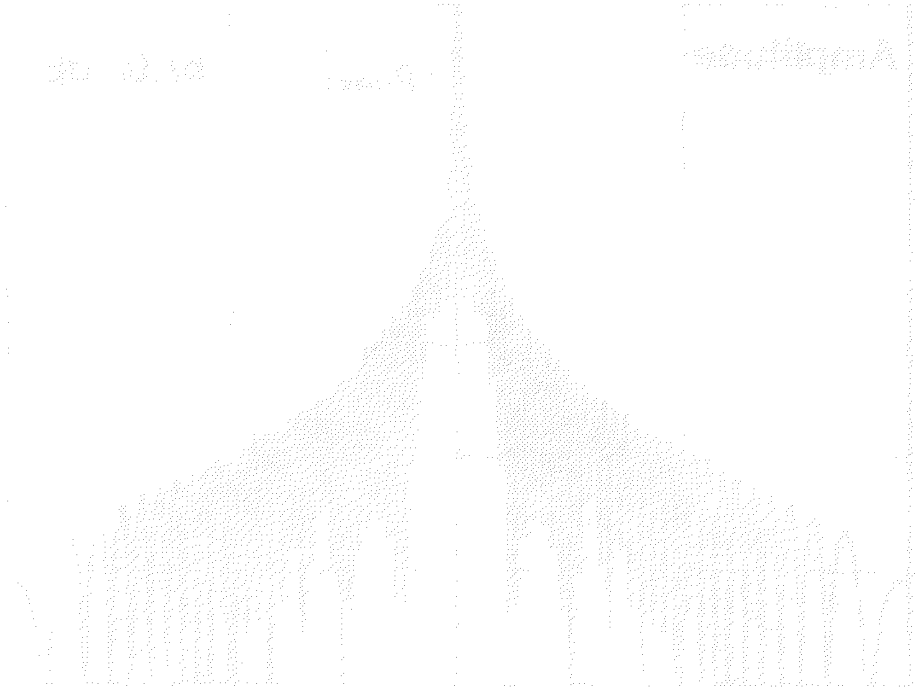

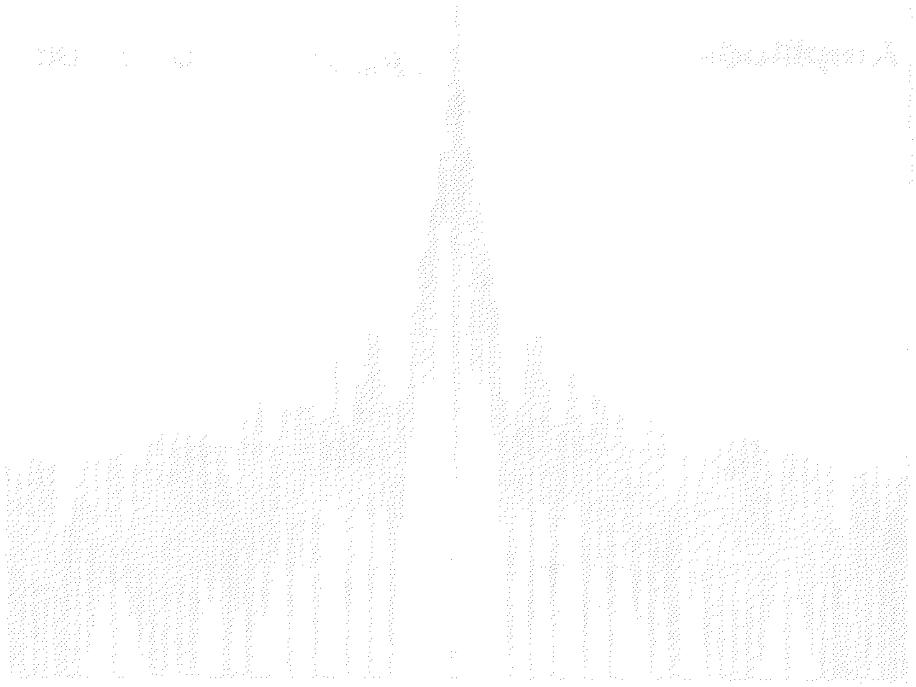

HOLLIS RYAN
CTA INCORPORATED

SPECULAR GROUND REFLECTIONS

CTA INCORPORATED

THE USE OF THE MLS COMPUTER SIMULATION TO MODEL SPECULAR GROUND REFLECTIONS

PRESENTED BY:

DR. HOLLIS F. RYAN

CTA INCORPORATED
AIR TRAFFIC SYSTEMS DIVISION
MCKEE CITY, NEW JERSEY 08232
(609) 645-5000

7 NOVEMBER 1991

165

PRESENTATION TOPICS

- OVERVIEW OF GROUND PLATE PROPAGATION MODEL
- INPUT CONTROL FLAGS FOR GROUND PLATES
- GROUND PLATE OPTIONS
- INPUT FLAG SETTINGS FOR GROUND PLATE OPTIONS

- [illegible] COLLAPSE WAS EXPOSED IN THE [illegible]
- CRACKS IN THE [illegible]
- [illegible] AND THE [illegible] [illegible]
- COMPARISON OF CHROMIUM IN THE MEDIUM CYANIDE INCIDENT

MINIMAL FARM ACRIDE

GROUND PLATE PROPAGATION MODEL

REFERENCE: "Multipath Parameter Computations for the MLS Simulation Computer Program, Jack Capon, Lincoln Laboratory, Massachusetts Institute of Technology, Project Report ATC-68, 8 April 1976, Report No. FAA-RD-76-55

- ONE OF SEVERAL PROPAGATION MODELS IN THE MLS COMPUTER SIMULATION PROGRAM
- SPECULAR REFLECTIONS FROM TERRAIN BETWEEN TRANSMITTER & RECEIVER
- MULTIPATH COMPONENTS COHERENTLY SUMMED - AMPLITUDE & PHASE
- CHARACTERISTICS

  - HIGHLY DIRECTIONAL
  - COHERENT
  - RERADIATION FROM FIRST FEW FRESNEL ZONES

GROUND PLATE PROPAGATION MODEL (CONTINUED)

- LINEAR POLARIZATION
- DEFAULT GROUND PLATE
- GROUND SURFACE APPROXIMATED BY PIECEWISE FLAT SECTIONS (PLATES OR PLANES)
- RECTANGULAR OR TRIANGULAR
- EACH PLATE IS HOMOGENEOUS IN PERMITTIVITY & CONDUCTIVITY
- EACH PLATE IS HOMOGENEOUS IN SMALL SCALE ROUGHNESS
- ATTENUATION OF REFLECTED SIGNAL INCREASES WITH ROUGHNESS

[illegible]

- [illegible]
- [illegible]

[illegible]

- [illegible]

[illegible]

- [illegible]

[illegible]

- [illegible]
- [illegible]
- [illegible]

[illegible]

GROUND PLATE PROPAGATION MODEL (CONTINUED)

- PERMITTIVITY COMBINED WITH CONDUCTIVITY TO FORM COMPLEX DIELECTRIC CONSTANT

$$\epsilon_C = \frac{\epsilon}{\epsilon_0} - j\frac{\sigma}{\omega\,\epsilon_0}$$

- SCATTERING MODELS FOR BUILDINGS AND AIRCRAFT INCLUDE DEFAULT GROUND REFLECTIONS

- SHADOWING MODELS FOR BUILDINGS AND AIRCRAFT INCLUDE DEFAULT GROUND REFLECTIONS

- DIFFERENT GROUND DIELECTRIC CONSTANTS FOR

  - THE DEFAULT GROUND PLATE
  - THE SCATTERING AND SHADOWING MODELS
  - EACH INDIVIDUAL GROUND PLATE

169

- [illegible]
- [illegible]
- [illegible]

- [illegible]

[illegible]
- [illegible]

[illegible]
- [illegible]

[illegible]
- [illegible]

[illegible]

GROUND PLATE PROPAGATION MODEL (CONTINUED)

- GROUND PLATE REFLECTIONS ADDED TO DEFAULT GROUND REFLECTION - OR -
- KEPT SEPARATE AND PASSED TO EDITING ROUTINE (FOCUSING GROUND EFFECT OPTION)
- PRECEDENCE: A/C & BLDG SHADOWING, HUMP SHADOWING, GROUND PLATES (ONE ONLY)
- A/C & BLDLG SHADOWING COMPUTATION FOR EVERY FLIGHT PATH POINT WHEN DATA PRESENT IN INPUT FILE
- HUMP SHADOWING ONLY WHEN HUMP CLOSE TO DIRECT RAY PATH
- MODEL FOR DIFFUSE SCATTERING FROM THE GROUND

- [illegible] [illegible] [illegible] [illegible] [illegible]

[illegible]

- [illegible] [illegible] [illegible] [illegible] [illegible] [illegible]

[illegible]

- [illegible] [illegible] [illegible] [illegible] [illegible] [illegible]

[illegible]

- [illegible] [illegible] [illegible] [illegible] [illegible]

[illegible]

- [illegible]

GROUND PLATE PROPAGATION MODEL (CONTINUED)

- 2 METHODS TO CALCULATE SPECULAR GROUND REFLECTION

  - SIMPLE FRESNEL REFLECTION
  - COMPLEX NUMERIC (FULL) INTEGRATION

- SIMPLE FRESNEL REFLECTION

  $\rho_s = \rho_r \cdot R_v(\theta_t)$ FOR VERTICAL POLARIZATION

  $\rho_s = \rho_r \cdot R_h(\theta_t)$ FOR HORIZONTAL POLARIZATION

- FULL INTEGRATION

  - FRESNEL-KIRCHOFF DIFFRACTION FORMULA
  - SURFACE INTEGRAL OVER AREA SURROUNDING SPECULAR POINT
  - OVER THE FIRST 2.8 FRESNEL ZONES
  - EQUIVALENT EQUAL AREA RECTANGLE CENTERED ON FRESNEL ELLIPSE

[illegible]

- [illegible]
- [illegible]
- [illegible]
- [illegible]
- [illegible]
- [illegible]

- [illegible]

  - [illegible]

  - [illegible]

- [illegible]

  - [illegible]
  - [illegible]

- [illegible]

  [illegible]

GROUND PLATE PROPAGATION MODEL (CONTINUED)

- NUMERIC INTEGRATION OVER RECTANGULAR GRID OF 25 BY 11 POINTS

172

INPUT CONTROL FLAGS FOR GROUND PLATES

- 1 - GROUND REFLECTION PROCESSING FLAG - SECTION 2, LINE 1
- 2 - FULL INTEGRATION FLAG - SECTION 2, LINE 2
- 3 - RECTANGULAR GROUND SURFACES FLAG - SECTION 5, LINE 2
- 4 - TRIANGULAR GROUND SURFACES FLAG - SECTION 6, LINE 2
- N - A SURFACE FLAG FOR EACH PLATE - SECTIONS 5 & 6, FIRST DATA LINE FOR EACH PLATE
- ALL FLAGS ARE BINARY VALUED - Y, y, N, OR n - EXCEPT FOR SURFACE FLAGS WHICH ARE 1 (YES) OR 0 (NO)

CONTROL FLAGS (CONTINUED)

- **FLAG #1:** YES - TO INCLUDE DEFAULT GROUND OR DEFAULT GROUND & GROUND PLATES
  NO - TO OMIT DEFAULT GROUND & GROUND PLATES

- **FLAG #2:** YES - TO USE FULL INTEGRATION ON DEFAULT GROUND OR ON DEFAULT GROUND & GROUND PLATES
  NO - TO USE SIMPLE CALCULATION ON DEFAULT GROUND

- **FLAG #3:** YES - TO READ IN RECTANGULAR GROUND PLATE DATA
  NO - TO NOT READ IN RECTANGULAR GROUND PLATE DATA

- **FLAG #4:** YES - TO READ IN TRIANGULAR GROUND PLATE DATA
  NO - TO NOT READ IN TRIANGULAR GROUND PLATE DATA

		[illegible]
	AC	AC ADJ BEND IN ABSTRACT VB GROUND
		WALK
[illegible]	ARP	AD BEND IN ABSTRACT VB GROUND IN WALK
		[illegible]
		[illegible]
	NO	IN ADJ BEND IN ABSTRACT VB GROUND
		WALK
[illegible]	ANP	AD BEND IN ABSTRACT VB GROUND IN WALK
		GROUND
	NO	AD BEND ABSTRACT VB GROUND WALK OR DRIVE
		STYLES
		GROUND OR OR ABSTRACT GROUND S GROUND
[illegible]	ANP	AD BEND ABSTRACT VB GROUND OR DRIVE
		STYLES
	AC	AD ORIL DRIVE ABSTRACT GROUND
		GROUND S GROUND STYLES
[illegible]	ARP	AD BEND ABSTRACT VB GROUND OR DRIVE

CONTROL FLAGS (CONTINUED)

- FLAG #N: YES - TO CALCULATE A SEPARATE MULTIPATH COMPONENT FOR THE GROUND PLATE
  NO - TO ADD THE CONTRIBUTION FROM THE GROUND PLATE TO THE DEFAULT GROUND PLATE

- DEFAULT VALUES FOR FLAGS #1 & #2 WHEN SECTION 2 IS OMITTED ARE YES & YES

175

GROUND PLATE OPTIONS

- 1 - NO EXPLICIT GROUND REFLECTIONS
- 2 - EXPLICIT SPECULAR GROUND REFLECTION FROM DEFAULT GROUND ONLY - SIMPLE CALCULATION
- 3 - EXPLICIT SPECULAR GROUND REFELCTION FROM DEFAULT GROUND ONLY - FULL INTEGRATION
- 4 - EXPLICIT SPECULAR GROUND REFLECTIONS FROM DEFAULT GROUND AND FROM GROUND PLATES - FULL INTEGRATION - ALL PLATE REFLECTIONS COMBINED WITH DEFAULT GROUND REFLECTION
- 5 - EXPLICIT SPECULAR GROUND REFLECTIONS FROM DEFAULT GROUND AND FROM GROUND PLATES - FULL INTEGRATION - SOME OR ALL PLATE REFLECTIONS CALCULATED SEPARATELY - REMAINDER COMBINED WITH DEFAULT GROUND REFLECTION

GROUND RULE NINE

GOLF BALLS. EQUIPMENT COVERED BY RULE EIGHT.

ZONE OF THE LEVEL REFERENCE CYLINDER

GROUND AND NON GROUND LEVEL - NOT PARTICULARLY

EXTRICAL RELATIVE GROUND REFERENCE NON DEFINED

GROUND TEN.

THE LEVEL REFERENCE CYLINDER MAY BE

GROUND AND NON GROUND LEVEL - NOT PARTICULARLY

EXTRICAL RELATIVE GROUND REFERENCE NON DEFINED

GROUND ONE - NOT PARTICULARLY

EXTRICAL RELATIVE GROUND STRAY WALL NON DEFINED

GROUND TWO - SAME PARTICULARLY

EXTRICAL RELATIVE GROUND REFERENCE NON DEFINED

NO ALGEBRICAL GROUND REFERENCE

GROUND LEVEL ONLY

INPUT FLAG SETTINGS FOR GROUND PLATE OPTIONS

- 1 - FLAG #1 = NO

- 2 - FLAG #1 = YES
  FLAG #2 = NO

- 3 - FLAG #1 = YES
  FLAG #2 = YES
  FLAG #3 = NO
  FLAG #4 = NO

- 4 - FLAG #1 = YES
  FLAG #2 = YES
  FLAG #3 = YES
  FLAG #4 = YES
  FLAG #N = 0

INPUT FLAG SETTINGS FOR GROUND PLATE OPTIONS (CONTINUED)

- 5 - FLAG #1 = YES
  FLAG #2 = YES
  FLAG #3 = YES
  FLAG #4 = YES
  FLAG #N = 0 OR 1

- NOTE: THE SPECULAR REFLECTION FROM THE DEFAULT GROUND PLATE CAN BE SUPPRESSED BY GIVING THE PLATE A LARGE ROUGHNESS FACTOR

178

[illegible] VISCOUS SOLUTIONS BY USING
GROUND STATE CAN BE BUILDING AS STARTING POINT
[illegible] THE CONCAVITY INEQUALITY UNDER THE DIVERGENCE

$$\mathrm{MVC}\ W = \{ [illegible] \}$$
$$\mathrm{MVC}\ W = \mathrm{AB}^2$$
$$\mathrm{MVC}\ W = \mathrm{AB}^2$$
$$\mathrm{MVC}\ W = \mathrm{AB}^2$$
$$\mathrm{MVC}\ W = \mathrm{AB}^2$$

[illegible] MVC [illegible] BOX GROUND STATE [illegible] [illegible]

```
*******************MLS MATHEMATICAL MODEL INPUT DATA FILE************************
SECTION  0
          = SCENARIO DATA
          RUN ID# :9999
          TITLE   :SAMPLE INPUT FILE
          AIRPORT :LAX
          RUNWAY  :24R
          LENGTH  :8700.
          WIDTH   :150.
          ARDH    :50.
          MGPA    :3.0
          UNITS   :FEET  (feet, meter) FOR ENTRIES IN FILE
SECTION 1A
          = ANGLE TRANSMITTER DATA
          PHASE CENTER:  X        Y        Z    FREQ(mhz)  LSL   USL    TYPE
                       -------- -------- -------- --------- ----- ----- --------
          AZIMUTH  :  -1000.0      0.0      5.0  4992.291 -60.0 60.0  AZBN
          ELEVATION:   7900.0   -400.0     13.0  4992.291   0.9 20.0  ELBN
SECTION 1D
          = DME/P TRANSMITTER DATA
          PHASE CENTER:  X        Y        Z      TYPE
                       -------- -------- -------- --------
          DME/P    : -1000.0  0.0      5.0      DMBN

          = OTHER DME DATA
                       FREQ(mhz)   SHAPE   TRG  F   SW    AS    TRS  SIGM   RMI
                       --------- --------- --- --- ----- ----- ----- ----- -----
          UPLINK   : 983.4813  COS/P     DAC B4P .5    .5    .125  0.0   0.0
          DOWNLINK : 983.4813  COS/P     DAC B4P .5    .5    .125  0.0   0.0
SECTION  2
          YES - DO ANY GROUND REFLECTION PROCESSING (CALL GREFC) (yes,no)
          YES  - DO FULL INTEGRATION FOR SPECULAR GROUND SCATTERING (yes,no)
          = DEFAULT DIELECTRIC CONSTANT AND ROUGHNESS HEIGHT
          DIELECTRIC CONSTANT : 1.2        0.0
          ROUGHNESS HEIGHT    : 0.0
        * FOR MULTIPLE SCATTERING PATHS FROM AIRCRAFT AND BUILDINGS
          DIELECTRIC CONSTANT : 1.2        0.0
          ROUGHNESS HEIGHT    : 0.0
SECTION  3
          = SCATTERING FROM AIRCRAFT (MAXIMUM OF 10)
          YES - RUN AIRCRAFT SCATTERING (yes,no)
        ##  X-TAIL   Y-TAIL   X-CKPT   Y-CKPT     ALT   AT  GRCORR
        -- -------- -------- -------- -------- -------- -- --------
        nn xxxxxxxx yyyyyyyy xxxxxxxx yyyyyyyy aaaaaaaa tt cccccccc
        01 5700.0   -1150.0  5900.0   -1150.0  0.0       1 0.0
        02 6700.0   -1150.0  6900.0   -1150.0  0.0       1 0.0
        03 8758.6   -1150.0  8900.0   -1008.6  0.0       1 0.0
        04 8900.0    -900.0  8900.0    -700.0  0.0       1 0.0
SECTION  4
          = SCATTERING FROM BUILDINGS (MAXIMUM OF 10)
          YES - RUN SCATTERING BUILDINGS (yes,no)
        ##  X-LEFT   Y-LEFT   X-RGHT   Y-RGHT   ELV   HGT   TLT   GRCORR   CMP
        -- -------- -------- -------- -------- ----- ----- ----- -------- -----
        nn xxxxxxxx yyyyyyyy xxxxxxxx yyyyyyyy eeeee hhhhh ttttt cccccccc mmmmm
        01 3975.0   -3400.0  4400.0   -3400.0  0.0   100.0 0.0   0.0      METAL
        02 4550.0   -2100.0  5080.0   -2100.0  0.0   100.0 0.0   0.0      METAL
        03 4800.0   -3100.0  5200.0   -3100.0  0.0   100.0 0.0   0.0      METAL
        04 6825.0   -1800.0  7125.0   -1800.0  0.0    50.0 0.0   0.0      METAL
        05 7780.0   -1800.0  8080.0   -1800.0  0.0    50.0 0.0   0.0      METAL
        06 7125.0   -1800.0  7252.0   -1706.0  0.0    50.0 0.0   0.0      METAL
        07 8080.0   -1800.0  8209.0   -1706.0  0.0    50.0 0.0   0.0      METAL
SECTION  5
          = SPECULAR SCATTERING FROM RECTANGULAR GROUND SURFACES (MAX OF 10)
          YES - RUN RECTANGULAR GROUND (yes,no)
          THIS DATA MAY BE SKIPPED
        ##  X-VALU   Y-VALU   Z-VALU   DCREAL   DCIMAG   ROUGHN  SF
        -- -------- -------- -------- -------- -------- -------- --
        nn x1x1x1x1 y1y1y1y1 z1z1z1z1 rrrrrrrr iiiiiiii rrrrrrrr is
           x2x2x2x2 y2y2y2y2 z2z2z2z2
           x3x3x3x3 y3y3y3y3 z3z3z3z3
        01 0.0      -75.0    0.0      5.0      0.0      .006562   0
           0.0       75.0    0.0
           8700.0    75.0    0.0
SECTION  8
          = SHADOWING BY AIRCRAFT
          YES - RUN SHADOWING AIRCRAFT (yes,no)
```

```
        ##  X-VALU   Y-VALU   Z-VALU   VEL   ANG  AT
        -- -------- -------- -------- ----- ----- --
        nn sax1sax1 say1say1 saz1saz1 vvvvv aaaaa tt
           sax2sax2 say2say2 saz2saz2
        01  4076.0    -25.0      0.0  275.0 14.0   6
            2167.0    -29.0    127.0
SECTION  9
           = SHADOWING BY BUILDINGS
           YES - RUN SHADOWING BUILDINGS (yes,no)
        ##  X-LEFT   Y-LEFT   X-RGHT   Y-RGHT   ELV   HGT
        -- -------- -------- -------- -------- ----- -----
        nn xxxxxxxx yyyyyyyy xxxxxxxx yyyyyyyy eeeee hhhhh
        01   250.0    750.0   -400.0    750.0   0.0  100.0
        02  1900.0    850.0    700.0    850.0   0.0  100.0
        03  3000.0    700.0   2300.0    700.0   0.0  100.0
SECTION 10
           = SHADOWING BY RUNWAY HUMP
           YES - RUN SHADOWING HUMP (yes,no)
            X-FRONT  Z-FRONT  X-HUMP   Z-HUMP   X-BACK   Z-BACK
           -------- -------- -------- -------- -------- --------
           xfxfxfxf zfzfzfzf xhxhxhxh zhzhzhzh xbxbxbxb zbzbzbzb
           3300.0   0.0      3800.0   5.0      4300.0   0.0
SECTION 12
           = FLIGHTPATH
           FAF      : 6.2      NAUTICAL MILES
           DATUM    : 7900.0   0.0      0.0
           TYPE     : SEGMENTED    (measured, distance, orbit, radial,
         *                          segmented, straight)
           VELOCITY : 219.56
           INCREMENT: 43.91
           DATA RATE:  0.20
         *  IF "straight" SUFFICIENT DATA IS AVAILABLE TO COMPUTE FLIGHTPATH
         *  IF "radial" ENTER ANGLE, ELEVATION, STARTING and ENDING DISTANCE
         * (nm from dme/p)
           ANGLE: aaaaaaaa
           SDIST: dddddddd
           EDIST: dddddddd
           ELEV : eeeeeeee
         *  IF "orbit" ENTER RADIUS (nm from dme/p) & ELEVATION
           RADIUS: rrrrrrrr
           ELEV  : eeeeeeee
         *  IF "measured" X,Y,Z COORDINATES AND TIME WILL BE READ FROM UNIT 15
         *      WITH VELOCITY AND DATA INCREMENT COMPUTED FROM INPUT
         *  IF "segmented" or "distance" ENTER SEGMENT #,X,Y,Z,VELOCITY AND
         *      INCREMENT
        ##    XS       YS       ZS       VEL      INC
        -- -------- -------- -------- -------- --------
        nn xxxxxxxx yyyyyyyy zzzzzzzz vvvvvvvv iiiiiiii
        01  17700.0      0.0    500.0   219.56    43.91
        02   7700.0      0.0      0.0     0.0      0.0
SECTION 13
           = FLIGHTPATH AND AIRPORT LAYOUT AXIS LIMITS
         * FLIGHTPATH PLOTS:
                                X/Y PLOT     X/Z PLOT     D/Z PLOT
                               ----------   ----------   ----------
             MINIMUM X VALUE :  -3000.00 ft  -3000.00 ft     -0.25 nm
             UNITS PER INCH  :   3000.00 ft   3000.00 ft      0.25 nm
             MINIMUM Y VALUE :  -3000.00 ft   -100.00 ft   -100.00 ft
             UNITS PER INCH  :   1000.00 ft    100.00 ft    100.00 ft
         * AIRPORT LAYOUT PLOT:
                                X/Y PLOT
                               ----------
             MINIMUM X VALUE :  -2000.00 ft
             UNITS PER INCH  :   2000.00 ft
             MINIMUM Y VALUE :  -4000.00 ft
             UNITS PER INCH  :   1000.00 ft
SECTION 14
           = ANGLE EQUIPMENT AXIS LIMITS
         * MULTIPATH DIAGNOSTIC PLOTS:
                                M/D        SEP ANG    SHADOWING
                               ---------  ---------  ---------
             MINIMUM X VALUE :    -0.50 nm   -0.50 nm   -0.50 nm
             UNITS PER INCH  :     0.25 nm    0.25 nm    0.25 nm
             MINIMUM Y VALUE :    -40.0 db   -40.0 deg  -10.0 db
             UNITS PER INCH  :     10.0 db    10.0 deg    2.0 db
         * RECEIVER OUTPUT ERROR & FILTERED ERROR PLOTS:
```

	RAW	PFE	CMN
MINIMUM X VALUE :	-0.50 nm	-0.50 nm	-0.50 nm
UNITS PER INCH :	0.25 nm	0.25 nm	0.25 nm
MINIMUM Y VALUE :	-0.30 deg	-0.30 deg	-0.30 deg
UNITS PER INCH :	0.10 deg	0.10 deg	0.10 deg

SECTION 15

= DISTANCE MEASURING EQUIPMENT AXIS LIMITS

* MULTIPATH DIAGNOSTIC PLOTS:

	M/D	TIM DELAY	SHADOWING
MINIMUM X VALUE :	-0.50 nm	-0.50 nm	-0.50 nm
UNITS PER INCH :	0.25 nm	0.25 nm	0.25 nm
MINIMUM Y VALUE :	-40.0 db	0.0 ns	-10.0 db
UNITS PER INCH :	10.0 db	500.0 ns	2.0 db

* RECEIVER OUTPUT ERROR & FILTERED ERROR PLOTS:

	RAW	PFE	CMN
MINIMUM X VALUE :	-0.50 nm	-0.50 nm	-0.50 nm
UNITS PER INCH :	0.25 nm	0.25 nm	0.25 nm
MINIMUM Y VALUE :	-90.0 ft	-90.0 ft	-90.0 ft
UNITS PER INCH :	30.0 ft	30.0 ft	30.0 ft

END DATA

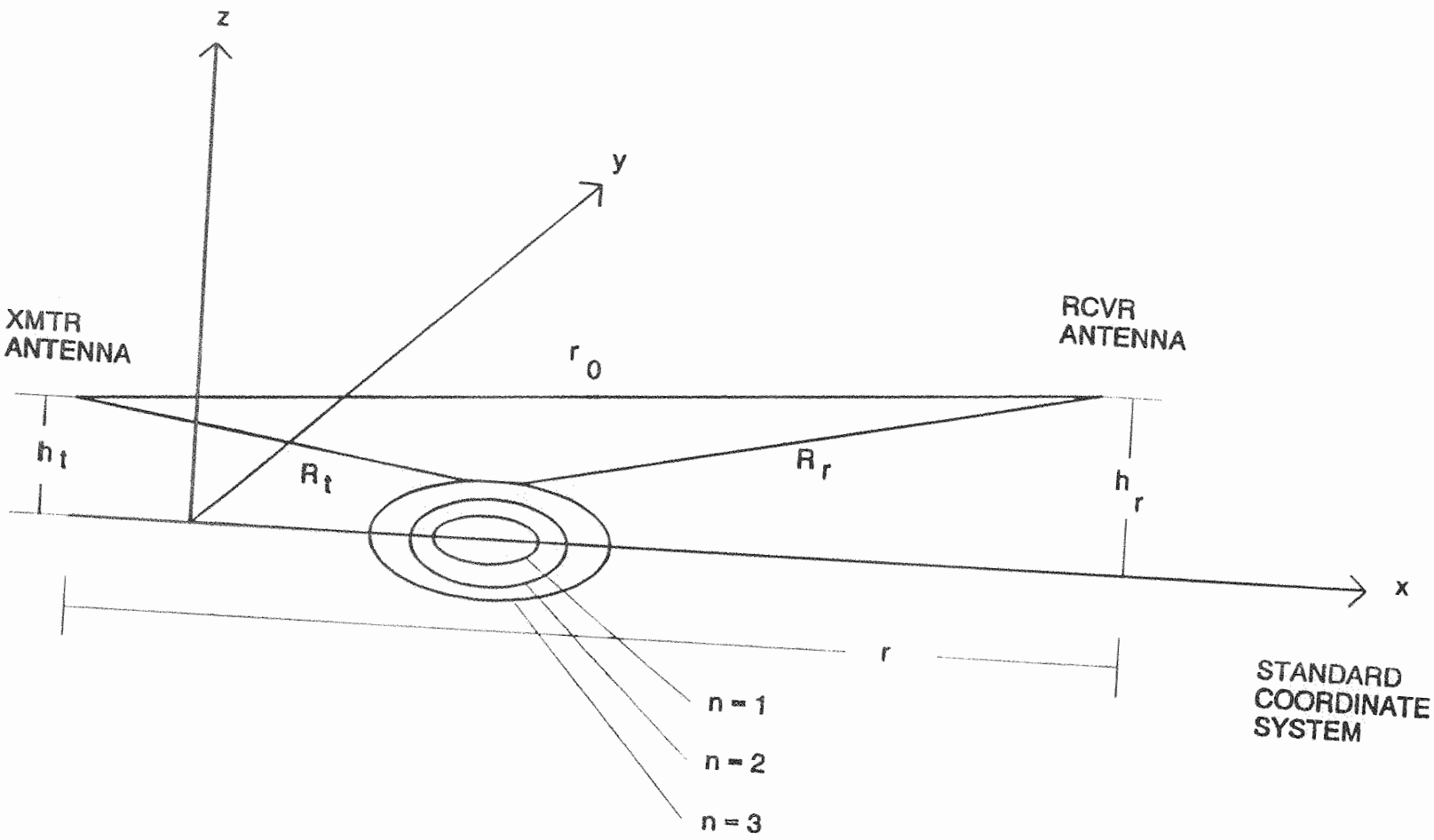

Fresnel Zones

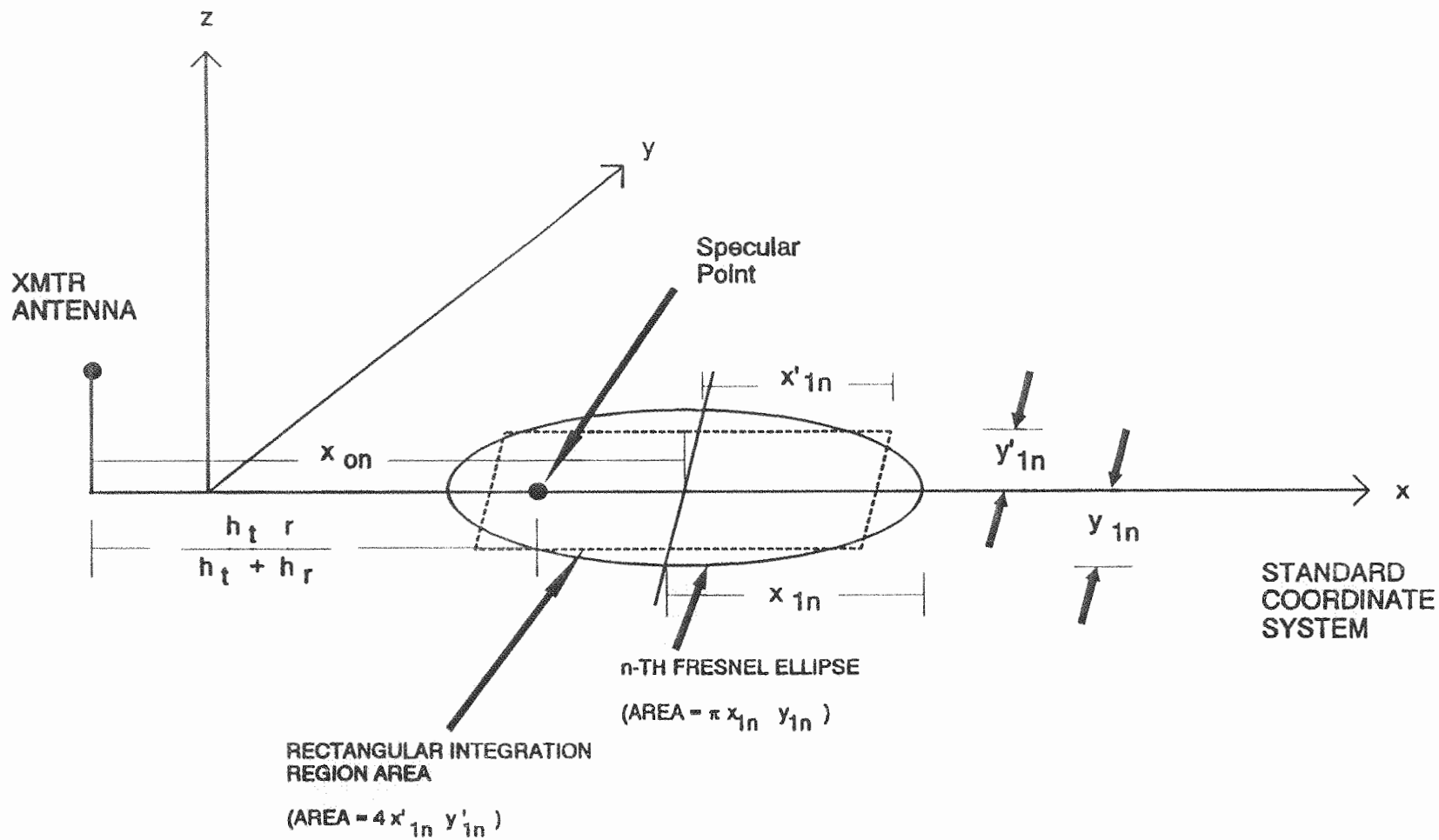

Fresnel Zones

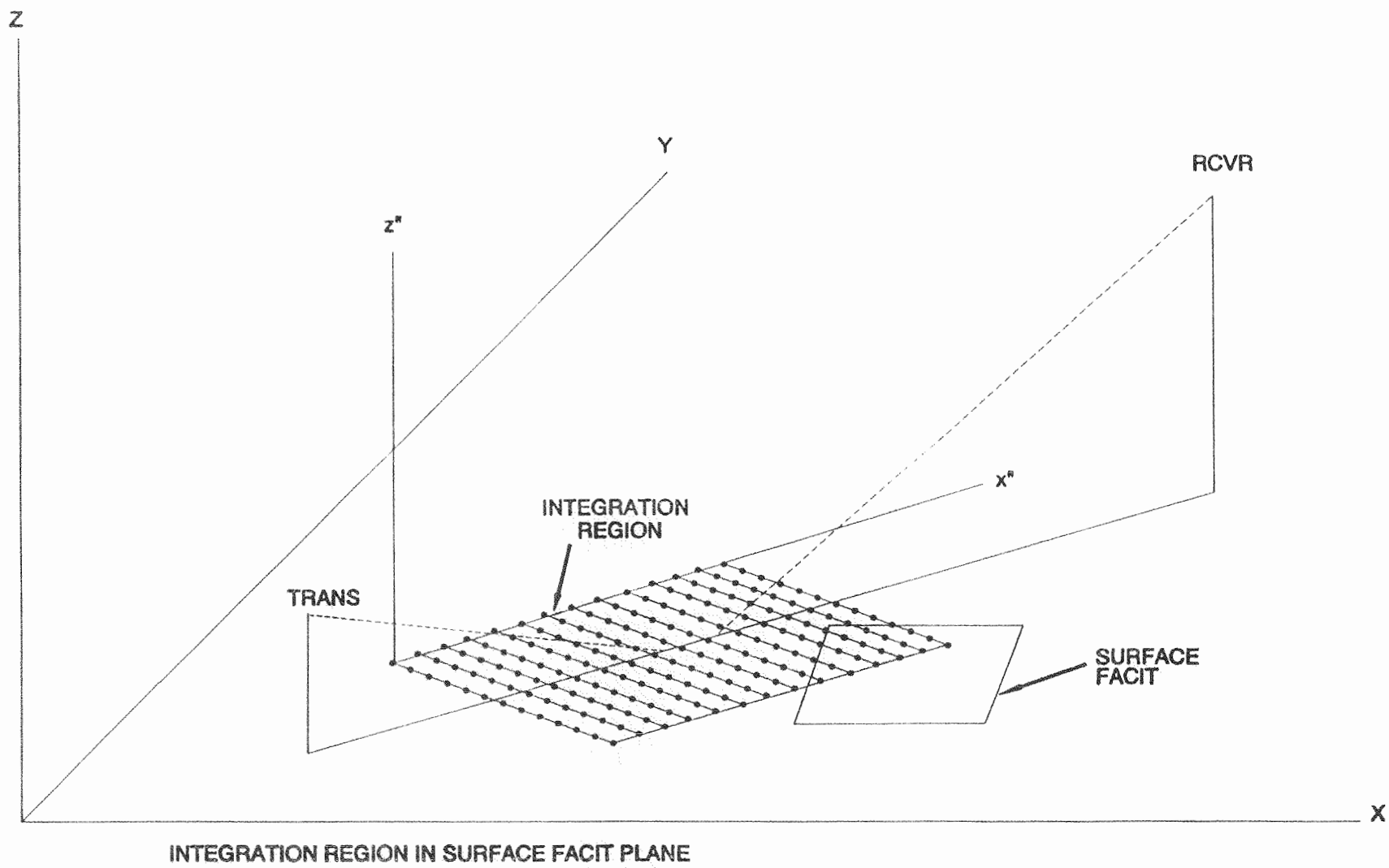

Relationship of Gridpoints to Surface Element

Small Scale Surface Roughness Attenuation Factor

$$\rho_r = \epsilon^{-\frac{1}{2}(4\pi/\lambda\ \sigma_h \cos\theta_t)^2}$$

σ_h = root-mean-square roughness height

θ_t = reflection angle

Reference: Beckman and Spizzichino[3], p.81

Total Reflection Coefficient

$$\rho_s = jR_o/\lambda * \int\int_{\text{Integration region}} 1/R_r R_t \, \epsilon^{-jk(Rr+Rt-Ro)} \cdot \rho_r R_{eq} \frac{\cos\theta_t + \cos\theta_r}{2} \, dS$$

R_o = distance between transmitter and receiver antennas

R_t = distance between transmitter antenna and specular point

R_r = distance between receiver antenna and specular point

λ = wavelength

θ_t = incidence angle

θ_r = reflection angle

Fresnel Reflection Coefficient for Reflection from Tilted Surface

$$R_{eq} = R_v(\theta_i) \cos \alpha_1 \cos \alpha_2 + R_h(\theta_i) \sin \alpha_1 \sin \alpha_2$$

R_v = Fresnel reflection coefficient for vertical polarization

R_h = Fresnel reflection coefficient for horizontal polarization

Reference: Goodman[4] p.41, or Sommerfield[5] p.201

Fresnel Reflection Coefficient for Vertical Polarization:

$$R_v(\theta_i) = \frac{\epsilon_r \cos\theta_i - (\epsilon_r - \sin^2\theta_i)^{1/2}}{\epsilon_r \cos\theta_i + (\epsilon_r - \sin^2\theta_i)^{1/2}}$$

Fresnel Reflection Coefficient for Horizontal Polarization:

$$R_h(\theta_i) = \frac{\cos\theta_i - (\epsilon_r - \sin^2\theta_i)^{1/2}}{\cos\theta_i + (\epsilon_r - \sin^2\theta_i)^{1/2}}$$

ϵ_r = surface dielectric constant

θ_i = incidence angle

Reference: Kerr[2], p.396

Rectangular Integration Region

$$x_{on} = r/2 \quad \frac{1+2h_t(h_r+h_t)/(n\ \lambda\ r)}{1+(h_r+h_t)^2/(n\ \lambda\ r)}$$

$$x_{in} = r/2 \quad \frac{[1+2\delta_o/(n\ \lambda)]^{1/2}}{1+(h_r+h_t)^2/(n\ \lambda\ r)}$$

$$y_{in} = 1/2 \quad \left[\frac{1+2\delta_o/(n\ \lambda)}{1+(h_r+h_t)^2/(n\ \lambda\ r)}\right]^{1/2}$$

$\delta_o = 2h_rh_t/r$

n = subscript of Fresnel ellipse being considered

h_t = height of transmiter antenna

h_r = height of receiver antenna

λ = wavelength

Table I. Dielectric Constant Values for Reflecting Surfaces

Composition	Name (CMP)	Dielectric Constant Real	Imaginary
Concrete	CONCR	10.0	-9.0
Smooth Metal	METAL	1.0	-1.0E8
Glass	GLASS	6.0	-0.042
Marble	MARBL	8.7	-0.2
Asphalts	ASPHA	2.6	-0.016
Plastics	PLAST	3.0	-0.09
Bakelite	BAKEL	4.5	-0.1
Laminated Fiberglass	FIBER	4.4	-0.13
Polyvinyl Chloride	POLYV	3.0	-0.15
Formica	FORMI	4.0	-0.1
Sandy Dry Soil	SSDRY	2.5	-0.016
Sandy soil, 20% Moisture	SS20%	20.0	-2.6
Loamy Dry Soil	LSDRY	2.4	-0.0027
Loamy Soil, 15% Moisture	LS15%	20.0	-2.4
Clay Dry Soil	CSDRY	2.27	-0.034
Clay Soil, 20% Moisture	CS20%	11.3	-2.8
Rocky Soil 10% Moisture	RS20%	30.0	-0.06
Dry Turf, Short Grass	DTWSG	3.0	-0.9
Wet Turf, Short Grass	WTWSG	6.0	-1.8
City Industrial Area	CITYI	5.0	-0.02
Fresh Water	FRESH	80.0	-0.18
Sea Water	SEA	80.0	-54.0
Fresh Snow	SNOW	1.2	-1.3
Ice	ICE	3.2	-0.0029